

OKINAWA INSTITUTE OF SCIENCE AND TECHNOLOGY
GRADUATE UNIVERSITY

Thesis submitted for the degree

Doctor of Philosophy

**Dynein Light Chain Roadblock 1 Regulates
FMRP Axonal Transport and Degradation**

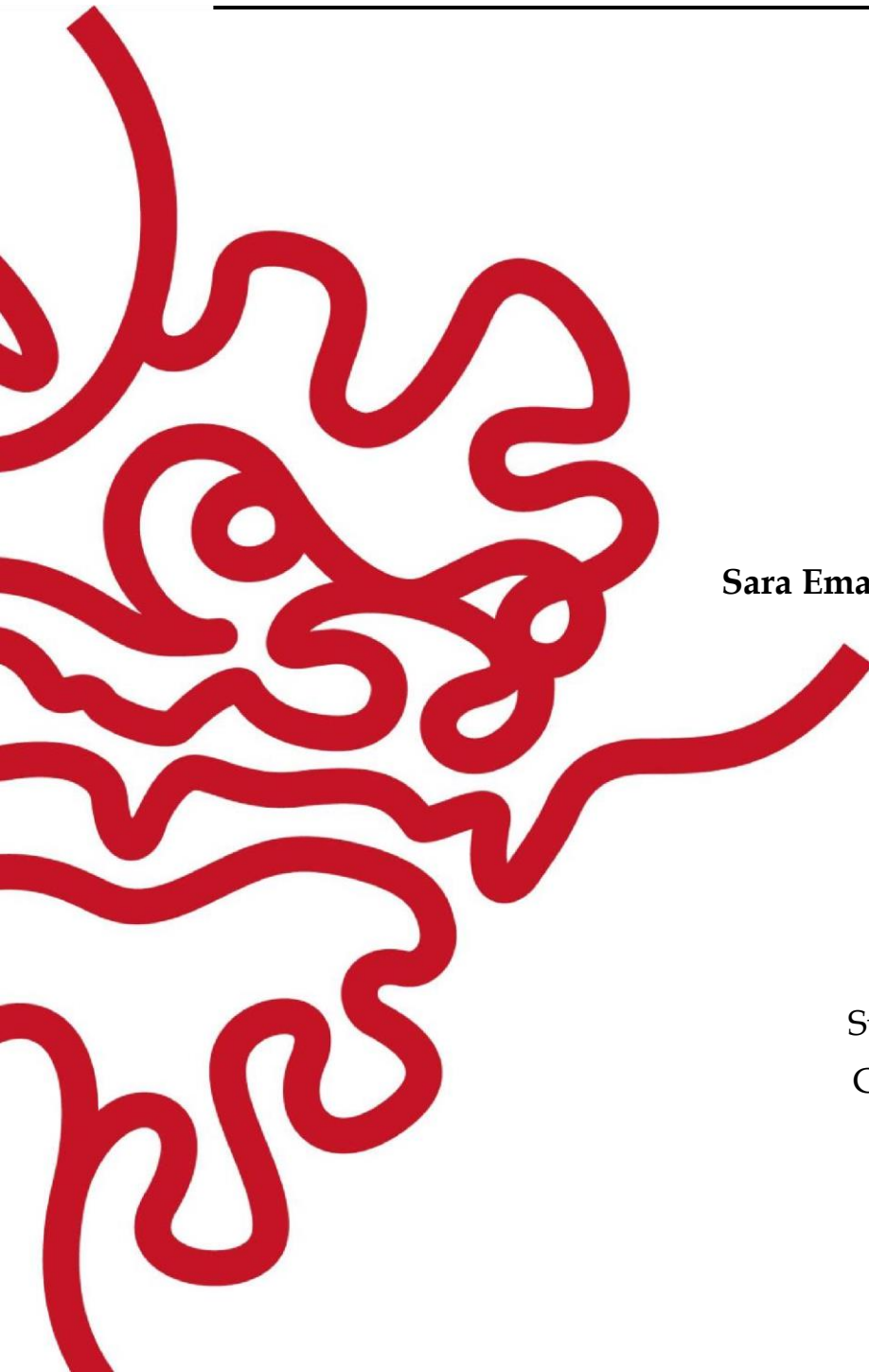
By

Sara Emad Mohamed Elagamy Abdelaal

Supervisor: **Prof. Marco Terenzio**

Co-supervisor: **Prof. Keiko Kono**

January 2024



Declaration of Original and Sole Authorship

I, Sara Emad Mohamed Elagamy Abdelaal, declare that this thesis entitled “Dynein Light Chain Roadblock 1 Regulates FMRP Axonal Transport and Degradation” and the data presented in it are original and my own work.

I confirm that:

- No part of this work has previously been submitted for a degree at this or any other university.
- References to the work of others have been clearly acknowledged. Quotations from the work of others have been clearly indicated and attributed to them.
- In cases where others have contributed to part of this work, such contribution has been clearly acknowledged and distinguished from my own work.
- None of this work has been previously published elsewhere, with the exception of the following:

El-Agamy, S. E., Guillaud, L., Kono, K., Wu, Y., & Terenzio, M. FMRP Long-Range Transport and Degradation Are Mediated by Dynlrb1 in Sensory Neurons, Molecular and Cellular Proteomics, 2023.

Contributions:

S.E.E-A. and M.T. conceived the project, performed the experiments, and analyzed the data. Y.W. acquired the mass spectrometry data. L.G. performed the airyscan acquisition and analysis. M.T. and K.K. provided resources and supervision. S.E.E-A. wrote the original draft. S.E.E-A., M.T., L.G., and K.K. participated in the editing of the manuscript.

Date: January 2024

Signature: 

Abstract

The fragile X messenger ribonucleoprotein 1 (FMRP) is a multifunctional RNA binding protein (RBP) implicated in human neurodevelopmental and neurodegenerative disorders. FMRP mediates the localization and activity-dependent translation of its associated mRNAs through the formation of phase separated condensates that are trafficked by microtubule-based motors in axons. Axonal transport and localized mRNA translation are critical processes for long-term neuronal survival and are closely linked to the pathogenesis of neurological diseases. FMRP dynein-mediated axonal trafficking is still largely unexplored, but likely to constitute a key process underlying FMRP spatiotemporal translational regulation. Here, we show that roadblock 1 (Dynlrb1), a subunit of the dynein complex, is a critical regulator of FMRP function in sensory neurons. In axons, FMRP associates with the dynein complex and is retrogradely trafficked in a Dynlrb1-dependent manner. Moreover, Dynlrb1 silencing induced FMRP granules accumulation and repressed the translation of Map1b, one of its primary mRNA targets. Our findings suggest that Dynlrb1 regulates FMRP function through the control of its transport and degradation.

Acknowledgments

I would like to express my gratitude to my supervisor Prof. Marco Terenzio for seeing my potential and taking me in as his first PhD student, for his continuous support and help with the practical work and data analysis. His feedback and experience were instrumental in bringing my work to a higher level.

I would like to express my deepest appreciation to my co-supervisor prof. Keiko Kono for the invaluable scientific discussions and for standing by my side throughout the most challenging moments of this journey. Without her unconditional support, this PhD wouldn't have been possible.

I am thankful to my mentor, prof. Hiroki Ishikawa for the constructive feedback during my progress reviews and his support throughout my Ph.D.

I would like to thank all members of the Terenzio unit. I am particularly grateful to our group leader Dr. Laurent Guillaud for his scientific and moral support, for always being available whenever I needed guidance, and for all the encouragement to reach my goals.

I am thankful to all past and current members of the Kono unit for supporting my experiments for the first 6 months. I am truly grateful to Dr. Yohsuke Moriyama for his insightful advice and help.

I would like to extend my thanks to Alejandro Villar-Briones for teaching me how to process the proteomics samples as well as the data analysis. I am also thankful to Clive Barker for his help with the mass spectrometry data acquisition. Additionally, I am grateful to the Student Support section and OIST Graduate School for their tremendous help and assistance throughout my Ph.D.

I would like to thank all the kind people I met in Okinawa, especially Dr. Amine Aladag, Dr. Nurhanani Binti Razali, Dr. Afshan Jamshaid, and Dr. Alemeh Zamani for the cherished time spent on this beautiful island. They made graduate life a much more pleasant experience. Many thanks go to my friends from home, especially Dr. Amal Kamal Abdelaziz for cheering for me from afar, for sharing my ups and downs, and for always being there for me.

Finally, but of great importance, I am forever grateful to my beloved mother for her immense sacrifices and patience along the way to help me, for believing in me and my ability to achieve my ambitions, for pushing me to challenge myself, for being “my backbone”, I would have never made it this far if it weren't for her. I'm also truly thankful for my father who has been a great source of motivation and inspiration over the years.

List of Abbreviations

AAV	Adeno-associated virus
Actr1b	Actin related protein 1b
ALS	Amyotrophic lateral sclerosis
Anxa11	Annexin A11
AP	Affinity purification
APC	Adenomatous polyposis coli
APP	Amyloid precursor protein
ASD	Autism spectrum disorder
BAG3	Bcl-2-associated athanogene 3
BicD	Bicaudal-D
BDNF	Brain-derived neurotrophic factor
BSA	Bovine serum albumin
CAP-Gly	Cytoskeleton-associated protein and glycine-rich
CDS	Coding sequence
CMT	Charcot-Marie-Tooth disease
Co-IP	Co-immunoprecipitation
CLIP	Cross-linking and immunoprecipitation
Cra1	Cramping 1
CYFIP1	Cytoplasmic FMRP-interacting protein 1
Dync1h1	Dynein heavy chain
Dync1i	Dynein intermediate chain
Dync1li	Dynein light intermediate chain
Dynll	Dynein light chain LC8-type
Dynlt	Dynein light chain Tctex-type
Dynlrb	Dynein light chain roadblock-type
DRG	Dorsal root ganglia
DIV	Days <i>in vitro</i>
FBS	Fetal bovine serum
FMRP	Fragile X messenger ribonucleoprotein 1
FUS	Fused in sarcoma
FXGs	Fragile X granules
FXRP	Fragile X related protein
FXS	Fragile X syndrome
FXTAS	Fragile X-associated tremors/ataxia syndrome
G3bp	G3BP stress granule assembly factor
HDAC6	Histone deacetylase 6
hSynI	Human synapsin I
IDR	Intrinsically disordered region

ISH	<i>In situ</i> hybridization
JIP	JNK-interacting protein
Lamp1	Lysosomal-associated membrane protein 1
LC-MS/MS	Liquid chromatography tandem mass spectrometry
LCR	Low complexity region
LLPS	Liquid-liquid phase separation
Loa	Legs at odd angles
m6A	N6-methyladenosine
Map1b	Microtubule-associated protein 1
MCD	Malformations of cortical development
MT	Microtubules
MTBD	Microtubule binding domain
MS	Mass spectrometry
NAGK	N-acetyl D-glucosamine kinase
NDD	N-terminal dimerization domain
NES	Nuclear export signal
NLS	Nuclear localization signal
P-bodies	Processing bodies
PFA	Paraformaldehyde
PLA	Proximity ligation assay
PPI	Protein-protein interaction
PP2A	Protein phosphatase 2A
RBP	RNA binding protein
RILP	Rab7 interacting lysosomal protein
RNP	Ribonucleoprotein
RT	Room temperature
SOD1	Superoxide dismutase 1
Smad2	SMAD family member 2
SMA-LED	Spinal muscular atrophy with lower extremity dominance
SQSTM1	Sequestosome 1
TDP43	TAR DNA binding protein
TRAK	Trafficking kinesin protein
UPS	Ubiquitin-proteasome system
Vps29	Vacuolar protein sorting associated protein 29
Vta1	Vacuolar protein sorting associated protein VTA1 homolog
YTHDF	YTH (YT521-B homology) domain-containing protein family

إهداء إلى أُمِّي، لِحُبِّها وَعَطَائِها الّلا مَنتهى ودعمها الدائم لي في مسيرتي.

Dedicated to my mother, for her endless love and unwavering support.

List of Contents

Declaration of Original and Sole Authorship	ii
Abstract	iii
Acknowledgments	iv
List of Abbreviations	vi
List of Contents	ix
List of Figures	xii
Chapter 1. Introduction	1
1.1. Axonal transport	1
1.2. Dynein subunit composition	2
1.2.1. Dynein heavy chain	2
1.2.2. Dynein intermediate chains	3
1.2.3. Dynein light intermediate chains	3
1.2.4. Dynein light chains	3
1.3. Dynein activation	4
1.4. Dynein cargos	5
1.4.1. Endolysosomes and autophagosomes	5
1.4.2. Messenger ribonucleoprotein granules	6
1.4.3. Mitochondria	7
1.4.4. Signaling endosomes	7
1.4.5. Protein cargos (aggresomes)	7
1.5. Dynlrb1 role in neuronal homeostasis	8
1.6. Dynein mutations in neurological disorders	8
1.7. FMRP involvement in neurological diseases	10
1.8. FMRP structure meets the function	10
1.9. FMRP regulates translation and mRNA transport	11
1.9.1. Models of translation regulation	11
1.9.2. Regulation of mRNA in mRNP granules	12
1.10. Proximity-dependent biotinylation	15

1.11. Aim and structure of the thesis	16
Chapter 2. Materials and Methods	17
2.1. Animal experiments	17
2.2. Reagents, chemicals, and antibodies	17
2.3. DRG culture	18
2.4. HEK cells and AAV production	18
2.5. NIH/3T3 cell line culture and transfection	18
2.6. Plasmid DNA	19
2.7. Axoplasm pulldown	20
2.8. Co-immunoprecipitation	20
2.9. Expression of miniTurbo constructs, biotinylation, and streptavidin pulldown	21
2.10. Mass spectrometry sample preparation and data analysis	21
2.11. Cytotoxicity assay	22
2.12. Immunofluorescence	22
2.13. Airyscan image acquisition and analysis	23
2.14. Proximity ligation assay	23
2.15. Puromycinylation and puro-PLA	23
2.16. RNAscope multiplex fluorescent assay combined with immunofluorescence	24
2.17. Pharmacological treatments	24
2.18. Protein extraction and western blotting	25
2.19. Gene expression analysis by quantitative reverse-transcription polymerase chain reaction	25
2.20. siRNA transfection	25
2.21. Axonal transport experiments	26
2.22. Statistical analysis	26
Chapter 3. Results	27
3.1. Design and optimization of Dynlrb1-miniTurbo fusion constructs for proximity labeling	27

3.2. Identifying Dynlrb1 interactors in DRG neurons via mass spectrometry	30
3.3. FMRP associates with dynein and endolysosomes in wild type sensory axons	34
3.4. FMRP axonal trafficking depends on Dynlrb1 levels	39
3.5. Dynlrb1 regulates FMRP protein levels and function	48
Chapter 4. Discussion	53
Chapter 5. Conclusion and Outlook	56
References	59
Appendix	68

List of Figures

Figure 1.1. Schematic representation of the axonal transport machinery	1
Figure 1.2. Schematic representation of the dynein complex composition	2
Figure 1.3. Schematic representation of dynactin's role in relieving dynein auto-inhibition	4
Figure 1.4. Schematic representation of hitchhiking as a mode of cargo transport	6
Figure 1.5. Schematic diagram of FMRP domain structure	11
Figure 1.6. Schematic of proximity-dependent proteomics workflow	15
Figure 3.1. Optimization of miniTurbo fusion constructs in 3T3 cells	28
Figure 3.2. Optimization of proximity labeling in cultured DRG neurons	29
Figure 3.3. Validation of recombinant Dynlrb1 association with the dynein complex in sensory neurons	30
Figure 3.4. Mass spectrometry (MS) analysis of Dynlrb1 interactors	31
Figure 3.5. Validation of Dynlrb1-Vps29 and Vta1 interaction in DRG neurons	33
Figure 3.6. Validation of Dynlrb1-FMRP association in DRG neurons	34
Figure 3.7. FMRP co-precipitates with the dynein complex in sensory axons	35
Figure 3.8. Analysis of FMRP trafficking in wild type sensory neurons	36
Figure 3.9. Efficiency of Anxa11 depletion in sensory neurons	37
Figure 3.10. Depletion of Anxa11 reduces FMRP association with Lamp1 vesicles	38
Figure 3.11. shRNA-mediated depletion of Dynlrb1 in DRG neurons	39
Figure 3.12. Dynlrb1 silencing impacts FMRP association with the dynein complex	40
Figure 3.13. siRNA-mediated depletion of Dynlrb1 in DRG neurons.....	40
Figure 3.14. Dynlrb1 depletion negatively impacts FMRP trafficking	42
Figure 3.15. Dynlrb1 silencing induces intra-axonal accumulations of FMRP	44
Figure 3.16. Super-resolution imaging of intra-axonal FMRP granules	45
Figure 3.17. Dynlrb1 silencing negatively impacts mitochondrial trafficking	47
Figure 3.18. Genetic depletion of Dynlrb1 promotes FMRP granule formation	48
Figure 3.19. Dynlrb1 silencing induces stress granules formation	49

Figure 3.20. Genetic depletion of Dynlrb1 impairs FMRP degradation	50
Figure 3.21. FMRP accumulations in Dynlrb1 depleted neurons sequester Map1b mRNA	51
Figure 3.22. Dynlrb1 silencing impairs Map1b translation	52

Chapter 1.

Introduction

1.1. Axonal transport

Neurons are highly polarized cells with an arborized dendritic network and an axon that can extend up to one meter in length in humans. Axons mostly rely on the biosynthetic and degradative capacity of the cell body to maintain themselves, thus bidirectional active transport of organelles, proteins, RNAs and other molecular complexes is pivotal for proper neuronal survival and functioning [1], [2]. The axonal transport machinery relies on microtubule-associated motor proteins (**Figure 1.1.**). Indeed, while actin and neurofilaments are key axonal cytoskeletal components, long-range axonal trafficking is mostly dependent on microtubules (MT) (**Figure 1.1.**). MT are polarized polymers of tubulin with the plus end pointing distally in axons, whereas the polarity is mixed in dendrites [1]. Kinesin and dynein superfamilies are motor proteins that utilize ATP to move along MT and transport various cargos towards the MT plus and minus ends respectively. The kinesin superfamily comprises 45 genes, 38 of which are expressed in the nervous system [1]. In contrast to the diversity of kinesins, the dynein superfamily comprises two major types, axonemal and cytoplasmic [3]. Cytoplasmic dynein 1 (hereafter referred to as dynein) is the main motor driving retrograde axonal transport [4] and is discussed in detail in the following sections.

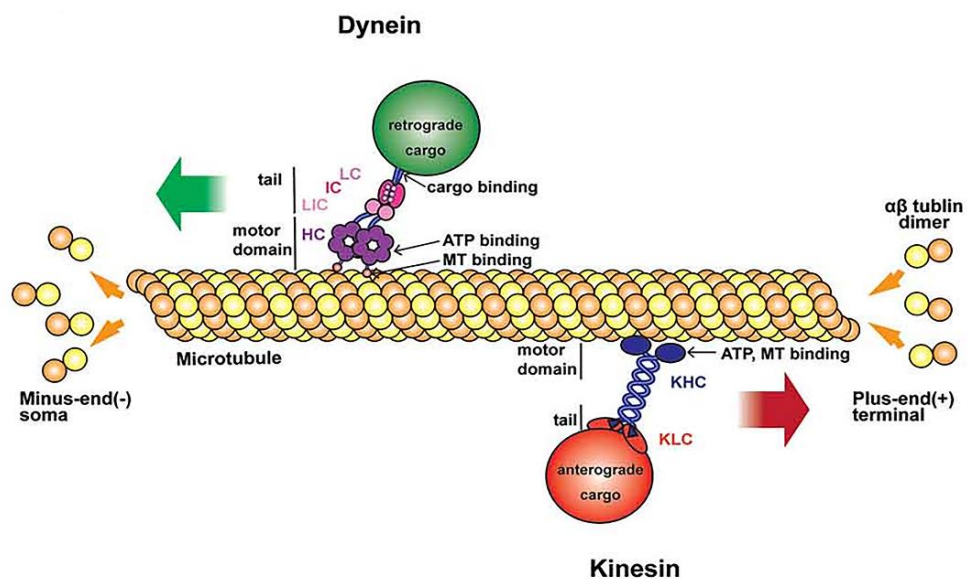


Figure 1.1. Schematic representation of the axonal transport machinery. Schematic modified from [2].

While utilizing the same motors, axonal transport is usually classified into either fast or slow categories. Fast axonal transport is characterized by a speed of 50-200 mm/day and delivers a variety of membranous organelles and vesicles. On the other hand, the slow component conveys cytoskeletal and cytosolic proteins with a speed range of 0.2-10 mm/day

[4]. Delivering cargo across a one-meter-long axon would then require a week or up to one year via fast and slow transport respectively. Accordingly, bidirectional active transport represents a bigger challenge in neurons and it is not surprising that trafficking deficits are evident in a multitude of neurological disorders [4]. Whether these deficits are the primary cause of the pathology or a secondary consequence of a dysfunctional nervous system is still a largely unresolved question [4]. Transport deficits were reported to precede Amyotrophic lateral sclerosis (ALS) symptoms in a mouse model expressing human mutant superoxide dismutase 1 (SOD1^{G93A}) [5]. Similarly, Charcot-Marie-Tooth disease type 2D (CMT2D) mice exhibited endosomal transport deficits early on in the pathology, which could be rescued through constitutive expression of brain-derived neurotrophic factor (BDNF) in the muscles [6]. Mutations of the components of the axonal transport machinery have been linked to a wide variety of neurological disorders [4]. Dynein mutations are discussed in section 1.6.

1.2. Dynein subunit composition

Dynein is a large (~1.5 MDa) complex formed by six subunits, all of which are incorporated into the complex as dimers (**Figure 1.2.**) [7].

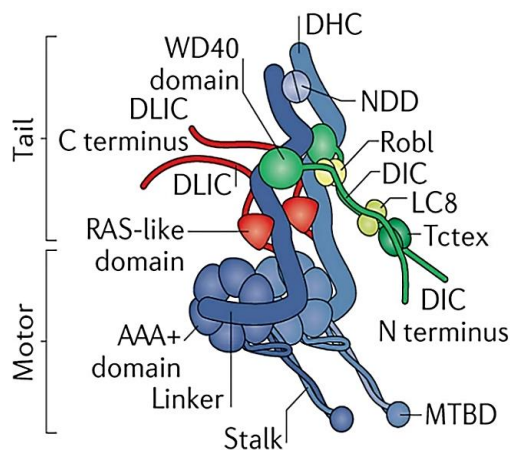


Figure 1.2. Schematic representation of the dynein complex composition [7]. Reproduced with permission from Springer Nature.

1.2.1. Dynein heavy chain

It is the largest subunit and represents the core of the complex. Unlike all other subunits, the heavy chain comprises only a single isoform (Dync1h1), which is formed by a C-terminus motor domain and an amino-terminal tail domain. The motor domain is responsible for the ATP hydrolysis and force generation and is composed of a hexameric AAA⁺ domain, a linker, and a stalk (**Figure 1.2.**) [8]. The six AAA⁺ subdomains are arranged in a ring shape with the stalk protruding from the AAA₄ domain. The stalk allows the docking of the heavy chain onto MT through a MT binding domain (MTBD) at its tip. The linker's C-terminus, an indispensable mechanical element, is connected to the AAA₁ domain and its N-terminus

extends to the tail region [7], [8]. The conformational changes within the AAA+ ring, together with the bending and straightening of the linker, allow dynein to move cargos along the MT tracks. On the other hand, the tail domain allows for the dimerization of the heavy chains as well as the association of intermediate and light intermediate chains, which consequently mediate the binding of a variety of cargos either directly or through adaptor proteins [7], [8].

1.2.2. Dynein intermediate chains

The intermediate chain, around 74 kDa in mass, acts as a scaffold for the binding of the three light chain families (**Figure 1.2.**) [9]. The C-terminus binds to the heavy chain while the N-terminus binds the light chains dimers [7]. Genetically, the intermediate chain is encoded by only two genes (*Dync1i1*, *Dync1i2*) however, the N-terminus harbors two sites of alternative splicing, which allow for the formation of numerous isoforms. Heterodimerization of these different isoforms gives rise to various dynein complex subtypes. Interestingly, this variety of complexes could partially explain how a single dynein motor is responsible for transporting a plethora of cargo in contrast to the 45 kinesin genes identified in mammals [9].

1.2.3. Dynein light intermediate chains

The light intermediate chain is also associated with the heavy chain (**Figure 1.2.**). There are three different isoforms expressed in vertebrates however, only *Dync1li1* and *Dync1li2* are incorporated in cytoplasmic dynein 1 [10]. The two isoforms form homodimers only, thus associating with the heavy chain in a mutually exclusive manner and determining two different dynein populations [10]. The C-terminus has been identified as a binding site for activating adaptors and it can also accommodate direct interaction with cargos [7].

1.2.4. Dynein light chains

There are 3 families of light chains that associate with the dynein complex: Tctex-type (*Dynlt*), LC8 (*Dynll*), and roadblock (*Dynlr*) (**Figure 1.2.**). Due to their ability to bind to a plethora of proteins and signaling molecules, *Dynlt* and *Dynll* are presumed to function in tethering cargo to the complex. Structural studies however, showed that their motif-binding site mediates their association with the intermediate chain thus preventing the simultaneous recruitment of cargos to the complex [7]. Further structural studies are required to determine if proteins can bind to *Dynlt* and/or *Dynll* chains that are incorporated into the dynein complex [7]. *Dynlr* is the least studied of light chains. The highly conserved *Dynlr* sequence among different organisms could arise from functional constraints on the protein [10]. The role of *Dynlr1* in neuronal retrograde transport is discussed in section 1.5.

1.3. Dynein activation

The dynein complex as described previously lacks major processive motility (ability to undertake consecutive steps without dissociating from MT) [11]. For dynein to perform its functions and transport a myriad of cargos, it needs to form a tripartite complex with dynactin, another 1.1 MDa complex, and an activating adaptor [11], [12]. Interestingly, dynein is present in the cytoplasm in an auto-inhibited form through self-dimerization of the motor domains, forming a structure resembling the Greek letter phi (Φ). This self-dimerized form is characterized by poor MT binding capacity. Dynein can shift to a more open form that can bind MT but with limited processivity. In the presence of an activating adaptor, dynactin recruitment promotes dynein processivity by re-orienting the motor domain of the open-dynein into a stable parallel conformation that can properly re-bind MT during stepping [11] (**Figure 1.3.**). Activating adaptors are bifunctional, they promote dynein processivity by facilitating dynein-dynactin association through providing a long residue that connects the two complexes. In addition, they recruit specific cargo to the machinery for transport [7], [12]. Several activating adaptors were described in the literature, the most studied one being bicaudal 2 (BICD2) [7]. BICD2, the homo sapiens homolog of *Drosophila* BicD, is one of four members of the bicaudal family which were all described to promote dynein processivity. They connect dynein and dynactin through their N-terminus whereas the C-terminus mediates cargo association [7].

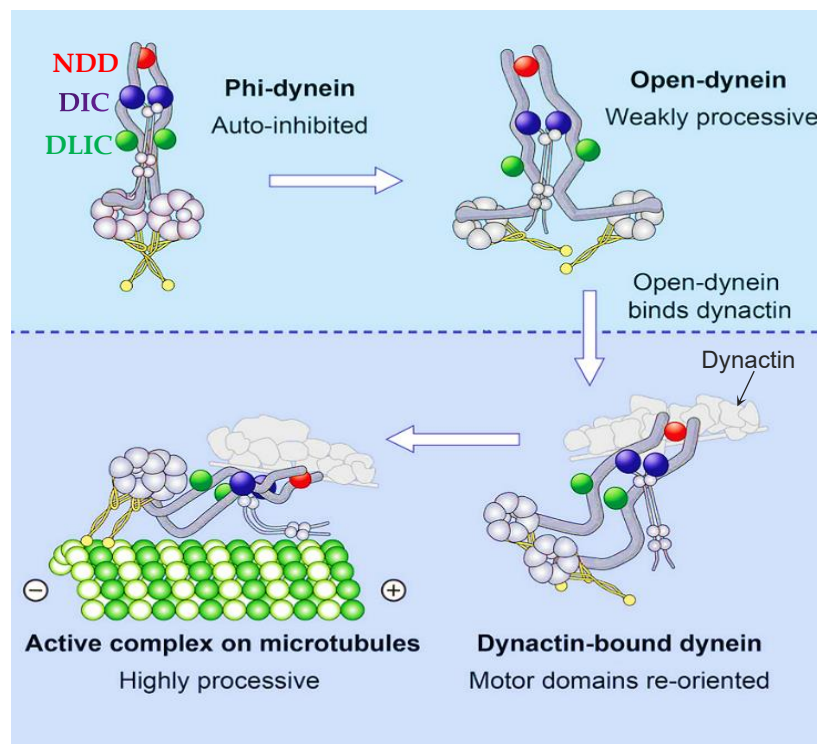


Figure 1.3. Schematic representation of dynactin's role in relieving dynein auto-inhibition. Schematic modified from [11]. NDD; N-terminal dimerization domain.

1.4. Dynein cargos

Dynein-mediated trafficking is linked to different processes including endosomal maturation, degradation as well and trophic signaling. The selective binding of adaptor proteins to specific cargos ensures the specificity of these processes. Listed below, a few of dynein cargos that are relevant to the work done in this thesis.

1.4.1. Endolysosomes and autophagosomes

Cells shuffle a variety of organelles connected to the degradative pathway [7]. This transport is particularly challenging in neurons due to the distance to be covered. Indeed, accumulation of protein aggregates is a hallmark of several neurodegenerative diseases and is attributed to genetic or environmental conditions that promote protein misfolding and aggregation or due to an impairment of the protein quality control system [13]–[15]. The dynein machinery is required for trafficking throughout the endolysosomal system and dynein mutations were shown to impair the clearance of several aggregation-prone proteins [16], [17]. The recruitment of dynein to endolysosomes could be mediated by Rab7 and the scaffolding protein RILP (Rab7 interacting lysosomal protein) [18]. In addition, knockout of JIP-3 (JNK-interacting protein 3), a scaffolding protein with the possible role of enhancing retrograde lysosomal trafficking through dynein recruitment, resulted in the accumulation of lysosomes in axonal swellings and further augmented amyloid beta pathology, two of the defining features of Alzheimer's disease [19].

Autophagy has also been associated with axonal transport. Autophagosomes are constitutively generated at axonal tips through the formation of cup-shaped double membraned structure (phagophore). After engulfment of portions of the cytoplasm together with ubiquitinated or aggregated proteins and damaged organelles, the membrane fuses forming the autophagosome [20]. While some degradation can occur locally through degradative lysosomes being continuously delivered to axonal tips [21], autophagosomes are mostly transported back to the soma where lysosomes are enriched [20]. Multiple dynein adaptors were reported to associate with autophagic vesicles [22]. Autophagosomes generated at axonal tips undergo inefficient back-forth transport driven by kinesin and dynein motors, which is then converted to unidirectional processive dynein-mediated mobilization through the recruitment of JIP-1 [22]. Autophagic vesicles are acidified while transported along the axon until they eventually fuse with a mature lysosome in the soma [22].

1.4.2. Messenger ribonucleoprotein granules

Eukaryotic cells impose a tight spatiotemporal regulation over complex biochemical interactions and processes through compartmentalization into microenvironments. These microenvironments are achieved either through membrane-delimited subcellular compartments or membraneless biomolecular condensates [23]. Cytoplasmic messenger ribonucleoprotein (mRNP) granules (mRNA and RNA-binding proteins (RBPs) assemblies) including transport granules, stress granules, and processing bodies represent a class of condensates formed through the process of liquid-liquid phase separation (LLPS) [23].

Dynein intermediate chain was reported to co-precipitate with staufen and La RBPs and is presumed to mediate their transport and accordingly mRNA localization [24], [25]. Dynein heavy chain mutation, or injection of antibodies targeting dynein heavy chain or dynactin subunits, resulted in mRNA localization deficits in *Drosophila* [26]. Additionally, BicD, a dynein activating adaptor, was shown to interact and promote the bidirectional trafficking of fragile X messenger ribonucleoprotein 1 (FMRP) in fly neurons [27]. Over the last few years, there has been growing evidence that RNA granules hitchhike onto membranous organelles for long-range axonal transport (**Figure 1.4.**) [28]–[30]. RNA granules were reported to associate with late endosomes, a retrogradely trafficking organelle, to sustain local axonal translation [28]. In addition, G3BP stress granule assembly factor (G3bp1) granules were shown to hitchhike onto lysosomal-associated membrane protein 1 (Lamp1)-positive vesicles, utilizing annexin A11 (Anxa11) as a tethering adaptor [29].

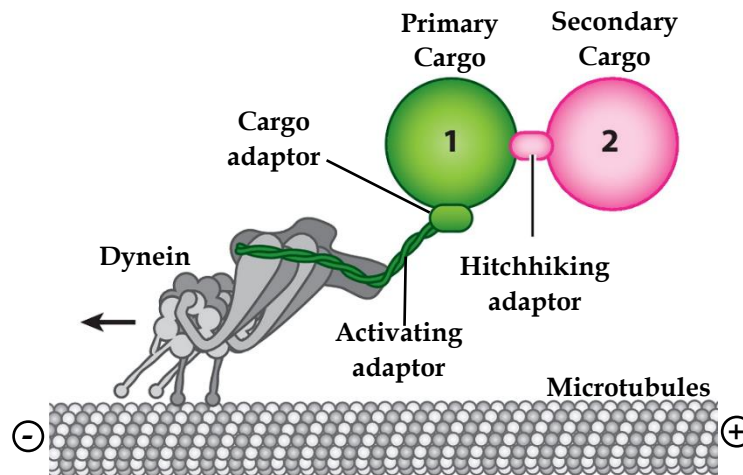


Figure 1.4. Schematic representation of hitchhiking as a mode of cargo transport. Schematic modified from [30]. Republished with permission of Annual Reviews, Inc.

RBPs regulate the fate of their bound mRNAs at different life stages [31]. The significance of the post-transcriptional regulation of gene expression by RBPs is highlighted by the number of diseases associated with mutations or aberrant expression of RBPs [31], [32]. Sections 1.7 - 1.9 discuss the involvement of one notable RBP, FMRP, in neurological disorders as well as its role in post-transcriptional regulatory processes, in particular mRNA localization and translational regulation.

1.4.3. Mitochondria

Mitochondria, the main organelle responsible for energy production, are actively transported bidirectionally in axons to meet the local energy needs [33]. Only a subset of the mitochondrial population is motile, with the majority seems to be anchored in position [1], [34]. TRAK (trafficking kinesin proteins) were reported to mediate dynein-dependent mitochondrial transport [35]. The dynamic retrograde shuttling of a pool of mitochondria acts to clear dysfunctional organelles by degradation in the soma where lysosomes are enriched or supports mitochondrial recovery by facilitating fusion with healthy mitochondria [35]. The significance of mitochondria transport is highlighted by the neurodegenerative disorders associated with its defects [4].

1.4.4. Signaling endosomes

Neurotrophic factors are a family of homodimeric ligands including nerve growth factor, BDNF, neurotrophin-3, and neurotrophin-4. They are secreted by the target tissue to support the connection with the innervating neurons. They bind two types of receptors: tropomyosin-related kinase receptor and p75 neurotrophin receptor [36]. Ligand-bound neurotrophin receptors are endocytosed, sorted into signaling endosomes, and retrogradely trafficked through the Rab5 and Rab7 endosomal pathway [37]. The long-range trafficking of these factors induces transcriptional changes that promote neuronal survival [36]. Indeed, loss of trophic signaling was linked to multiple neurodegenerative diseases including ALS and CMT2D [6], [36].

1.4.5. Protein cargos (aggresomes)

To maintain a state of proteostasis, chaperons and the ubiquitin-proteasome system (UPS) constitute a surveillance mechanism that refolds misfolded and aggregation-prone proteins or if this cannot be attained, directs them for proteolysis [7], [38]. Additionally, cells can sequester the aggregated protein into “holding stations” (mini-aggresome, ~200 nm) that are transported by the dynein machinery to the MT organizing center, where multiple mini-aggresomes pack together forming a larger particle (~1-3 μm) that activates autophagic clearance and lysosomal degradation [7], [38]. Three factors were reported to mediate the recognition of misfolded proteins by the dynein machinery: histone deacetylase 6 (HDAC6), sequestosome 1 (SQSTM1), and the co-chaperone Bcl-2-associated athanogene 3 (BAG3) [39]–[41]. HDAC6 and SQSTM1 link polyubiquitinated proteins to dynein. On the other hand, BAG3 doesn't require a ubiquitination tag to target misfolded or aggregated proteins to the aggresome. Instead, it utilizes heat shock protein 70 specificity towards misfolded proteins and target those substrate to the dynein motor and thereby the aggresome [39]–[41].

1.5. Dynlrb1 role in neuronal homeostasis

Roadblock was first identified in a genetic screen of *Drosophila* mutants, where the Dynlrb mutant exhibited intra-axonal accumulation of cargos and severe axonal degeneration [42]. Unlike the *Drosophila* counterpart, mammalian Dynlrb has 2 isoforms: Dynlrb1 and 2, which share a high degree of homology and can homo or heterodimerize [10], [43]. Until recently, mammalian Dynlrb1 was regarded as an accessory subunit recruited for specific cargos. The identified cargos include Rab6, Smad2 (SMAD family member 2), and NAGK (N-acetyl-D-glucosamine kinase) [44]–[47]. While Dynlrb1 was shown to co-immunoprecipitate with Rab6, the biological significance of this interaction remains elusive [46]. On the other hand, Dynlrb1-smad2 interaction was shown to mediate TGF β signaling [47]. The only neuronal specific interactor already identified for Dynlrb1 is NAGK. Dynlrb1-NAGK was shown to localize to MT tracks and was proposed to support the delivery of Golgi outposts to dendritic branching points and axonal growth cones of developing hippocampal neurons to promote their outgrowth [44], [45]. Interestingly, recent work from our group similarly identified Dynlrb1 as a regulator of axonal outgrowth in cultured sensory neurons from adult mice [43]. Importantly, this work has also shown that Dynlrb1 contributes to the maintenance of proprioceptive neurons, both during development and adulthood. Complete loss of Dynlrb1 expression resulted in embryonic lethality, while viral-mediated genetic reduction of Dynlrb1 in adult animals caused a loss of proprioceptive neurons [43]. The negative effect on neuronal survival was proposed to be an aftermath of impaired endosomal retrograde trafficking. In that context, time-lapse imaging revealed a significant reduction in the fraction of motile acidified carriers as well as the traveling speed of individual organelles. Comparably, a marked increase in the number of stationary signaling endosomes was evident. These findings suggest that Dynlrb1 is an indispensable subunit for dynein-mediated survival signaling in neurons [43].

1.6. Dynein mutations in neurological disorders

Cytoplasmic dynein mutations in *Drosophila* are lethal, suggesting its essential role in eukaryotes [48]. This finding was further confirmed in mammals using a dynein heavy chain mouse knockout model (*Dync1h1^{tm1Noh}*). Embryos implanted from homozygous knockout blastocysts died at an embryonic age of 8.5 days [49]. Cultured cells from homozygous null blastocysts showed a fragmented Golgi apparatus, and abnormal cytoplasmic distribution of endosomes and lysosomes [3], [49]. Two dynein mutant mouse strains, Legs at odd angles (Loa) and Cramping 1 (Cra1), were identified in a screen for genes involved in motor neuron disease [3]. The naming arises from a hind limb clenching phenotype that is observed when the animals are suspended from the tail for more than 30 seconds. Loa and Cra1 models represent a single point mutation within the tail domain of the heavy chain [3]. Homozygous mice die within 24 h from birth due to the inability to move or feed, resulting from a significant loss of α -motor neurons within the anterior horn of the spinal cord [50]. Interestingly, further work failed to detect motor neuron degeneration [51]. Instead, a severe sensory deficit that emerges early in life and does not worsen with age was observed, suggesting developmental loss of proprioceptive neurons [51]. Loa mutation was shown to alter dynein processivity through the impairment of the communication between the two motor domains within the dimer [52]. The authors described an altered “gating” model. Gating promotes processivity by ensuring that one motor domain dissociates from the MT,

while the other remains strongly attached to the tracks to avoid premature dissociation [52]. The aforementioned mutant models have been extremely useful for probing the involvement of dynein mutations in several neurological diseases. More than 30 missense mutations have been identified in patients diagnosed with spinal muscular atrophy with lower extremity predominance (SMA-LED) and CMT, two closely related motor neuropathies characterized by muscle weakness, wasting, and loss of motor functions [53]–[55]. CMT patients are also afflicted by sensory deficits [55]. Moreover, dynein mutations have been implicated in malformations of cortical development (MCD), a neurodevelopmental disorder characterized by severe intellectual disability and intractable epilepsy mostly due to cortical migratory defects [53].

Dynactin mutations have been reported in Perry syndrome, a progressive neurodegenerative disease characterized by TDP43 (TAR DNA binding protein) inclusions mainly in the extrapyramidal system [56], [57]. Multiple mutations within or adjacent to the cytoskeleton-associated protein and glycine-rich (CAP-Gly) domain of the p150^{Glued} subunit have been reported. The CAP-Gly domain mediates dynactin's ability to bind MT and its enrichment within axonal tips and accordingly promotes the engagement of dynein and retrograde trafficking [57]. p150^{Glued} CAP-Gly domain mutation was also previously reported to cause distal hereditary motor neuropathy [57]. A knock-in mouse model of the mutant human dynactin displayed neuronal degeneration and impairment of axonal transport, as evident by the formation of axonal swellings [58].

1.7. FMRP involvement in neurological diseases

FMRP is a ubiquitously expressed RBP involved in both neurodevelopmental and neurodegenerative disorders: fragile X syndrome (FXS) and fragile X-associated tremors/ataxia syndrome (FXTAS) respectively [59], [60]. While the two diseases are induced by mutation of the same gene, their clinical features are completely distinct. FXS is the most common cause of inherited intellectual disability and strongly associates with autism spectrum disorder (ASD) [59]. FXS is caused by epigenetic silencing of the *Fmr1* gene due to triplet nucleotide repeat expansion in its 5' UTR (>200 repeat), resulting in a complete loss of FMRP expression [59]. On the other hand, FXTAS is a late-onset progressive neurodegenerative disease associated with tremors, cerebellar ataxia, and cognitive deficits [60]. FXTAS is a result of CGG repeat expansion that's within the premutation range (55-200 repeat) and in contrast to FXS, the levels of the protein are normal or slightly reduced [60]. The toxicity is mostly caused by the elevated levels of the mutated *Fmr1* mRNA which was shown to sequester several proteins essential for neuronal homeostasis. FMRpolyglycine protein was also described to augment the mRNA toxicity [60], [61].

1.8. FMRP structure meets the function

FMRP's most studied roles involve translation regulation and mRNA localization [59], [62]. These functions are dependent on FMRP dynamic assembly and disassembly into RNP particles through LLPS and the trafficking of these granules by molecular motors [27], [59]. Substantial evidence has shown that LLPS is driven by multivalent interactions formed by intrinsically disordered regions (IDRs) and RNA-binding residues within RBPs sequences [23]. IDRs are regions that have low amino acid sequence complexity and thus lack a stable structure and can exhibit a variety of conformations. This conformational flexibility supports the formation of a multitude of multivalent weak interactions that allow molecules to locally concentrate and once this network reaches a certain threshold/saturation limit, it separates into a distinct phase forming membraneless organelles/foci/condensates/droplets/granules [23]. The number of domains that support interactions is a critical determinant of the concentration threshold required to undergo LLPS, with proteins with higher valency undergoing phase separation at lower concentrations [23], [63].

FMRP domain structure includes agenet-like domains that mediate protein interactions, nuclear localization and export signal (NLS, NES) domains that could mediate rapid shuttling in and out of the nucleus, three canonical RNA-binding domains: two hnRNP K-homology (KH) domains and an RGG box domain that recognize kissing complex RNA motifs and G-quadruplex structures *in vitro* respectively (**Figure 1.5.**) [59], [64]. A third potential KH domain, KH0, has also been recently identified, however its RNA-binding capability is not confirmed yet [59]. The C-terminus of FMRP represents a low complexity region (LCR) (**Figure 1.5.**). Work from Forman-Kay lab has shown that the C-terminus region is sufficient to promote LLPS separation of FMRP together with RNA *in vitro* [65]. Importantly, post-translational modifications were shown to act as a molecular switch to tune FMRP LLPS and its ability to form mRNP granules. In particular, synaptic activity induced dephosphorylation of FMRP via protein phosphatase 2A (PP2A) was shown to promote the granules disassembly [65]. This is in agreement with previous literature showing

phosphorylated FMRP to preferentially associate with stalled ribosomes [66]. FMRP dephosphorylation was also shown to control its protein levels by promoting its ubiquitination and subsequent proteasomal degradation [67].

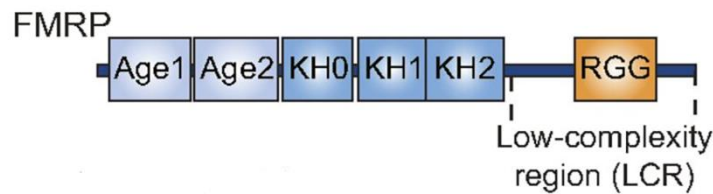


Figure 1.5. Schematic diagram of FMRP domain structure. Schematic modified from [65].

1.9. FMRP regulates translation and mRNA transport

1.9.1. Models of translation regulation

Three decades have passed since FMRP was first shown to bind RNA [68]. This finding raised a critical question regarding the biological significance of this association. One of the earliest indications that FMRP acts as a translational repressor was the observation that hippocampal slices from *Fmr1* knockout mice incorporated more ³⁵S methionine than those from wild type littermates [69]. Seminal cross-linking and immunoprecipitation (CLIP)-sequencing work from Darnell and colleagues showed that FMRP binds >800 mRNA in juvenile mouse brain. These transcripts were largely involved in synaptic transmission, with FMRP mostly binding within the coding sequence (CDS) rather than their 5' or 3' UTR [70]. Importantly, this work reported a translational dysregulation in *Fmr1* knockout mice [70]. Translational changes in *Fmr1*-deficient cells were also reported from various groups [71]–[74]. The findings that FMRP binds to the CDS of its target transcripts [70] and co-sediments with polyribosomes [75] suggested that FMRP could repress translation by stalling or stopping translation at the elongation stage. How FMRP pauses translation on specific transcripts remains debatable. One explanation is that FMRP could block the association of tRNA and elongation factors on the ribosome [76]. An alternative model suggests that FMRP regulates translation by binding to optimal codons [77]. mRNAs whose corresponding tRNAs are abundant have optimal codons, while those whose cognate tRNAs are relatively scarce have non-optimal codons. Codon optimality has been reported to regulate mRNA translation and stability [78]. FMRP was shown to regulate the stability of its N6-methyladenosine (m6A) marked transcripts, presumably by impeding YTH (YT521-B homology) domain-containing protein family (YTHDF)-mediated degradation [79]. m6A modification is one of the most prevalent epigenetic modifications of mRNAs, the biological consequence of this modification depends on a group of m6A reader proteins that collectively work to fine tune the fate of RNA at different life stages [79]. This study raises the possibility that RNA modifications could play a role in how FMRP could recognize its target transcripts. Besides stalling elongation, FMRP was also reported to regulate translation at the levels of translation initiation and the miRNA pathway [80]–[82].

1.9.2. Regulation of mRNA in mRNP granules

FMRP was shown to associate with RNA granules that differ in their composition and function [62]. I discuss below FMRP association with neuronal transport granules, fragile X granules, stress granules, and processing bodies.

1.9.2.1. Neuronal transport granules

Neurons support spatiotemporal control over protein synthesis through the localization of mRNAs, incorporated in neuronal transport granules, across different subcellular compartments [83]. Neurons sort their mRNA for axonal localization through elements or motifs that are mostly, not exclusively, present in the UTR of the mRNA [84]. These motifs are recognized by RBPs [84], [85]. Interestingly, recent motility reconstitution assay from Simon Bullock's group showed that the presence of RNA fully activates dynein-dependent transport of Egalitarian RNP [86] suggesting that mRNAs could facilitate their minus-end directed transport by activating dynein. Comparably, the inclusion of RNA augmented kinesin-dependent axonal transport of adenomatous polyposis coli (APC) complex [87]. Transport granules are typically composed of transcripts in a translationally repressed state, RBPs, ribosomal subunits, and translation factors indicating their potential capacity to regulate translation as well [84], [85], [88]. These granules undergo bidirectional long-range transport by associating either directly or indirectly with molecular motors [30], [84].

FMRP plays a crucial role in neuronal morphogenesis, cytoskeleton stabilization, and synaptic transmission, through mediating the localization and translation of its target mRNAs [59]. FMRP association with neuronal granules was reported within both the dendritic and axonal compartments [89]–[91]. Several studies reported FMRP association with various members of the kinesin family [92], however FMRP association to dynein is less well characterized. To the best of my knowledge, a single study has thus far identified BicD as a regulator of FMRP trafficking and levels in a *Drosophila* model [27]. Time-lapse imaging of FMRP fused to a fluorescent reporter revealed activity dependent transport of FMRP granules [90], [93]. Synaptic activity was also shown to promote FMRP dephosphorylation, de-condensation of FMRP granules, and the release of mRNAs for translation [65]. This is in agreement with literature suggesting that FMRP transport granules emerge from polysome-interacting particles [88] and that phosphorylated FMRP associates with stalled polyribosomes [66]. Several studies have utilized the MS2 tagging system to visualize FMRP-dependent transport and localization of individual transcripts [93]–[95]. Interestingly, a recent study revealed that the RGG box mediates the localization of FMRP targets that exhibit G-quadruplexes within UTRs to distal sites, whereas interactions with one or both KH domains were essential for translational repression [85].

1.9.2.2. Fragile X granules

FMRP was also shown to be recruited together with two of its homologs to distinct membraneless granules termed fragile X granules (FXGs) [62]. Fragile X related 1 and 2 proteins (FXR1P, FXR2P) are two RBPs that share ~ 60% amino acid sequence homology with FMRP and localize to FXGs [62]. FXGs were detected in specific neuronal circuits and their protein composition varies accordingly, with FXR2P being a constitutive component in all FXGs [96]. Interestingly, these granules localize predominantly to the axonal compartment in CNS neurons [97], and were shown to mediate local axonal translation of a specific subset of FMRP targets [97]. While transport granules are expected to associate with ribosomes before initiation of the trafficking, a dynamic ribosomal and mRNA incorporation at axonal sites is evident for FXGs [97]. However, the nature of the signaling cascade that promotes this dynamic assembly has not been investigated. FXG could offer additional spatial control over the expression of specific transcripts at the presynaptic compartment.

1.9.2.3. Stress granules

In contrast to neuronal granules that are formed under normal physiological conditions, stress granule formation, as the name implies, is induced by cellular stress [63]. Stress granule assembly is concurrent with a translational shutdown through sequestration of stalled transcripts at the translation initiation phase [63] and is driven by additive, multivalent interactions of various RBPs and translation factors with the non-translating transcripts [63]. Stress granules may act as potential sites for mRNA triage, where transcripts are sorted and routed for re-initiation of translation, degradation, or storage into stable non-polysomal RNPs [63]. The proteomic composition of these granules varies according to the cell type and the stress-inducing context [98]. A central node for nucleation of stress granules is G3bp. A recently introduced 'network' model to describe G3bp role in stress granules formation classifies molecules as node, bridge, cap, or bystander based on the number of interaction sites (≥ 3 , 2, 1, or zero respectively). G3bp possesses 3 features that drive biomolecular condensation: an NTF2-like domain that promotes homotypic oligomerization and heterotypic interactions, RNA binding domains: RGG and RNA recognition motif, and LCRs [63].

FMRP is indeed a robust component of these stress granules as evident by their reduced assembly upon the loss of FMRP [99]. Interestingly, FMRP phosphorylation was shown to promote its co-phase separation with Caprin1 and RNA [100]. Caprin1 is a well-known promoter of G3bp driven stress granule formation [63]. Accordingly, phospho-regulated FMRP-Caprin1 co-condensation could be a paradigm through which FMRP localizes to and promotes the formation of stress granules. Additionally, it can provide a passage for the recruitment of specific transcripts to stress granules.

1.9.2.4. Processing bodies

Processing bodies (p-bodies) are mRNP granules composed of transcripts complexed with translational repressors and mRNA decay machinery [101]. They are proposed to act as a

storage site for translationally repressed mRNAs and inactive mRNA decay enzymes that undergo LLPS as a result of the interaction network formed when mRNA decay factors accumulate on mRNAs free from polysomes [101]. In contrast to transport and stress granules, most translation factors and ribosomal subunits are excluded from these granules [101]. FMRP localizes to p-bodies and was shown to recruit amyloid precursor protein (APP) mRNA to p-bodies and repress its translation [102]. APP is involved in neuritogenesis, and synaptic transmission and is linked to Alzheimer's disease pathogenesis [102].

Ultimately, FMRP is a multifunctional RBP that regulates RNA fate at different life stages [59]. FMRP's cytoplasmic roles include regulating mRNA localization and translation. The structural domains of FMRP allow for its phase separation and subsequent association with a variety of membraneless organelles including FXG, transport granules, stress granules, and p-bodies. Despite the myriad of studies focusing on FMRP targets, the sequences or the structural features recognized by FMRP are not fully characterized or understood. Target specificity could be attained through G-quadruplex structures, a repetitive feature of FMRP's targets [103]–[106]. The absence of this feature from the CLIP binding targets could be, at least in part, explained by the recent literature suggesting distinct localization and translation targets, with the RGG box interactions mediating target localization whereas translation repression is mediated by KH domains [85]. In addition, FMRP's ability to bind to the CDS of its targets was reported by various studies [70], [107]–[110], with further analysis identifying WGGA (W=A or U) and ACUK (K=G or U) as enriched motifs [107], [108], [111], however they are not a requisite [59]. The identification of FMRP binding motifs could be further compounded by cell-specific targets as well as protein interactions. FMRP was shown to bind specific transcripts in different cell types [74], [109]. Furthermore, FMRP likely forms cell-specific protein interactions. FMRP protein interactions regulate its target selectivity and function (ex: Cytoplasmic FMRP-interacting protein 1 (CYFIP1)) [112]. A full characterization of FMRP interacting proteome in different neuronal cell types has not been described yet. Nevertheless, FMRP target mRNAs appear to be involved mainly in synaptic transmission as well as cytoskeleton structure and morphogenesis [59]. Besides the aforementioned functions, FMRP has also been shown to regulate transcription and splicing events [59]. While these functions could be a downstream effect of FMRP-dependent translation regulation, FMRP structural domains include a NLS and NES that could mediate rapid shuttling in and out of the nucleus [59].

1.10. Proximity-dependent biotinylation

Screening for protein-protein interaction (PPI) in living cells has been commonly performed using affinity purification (AP) coupled with mass spectrometry (MS). This approach is effective in identifying binding partners, but it also has several limitations [113]. For instance, numerous PPI could be disrupted by the buffer/detergent required to solubilize the proteins from the cellular compartments. In addition, detection of lower affinity and less frequent interactions is restricted [114]. Proximity-dependent labeling overcomes the said limitations. This methodology relies on the use of an exogenous biotin ligase enzyme, which is genetically fused with the protein of interest and expressed in a relevant biological setting. The consequent addition of the enzyme substrate, biotin, initiates covalent labeling of proteins within ~10 nm radius of the enzyme [113]. The biotinylated proteins can then be captured using streptavidin-coated magnetic beads and identified by MS [113] (**Figure 1.6**). Since the interacting partners are biotinylated, which is a covalent modification, harsh lysis, and washing conditions can be implemented to reduce the background and improve the purity of isolated proteins without losing weak interactions. Furthermore, this technique allows for the detection of less frequent PPI interactions that are not standardly captured by AP-MS, by labeling all proteins coming in close proximity to the target [114]. Two main classes of enzymes have been taken advantage of: biotin ligases (ex: BioID, miniTurbo, TurboID) and peroxidase (ex: APEX). Biotin peroxidases require the addition of hydrogen peroxide to activate the labeling, which is toxic to the cell, thus limiting its utilization for *in vivo* experiments [113].

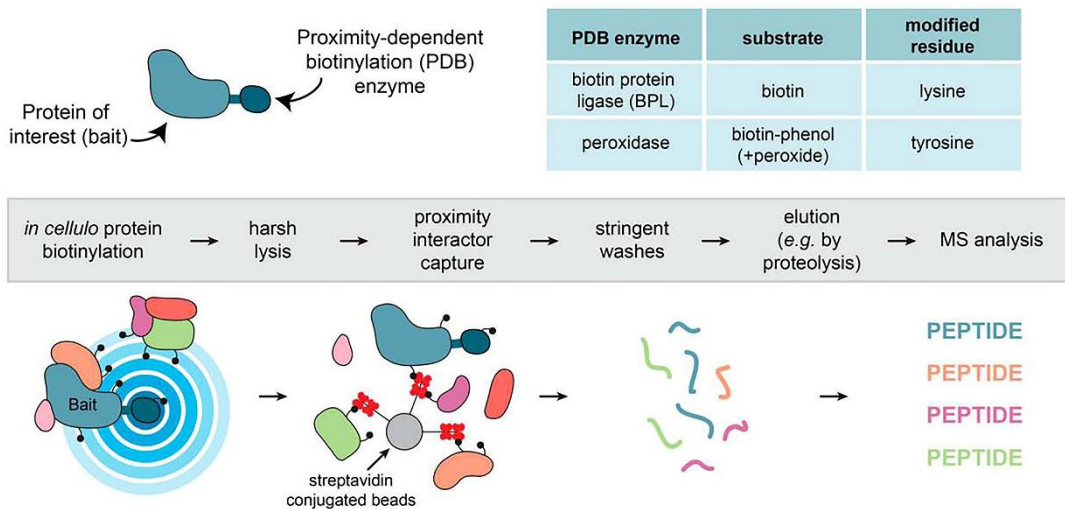


Figure 1.6. Schematic of proximity-dependent proteomics workflow. Schematic modified from [113].

1.11. Aim and structure of the thesis

Neuronal homeostasis requires an efficient long-range transport system to shuttle a variety of cargos to and from distal compartments. Indeed, mutations of the dynein transport machinery have been reported in a wide range of neurological diseases. Previous work from our group identified a novel role for Dynlrb1, a small subunit of the dynein motor, in sensory neuron survival however, the underlying mechanisms were not fully investigated.

Thus, the overall aim of this work is to **investigate the physiological role of Dynlrb1 in adult sensory neuron homeostasis, at the molecular level**. The work in **Chapter 3** of this thesis highlights two objectives that fulfill this aim:

- a. Identification of Dynlrb1 proximal interactome in cultured sensory neurons.**
Using a proximity-based labeling approach coupled with mass spectrometry, I identified 90 Dynlrb1 interactors in DRG neurons. The list was refined to highlight candidates involved in neuronal homeostasis; a notable interactor was FMRP.

FMRP was selected for further investigations due to its involvement in neurodevelopmental and neurodegenerative disorders resulting from perturbations of RNP granule assembly and mRNA translation, and the relative lack of data regarding its interaction with dynein in mammalian systems.

- b. Investigation of the functional significance of Dynlrb1-FMRP association.**
Utilizing RNA interference (RNAi) tools coupled with live imaging, immunocytochemistry, and biochemical assays, I investigated the perturbation of FMRP's axonal transport, protein levels, and function as a translational repressor upon Dynlrb1 depletion.

In **Chapter 4**, I will discuss the interpretation of the results presented in Chapter 3 and their significance in the context of the research question and the existing literature.

In **Chapter 5**, I propose a model through which Dynlrb1 contributes to neuronal homeostasis through its functional interaction with FMRP and an outlook for future studies that stem from this work.

Chapter 2.

Materials and Methods

This chapter is a slightly modified version of the materials and methods section of “FMRP long-range transport and degradation are mediated by Dynlrb1 in sensory neurons [115]”, published under Creative Commons Attribution 4.0 international license (CC-BY 4.0).

2.1. Animal experiments

All experiments involving animal subjects were carried out in accordance with the guidelines and regulations of Okinawa Institute of Science and Technology Graduate University (OIST) and approved by OIST animal care and use committee (Protocol No. 2020-304). Adult (8-10 weeks) male ICR mice were purchased from Jackson Laboratory, Japan. Animals were housed at $24.0 \pm 0.5^{\circ}\text{C}$ with alternating 12 h day/night cycles and allowed access to food and water ad libitum.

2.2. Reagents, chemicals, and antibodies

Culture media, sera, and chemicals were purchased from GibcoBRL, Invitrogen, and Sigma-Aldrich respectively, unless specified otherwise. Drugs used in this study include puromycin (Sigma-Aldrich, #P8833), anisomycin (Nacalai Tesque, #03046-14), leupeptin (Sigma-Aldrich, #L2884), pepstatin A (Sigma-Aldrich, #P5318), E-64d (Sigma-Aldrich, #E8640), and MG132 (Sigma-Aldrich, #M8699). Primary antibodies used in this study are anti-Tyr- α -tubulin (Synaptic systems GmbH, #302117), anti- β III-tubulin (Synaptic Systems GmbH, #302304), anti-FMRP (Invitrogen, #PA534584 & OT11C6 clone, #TA504290), anti-dynein intermediate chain (Chemicon International, clone IC74.1, #MAB1618), anti-flag (Sigma-Aldrich, Clone M2, #F3165), anti-Vps29 (Abcam, # ab236796), anti-Vtal (Invitrogen, #PA521831), anti-dynein heavy chain (Proteintech, # 12345-1-AP), anti-rabbit IgG isotype control (Cell Signaling, #2729), anti-puromycin (Merck, #MABE343), anti-Map1b (Invitrogen, #PA582798), anti- β -actin (Sigma-Aldrich, #A5441), anti-GFP (Roche, #11814460001), anti-G3bp1 (Sigma-Aldrich, #G6046), anti-Lamp1 ((D2D11) XP®, Cell Signaling Technology, #9091S), and anti-Anxa11 (Proteintech, # 68089-1-IG).

Secondary antibodies used for immunostaining are anti-mouse Alexa Fluor 488 (Invitrogen, #A11001), anti-guinea pig Alexa Fluor 568 (Invitrogen, #A11075), anti-rat Alexa Fluor (Invitrogen, #A-11077), anti-rabbit Alexa Fluor 568 (Invitrogen, #A11011), anti-guinea pig Alexa Fluor 647 (Invitrogen, #A21450), anti-rabbit Alexa Fluor 647 (Invitrogen, # A21245), and streptavidin Alexa Fluor 647 conjugate (Invitrogen, #S21374). Secondary HRP-conjugated mouse and rabbit antibodies for immunoblots were horse anti-mouse (Cell Signaling, #7076), goat anti-mouse (Invitrogen, #G-21040), goat anti-rabbit (Abcam Limited, #ab6721) and streptavidin HRP (Cell Signaling Technology, #3999S).

2.3. DRG culture

Coverslips/dishes were coated with 0.01% poly-L-lysine (Sigma-Aldrich #P4832) overnight at 4°C, rinsed with water, dried and coated with laminin (GibcoBRL #23017-015) for 1 h at 37°C. DRG neuronal cultures were prepared as previously described [116]. Briefly, DRG from all segmental levels were collected in HBSS (GibcoBRL, #14175095), supplemented with 5 mM HEPES (Sigma-Aldrich, #H0887), and 0.1 mg/ml primocin (Invivogen, #ant-pm-1). Extracted DRG were enzymatically dissociated with 100 U of papain (Worthington Biochemical Corporation, #PAP) in HBSS for 30 min at 37°C followed by another 30 min of incubation in collagenase (1 mg/ml) and dispase (1.2 mg/ml) in HBSS at 37°C (Worthington Biochemical Corporation, #CLS2, Roche Diagnostics GmbH, #04942078001). The ganglia were triturated in HBSS with 5 mM HEPES and 0.1 mg/ml primocin. Neurons were separated using a 20% percoll (Sigma-Aldrich, #P4937) in L15 medium (GibcoBRL #L-5520), supplemented with 5 mM HEPES, 10% fetal bovine serum (FBS) (Invitrogen, #10270106), and 0.1 mg/ml primocin. Percoll gradient centrifugation was performed at 1000 rpm for 8 min. Neurons were plated in F-12 medium (Invitrogen, #11765054) supplemented with 10% FBS, and 0.1 mg/ml primocin. After 2 days *in vitro* (DIV), the medium was supplemented with 5 μM of arabinofuranosylcytosine (Jena Bioscience GmbH, #N-20307-1) to inhibit glial proliferation. Neurons were fixed for immunostaining or lysed for protein or RNA extractions at DIV 6-8 as described in the following sections unless specified otherwise.

2.4. HEK cells and AAV production

HEK293T cells (ATCC®) were maintained in DMEM (Nacalai Tesque, #08458-45) supplemented with 10% FBS. AAV particles, (PHP.S serotype [117]), were produced as previously described [118] with minor modifications. Briefly, HEK cells were seeded to 70% confluency 24 h before transfection. A DNA mixture (gene of interest, ΔF6 helper, and PHP.S capsid plasmids) was introduced into the cells through a calcium phosphate transfection protocol. Four days later, cells were detached and suspended in artificial cerebrospinal fluid (124 mM NaCl, 3 mM KCl, 26 mM NaHCO₃, 2 mM CaCl₂·2H₂O, 1 mM MgSO₄·7H₂O, 1.25 mM KH₂PO₄, 10 mM D-Glucose). AAV particles were retrieved through four freeze-thaw cycles, treated with Benzonase® nuclease (Merck, #70664-3) at 45°C for 15 min, and further purified from the crude lysate through multiple rounds of centrifugation at 14,000 rpm for 10 min at 4°C. Purified AAV particles were used to infect primary neuronal cultures 3 h after plating.

2.5. NIH/3T3 cell line culture and transfection

The mouse fibroblast cell line was acquired from Riken BRC cell bank (RCB2767) and cultured in a humidified incubator at 37°C in low glucose DMEM (Fujifilm Wako, #041-29775) containing 10% FBS. Transient transfection was performed with lipofectamine 3000 (Invitrogen, #L3000015) according to the manufacturer's instructions. Forty-eight hours after transfection, 3T3 cells were either fixed for 25 min in 4% paraformaldehyde (PFA) (Electron Microscopy Sciences, #15710) in PBS at room temperature (RT) for

immunostaining or processed for protein extraction. Cells were lysed in 150 mM NaCl, 50 mM Tris (PH 7.4), 1% NP-40, 1 mM EDTA supplemented with cOmplete™ protease inhibitor cocktail (Roche Diagnostics GmbH, #4693132001) for 30 min on ice. Lysates were clarified by centrifugation at 12,500 rpm for 15 min at 4°C. The supernatant was collected and used for downstream experiments.

2.6. Plasmid DNA

All Recombinant DNA experiments were carried out in accordance with the guidelines and regulations of OIST genetic manipulation procedures and approved by the biosafety committee (Protocol number RDE-2020-013-4). *Dynlrb1* gene was subcloned using an mRNA library isolated from the mouse brain using the RNeasy Mini kit (QIAGEN). The mRNA was then retrotranscribed in cDNA (Superscript™ III, Thermo Fisher) and *Dynlrb1* was amplified by PCR and inserted into a pcDNA3.1 vector via digestion with the restriction enzymes BamHI and XhoI. The primers used to amplify and clone *Dynlrb1* in the pcDNA3.1 vector were the following:

Forward: CGGGATCCATGGCAGAGGTGGAGGAAAC

Reverse: CGCTCGAGTTCAGTTCAGTTGGATTCTGGATCAC

N- and C-terminal constructs with the *Dynlrb1* sequence fused to flag tag and the miniTurbo enzyme [119] in pcDNA3.1 were cloned by restriction-free cloning. A minimal linker (G4S1) between *Dynlrb1* and miniTurbo was used. The primers used to amplify and clone *Dynlrb1* in the miniTurbo vector are the following:

1) *Dynlrb1* cloned at the C-terminus of miniTurbo:

Forward:

CGATGACGACAAGCTTGCGGCCGCGATGGCAGAGGTGGAGGAAACACT

Reverse:

CGGGATGCTGGATCCGCCTCCGCCTTCAGTTGGATTCTGGATCACAATCAGGA

2) *Dynlrb1* cloned at the N-terminus of miniTurbo:

Forward: GCCCAAAGGGCGGAGGCGGATCCATGGCAGAGGTGGAGGAAACAC

Reverse:

ATGCCACCCGGGATGATATCCCTCTAGAGTCGAGTTATTCAGTTGGATTCTGGAT
CACAATCAGG

The N-terminal fusion protein sequence was then subcloned using restriction digestion (SgsI and EcoRV) in an AAV vector backbone under the human synapsin I promoter (hSynI).

For shRNA-mediated knockdown experiments, “AAV-shRNA-ctrl” vector, a gift from Hongjun Song (Addgene (plasmid #85741, [120]), was used as a non-targeting control. To generate the sh*Dynlrb1* vector, the shControl sequence was deleted using BamHI and XbaI restriction enzymes, and a sequence targeting *mus musculus* *Dynlrb1* was inserted and ligated to the digested vector. The primers used to insert sh*Dynlrb1* were as follows,

Forward:

GATCCGATTATGGTGGCACCAGATAAGAAGCTTGTTATCTGGTGCCACCATAATC
TTTTTTT

Reverse:

CTAGAAAAAAGATTATGGTGGCACCAGATAACAAGCTTCTTATCTGGTGCCAC
CATAATCG

shRNA constructs also express EYFP. All plasmids were verified by DNA sequencing (SeqStudio™, Applied Biosystems) and were delivered to neurons using AAV particles. “p-EGFP-C1-Flag-mFmr1(wt)” plasmid was a gift from Stephanie Ceman (Addgene plasmid #87929, [121]), and was transfected using jetPEI (Polyplus, #101-10N) to express EGFP-FMRP for axonal transport experiments.

2.7. Axoplasm pulldown

Axoplasm from mouse sciatic nerve was extracted as previously described [122]. Briefly, sciatic nerves from 2 mice were dissected and mechanically squeezed out in isotonic buffer (20 mM HEPES, 110 mM KAc, 5 mM MgAc, 0.5 mM EGTA, pH 7.4). The axoplasm was then centrifuged at 4°C for 15 min at 12,000 rpm to remove sciatic nerve fragments and the supernatant was incubated overnight at 4°C with 5 µg of anti-FMRP antibody or rabbit IgG isotype control conjugated to 50 µl protein-G coupled magnetic beads (Dynabeads™, Thermo Fisher, #10003D) according to the manufacturer’s instructions. The beads were washed twice in isotonic buffer (20 mM HEPES, 110 mM KAc, 5 mM MgAc, 0.5 mM EGTA, pH 7.4) at 4°C for 20 min and twice in PBS with 0.02% Tween-20 at 4°C for 20 min. Proteins were eluted from the bead by boiling in 2X Laemmli sample buffer and loaded on 4-12% Bis-Tris plus gel (Invitrogen, #NW04122BOX) and subsequently transferred to a nitrocellulose membrane (Invitrogen, #LC2000) for western blot analysis. The membrane was blocked with 5% bovine serum albumin (BSA) (Nacalai Tesque, #01860-65) for 30 min at RT and incubated with anti-FMRP or anti-dynein intermediate chain antibodies. After 3 washes with TBS-Tween-20 (0.05%), goat anti-mouse or goat anti-rabbit HRP conjugated antibodies were applied for 1 h at RT. The signal was developed using ECL prime (Cytiva, #RPN2232) and images were acquired using iBright FL 1500 imaging system (Invitrogen). The intensity of the FMRP bands was quantified using ImageJ software.

2.8. Co-immunoprecipitation

3T3 cells were lysed using an ionic detergent-free lysis buffer (150 mM NaCl, 50 mM Tris (PH 7.4), 1% NP-40, 1 mM EDTA) supplemented with a protease inhibitor cocktail. Anti-flag antibody was conjugated to protein-G coupled magnetic beads through a 45 min incubation at 4°C. Consecutively, the beads were washed with PBS-Tween-20 (0.02%) to remove any unbound antibody, and incubated with the lysates overnight at 4°C. The beads were washed with PBS-Tween-20 and the immobilized immune complexes were eluted by boiling the beads in 2X Laemmli buffer at 95°C for 5 min. The elute was loaded onto 4-15% Tris-glycine gels (Bio-Rad, #4561084) and proteins were subsequently transferred onto a PVDF membrane (Bio-Rad, #1704272). The membrane was blocked with 5% BSA for 30 min at RT and incubated with anti-dynein intermediate chain or anti-flag antibodies. After

TBS-Tween-20 (0.1%) washes, horse anti-mouse HRP conjugated antibody was applied for 1 h. The signal was developed using ECL prime and images were acquired using the ChemiDoc MP imaging system (Bio-Rad).

2.9. Expression of miniTurbo constructs, biotinylation, and streptavidin pulldown

Cultured DRG neurons were transduced with AAVs driving the expression of miniTurbo (MnT-control) or miniTurbo fused to Dynlrb1 (MnT-Dynlrb1). Six days later, transduced, and non-transduced neurons were incubated with 200 μ M of biotin (Sigma-Aldrich, #B4501) and incubated at 37°C for 2 h to initiate labelling. Cells were washed thoroughly with PBS before lysis to remove any excess biotin. Neurons were lysed in a buffer composed of 150 mM NaCl, 50 mM Tris (PH 7.4), 1% NP-40, 0.5% SDS, and supplemented with a protease inhibitor cocktail. Purification of Dynlrb1 interactors was performed using streptavidin-conjugated beads (Thermo Fisher, #88117). 500 μ L of beads were washed three times in a buffer composed of 150 mM NaCl, 50 mM Tris (PH 7.4), and 0.1% Tween-20. The beads were resuspended in the same buffer containing a protease inhibitor cocktail and then lysates were added and incubated overnight. Subsequently, the supernatant was removed, and the beads were washed three times with lysis buffer, twice with 2 M urea in PBS with 0.1% NP-40, followed by a final wash in 50 mM Tris (PH 7.4). All washes and binding steps were performed at 4°C on a rotator mixer. To effectively elute the biotinylated proteins, the beads were heated at 65°C in a reducing elution buffer (2% SDS, 150 mM NaCl, 150 mM Tris (PH 8.0), 10 mM DTT) for 30 min.

2.10. Mass spectrometry sample preparation and data analysis

Gel-aided sample preparation was used to generate proteomics samples [123]. Briefly, after eluting biotinylated proteins in the presence of 10 mM DTT (Wako, #047-08973), samples were cooled down and immediately incubated with 55 mM iodoacetamide (Wako, #095-02151). Proteins were then co-polymerized with acrylamide through incubating with acrylamide-bis solution (Supelco, #01709) at a final concentration of 20%, in the presence of Tetramethylethylenediamine and ammonium persulfate (Sigma-Aldrich, #T9281 and #GE17-1311-01). The formed microgel was shredded by pulse centrifugation through a plastic grid to increase the surface area for the removal of detergents and chaotropic agents. Proteins were digested with trypsin/lys-C cocktail (Promega, #V5073) at 37°C overnight. Peptides were extracted using trifluoroacetic acid (TFA) and acetonitrile (Wako, #206-10731 and #018-19853), and consecutively desalted using C18 stage tips [124]. For liquid chromatography tandem mass spectrometry (LC-MS/MS), the tryptic peptides were measured with data-dependent acquisition using a Q Exactive Plus Hybrid Quadrupole-Orbitrap Mass Spectrometer and an EASY nLC 1200 Liquid Chromatography System, together with a Nanospray Flex Ion Source (Thermo Fisher, USA).

MaxQuant (version 1.6.3.3) was used for identification and label-free quantification. Protein identities were assigned by searching against a UniProt *mus musculus* database.

Database search parameters included cysteine carbamidomethylation as a fixed modification, methionine oxidation, and protein N-terminal acetylation as variable modifications. MaxQuant output data were further processed using GraphPad Prism and Microsoft Excel softwares. Protein intensities were normalized by the average of the total abundance of all proteins in the corresponding sample. Mean intensities were generated by averaging the intensities of the individual runs (3 biological replicates, 2 technical repeats/biological replicate) per experimental sample. P-values for mean intensities of MnT-Dynlrb1 and MnT-control samples were calculated using multiple student t-tests. Abundance ratios were generated for Dynlrb1 fused miniTurbo compared to MnT-control and \log_2 transformed. Proteins with abundance ratios ≥ 2 and p-values ≤ 0.05 were considered potential Dynlrb1 interactors. Functional enrichment analysis was performed using the software suite [g:Profile](#) [51].

2.11. Cytotoxicity assay

Cell viability was evaluated using cytopainter cell viability assay kit (Abcam, #ab176744) as per the manufacturer's instructions. Briefly, DRG neurons were transduced with AAV harboring shControl or shDynlrb1. Six days after transduction, the neurons were incubated with the dye for 45 min at 37°C and 5% CO₂. Cells were washed to remove excess dye, incubated in Tyrode's solution, and transferred to a stage-top incubation chamber (P-set2000, Pecon, #133-800 261) on an LSM 900 confocal microscope and live imaged with a 20X objective (Plan apochromat NA=0.8). The number of dead and live cells was counted to estimate the degree of cytotoxicity imparted by Dynlrb1 depletion.

2.12. Immunofluorescence

Cells were fixed in 4% PFA for 25 min. Coverslips were washed with PBS and cells were permeabilized and blocked in 0.3% triton X-100, and 5% normal goat serum (NGS) (Invitrogen, #10000C) in PBS for 30 min. The following primary antibodies were incubated overnight at 4°C: anti-flag, anti-Tyr- α -tubulin, anti- β III-tubulin, and anti-G3bp1. After washing, fluorescent secondary bodies were applied for 1 h at RT: anti-mouse Alexa Fluor 488, anti-guinea pig Alexa Fluor 568, streptavidin Alexa Fluor 647 conjugate, anti-rat Alexa Fluor 568, anti-mouse Alexa Fluor 647, and anti-rabbit Alexa Fluor 647. For visualization of somal and axonal FMRP granules, cells were fixed in 4% PFA overnight or for 25 min respectively. Permeabilization was performed using 1% saponin in PBS for somatic granules and 0.1% saponin for axonal granules. Saponin solutions were freshly prepared and supplemented with 75 mM glycine as a quenching agent. Blocking was performed using 5% NGS for 30 min. 0.1% and 0.01% saponin were maintained during blocking, washes, and antibody incubation steps for somal and axonal granules respectively. The following antibodies were used: anti-FMRP and anti- β III-tubulin, anti-rabbit Alexa Fluor 568, and anti-guinea pig Alexa Fluor 647. Coverslips were mounted with Fluoromount GTM or ibidi mounting media and imaged using Zeiss LSM 780 or 900 confocal microscopes using a 63X oil-immersion objective (Plan apochromat NA=1.4). For visualization, maximum intensity projection images were adjusted for brightness and contrast levels using ImageJ or Zen softwares.

2.13. Airyscan image acquisition and analysis

Super-resolution images were acquired on LSM 900 with Airyscan 2.0 super-resolution module using a 63X oil-immersion objective (Plan apochromat NA=1.4). Initial image acquisition parameters were as follows: image size 1834x1834 pixels (78x78 μm), pixel resolution 0.043x0.043x0.150 $\mu\text{m}/\text{pixel}$, pixel dwell time 1.15 μs , laser power 1% (detector gain 900 V) and 0.4% (detector gain 850%) for laser line ex647 and ex568 respectively, and optimal z-section of 150 nm and around 20-30 stacks. Airyscan images were processed in Imaris 10 (Bitplane, Oxford instruments). FMRP granules were identified using Imaris spot tracking plugin with an initial spot size detection of 150 nm and automatic background subtraction, and the spot region growth was based on their absolute intensity. Axons were identified using the surface rendering plugin for the tubulin channel with smooth filter and a surface grain size of 0.085 μm . FMRP granule size, number, and clustering were calculated using Imaris measurement pro plugin. FMRP area was estimated from spot volume and clustering was estimated by measuring the average distance between 3 or 9 neighboring FMRP spots per image.

2.14. Proximity ligation assay

Proximity ligation assay (PLA) was performed using Duolink[®] reagents (Sigma-Aldrich) according to the manufacturer's protocol. Cells were fixed, permeabilized, and blocked as described in the immunofluorescence section. The antibodies used for the semi-endogenous PLA experiments were anti-flag, anti-FMRP, anti-Vps29, and anti-Vta1. For the endogenous PLA, anti-dynein heavy chain, anti-FMRP (OT11C6 clone), and anti-Lamp1 antibodies were used. The probes used were the anti-mouse minus and anti-rabbit plus probes (DUO92004 and DUO92002) and the signal was detected using the far-red detection kit (DUO92013). When indicated, cells were counterstained with anti- β III-tubulin for 1 h at RT. Coverslips were mounted with Duolink[®] mounting medium (DUO82040) and sealed with nail polish. Images were acquired using Zeiss LSM 900 confocal microscope using a 63X oil-immersion objective. PLA signal was quantified using ImageJ. The signal intensity was manually thresholded with the same value for controls and samples. The cell body size was manually outlined by the user, the axonal network was defined by the β III-tubulin or EYFP mask area. The number of puncta was calculated and divided by the cell body or the neuronal network area in maximum intensity projection images, after subtracting any areas of glia or cellular debris.

2.15. Puromycinylation and puro-PLA

Detection of newly synthesized Map1b was performed by incubating neuronal cultures with 5 μM puromycin (Sigma-Aldrich, #P8833) in F-12 for 10 min at 37°C in a 5% CO₂ incubator. Protein synthesis inhibition control groups were pre-incubated with 40 μM of anisomycin (Nacalai Tesque, #03046-14) in F-12 for 30 min before the addition of puromycin. The incubation was terminated by two quick washes in PBS and cells were fixed immediately using 4% PFA for 25 min. After permeabilization and blocking, PLA was performed as

described using anti-puromycin and anti-Map1b antibodies. Puro-PLA signal was quantified as previously described in the PLA section.

2.16. RNAscope multiplex fluorescent assay combined with immunofluorescence

The integrated co-detection workflow recommended by the manufacturer was followed with minor modifications. DRG neurons cultured on coverslips were fixed using fresh 4% PFA at RT for 30 min. After PBS washes, the samples were dehydrated through one min sequential incubations in 50%, 70%, and 100% ethanol and stored at -20°C in 100% ethanol until the assay was performed. The cells were rehydrated through one min sequential incubations in 70%, 50% ethanol, and water. Samples were then permeabilized using PBS-Tween (0.1%) for 10 min, treated with hydrogen peroxide for 10 min, washed with water, and incubated with the primary antibodies (anti-FMRP, and anti-GFP) overnight at 4°C. The anti-GFP antibody was used to enhance the AAV-EYFP signal impacted by the downstream protease treatment. Cells were then washed three times in PBS-Tween (0.1%), post-fixed using 4% PFA for 30 min, washed with PBS-Tween (0.1%), and treated with protease III (1:100 dilution, 10 min, RT). As reported by other groups [125], higher protease concentrations resulted in a significant loss of the primary antibodies signal. Different protease concentrations didn't have any influence on the mRNA signal obtained from primary cultures on coverslips [125]. After five washes in PBS, the multiplex v2 fluorescent *in situ* hybridization (ISH) assay was run as per the manufacturer's instructions. Briefly, the Map1b probe (Advanced Cell Diagnostics, #1045181-C3) or the negative (Advanced Cell Diagnostics, #320871) and positive control probes (Advanced Cell Diagnostics, #320881) were hybridized for 2 h at 40°C. Then Amp1, Amp2, and Amp3 hybridization cycles were performed, followed by developing the C3-HRP channel with TSA vivid™ fluorophore 650 (Tocris, #323273). After the final HRP blocking step, secondary antibodies: anti-mouse Alexa Fluor 488, and anti-rabbit Alexa Fluor 568 were incubated for 30 min at RT. Coverslips were then washed with PBS-Tween (0.1%), PBS, mounted with Fluoromount G™, and imaged using Zeiss LSM 900 confocal microscopes using a 63X oil-immersion objective. The fractional area of overlap between FMRP and Map1b signal was quantified using ImageJ. Axonal FMRP and Map1b signals were thresholded manually with a matched value for all experimental groups and the overlap area between the two channels was divided by the total FMRP area.

2.17. Pharmacological treatments

DRG neuronal cultures, transduced with either shControl or shDynlrb1, were treated on DIV8 with lysosomal inhibitors (200 μM leupeptin, 20 μM pepstatin A, 2 μM E-64d), a specific proteasomal inhibitor (MG132, 10 μM) or an equivalent volume of vehicles (DMSO and water) for 6 h. Neurons were washed with PBS and lysed to detect FMRP levels by western blotting.

2.18. Protein extraction and western blotting

Neurons were lysed in RIPA buffer (150 mM NaCl, 50 mM Tris (PH 8.0), 1% triton X-100, 0.1% SDS, 0.5% sodium deoxycholate) supplemented with protease inhibitor cocktail. Lysates were boiled with Laemmli buffer at 95°C for 5 min, loaded onto 4-12% Bis-Tris gels (Invitrogen, #NP0323BOX), and subsequently transferred to nitrocellulose or PVDF membranes (Invitrogen, #LC2000, #LC2002). The blotted membranes were blocked in 5% BSA for 40 min at RT and then incubated with primary antibodies overnight at 4°C. The following primary antibodies were used: anti-FMRP, anti- β -actin, anti-flag, anti-GFP, and anti-annexin A11. Afterward, membranes were washed 4 times with TBS-Tween-20 (0.1%), and secondary-HRP conjugated antibodies were applied for 1 h at RT: goat anti-mouse, goat anti-rabbit, and streptavidin HRP. After another set of 30 min TBS-Tween-20 washes, the chemiluminescence signal was developed using Cytiva ECL start detection reagents and detected using iBright FL 1500 imaging system (Invitrogen). The band's intensity was quantified by ImageJ software.

2.19. Gene expression analysis by quantitative reverse-transcription polymerase chain reaction

Total RNA was extracted and purified using NucleoSpin RNA plus kit (Macherey-Nagel, #740984.50). RNA concentration was assessed, and cDNA was synthesized according to the manufacturer's instructions (QIAGEN, #205311). PCR amplification was performed using PowerUp SYBR Green Master Mix (Thermo Fisher Scientific, #A25776) and target gene expression was measured using qTower³ real-time PCR system (Analytikjena). The following thermocycling parameters were used, an initial 20 sec denaturation step followed by 40 two-step cycles, a denaturation step at 95°C for 1 sec, and a combined annealing-extension step at 60°C for 30 sec. Relative gene expression presented as fold change was calculated using the $\Delta\Delta C_t$ method, where 18S ribosomal RNA was used as a reference gene to normalize the expression. The primers (*mus musculus*) used were as follows (Terenzio *et al*, 2020):

18S forward: AAACGGCTACCACATCCAAG

18S reverse: CCTCCAATGGATCCTCGTTA

Dynlrb1 forward: CAACCTCATGCACAACTTCATC

Dynlrb1 reverse: TCTGGATCACAATCAGGAAATAGTC

2.20. siRNA transfection

Four hours after plating, DRG neurons were transfected with an siRNA pool targeting Anxa11 (Sigma-Aldrich, #EMU006471), Dynlrb1 (Sigma-Aldrich, #EMU089881), or a universal non-targeting siControl (Sigma-Aldrich, #SIC001) using Dharmafect4 (Horizon discovery, #T-2004-03) according to the manufacturer's protocol.

2.21. Axonal transport experiments

To analyze the percentage of motile FMRP particles and lysotracker carriers as well as their respective speeds, DRG neurons (wild type, siControl, siDynlrb1) were transfected with EGFP-FMRP (Addgene plasmid #87929, [121]) using JetPEI (Polyplus, #101-10N) according to the manufacturer's instructions. On DIV3, 150 nM of lysotracker red DND-99 (Invitrogen, #L7528) was added to the cells for 30 min at 37°C and 5% CO₂. The medium was washed out to remove the excess dye and replaced with Tyrode's solution (Sigma-Aldrich, #T2397). Neurons were transferred to a stage-top incubation chamber (P-set2000, Pecon, #133-800 261) on an LSM 900 confocal microscope and imaged with a 63X oil immersion objective. Hundred and twenty frames (frame duration of 2.53 sec) were consecutively acquired for every time series. To analyze mitochondrial dynamics, DRG neurons transfected with siControl or siDynlrb1 were incubated with 100 nM of mitotracker deep red FM (Invitrogen, #M22426) for 20 min at 37°C and 5% CO₂. Cultures were washed, incubated in Tyrode's solution, and transferred to a stage-top incubation chamber on an LSM 900 confocal microscope and imaged with a 63X oil immersion objective. Hundred and ninety-five frames (frame time of 1.27 sec) were consecutively acquired for every time series. The percentage of stationary *vs* moving carriers was manually calculated on kymographs generated using Zen Blue software (Zeiss, version 3.2.). Statistical analysis was performed with two-way ANOVA using the software GraphPad Prism. Lysotracker and FMRP transport movies were tracked manually using the Manual Tracking plugin of the Fiji software. Mitotracker movies were tracked using a MATLAB script designed in-house [116] and archived [here](#).

2.22. Statistical analysis

All experiments were performed in at least three biological replicates. Analysis of multiple groups was performed using ANOVA. The choice between one or two-way ANOVA was based on the requirements for identification of specific factors' contribution to statistical differences between groups and was followed by Tukey's and Sidak's post hoc analysis tests respectively. For two groups analyses, unpaired Student's t-test was used. All statistical analyses were performed using GraphPad Prism (GraphPad Software, CA, USA). Data are presented as mean \pm SEM. Statistical significance tests and the number of samples used are described in the figure legends. Significance values are indicated as * $p < 0.05$, ** $p < 0.01$, *** $p < 0.001$; n.s. indicates not significant.

Chapter 3.

Results

This chapter is a modified version of the results section of “FMRP long-range transport and degradation are mediated by Dynlrb1 in sensory neurons [115]”, published under Creative Commons Attribution 4.0 international license (CC-BY 4.0).

3.1. Design and optimization of Dynlrb1-miniTurbo fusion constructs for proximity labeling

To identify Dynlrb1 interactome, we utilized a proximity-dependent biotinylation approach coupled with mass spectrometry. We fused the miniTurbo (MnT) enzyme and a flag tag to both the N- and C-terminus of Dynlrb1. A vector expressing only the miniTurbo enzyme was adopted as an internal control to allow for the exclusion of proteins that are randomly biotinylated in the cytoplasm, rather than being potential Dynlrb1 interactors. To reduce the number of animals in the study, we optimized the procedures for promiscuous protein biotinylation, purification, and identification in the 3T3 mouse cell line. To exclude the possibility that the fusion of the miniTurbo could affect the folding of Dynlrb1 or its integration into the dynein complex, flag immunofluorescence staining, and co-immunoprecipitation (Co-IP) assays were performed in 3T3 cells. Expression of the C-terminus fusion protein (Dynlrb1-MnT) in 3T3 cells resulted in its aggregation and reduced cell viability (**Figure 3.1A**). Additionally, while the flag IP efficiency was almost equivalent for both fusion proteins, dynein intermediate chain co-precipitated solely with the N-terminus protein (MnT-Dynlrb1) (**Figure 3.1B**). Thus, we decided to use only the N-terminal fusion construct moving forward. We then tested the efficiency of biotinylation and pulldown in 3T3 cells transfected with miniTurbo control (MnT-control) or MnT-Dynlrb1 constructs and treated with 200 μ M of biotin for 2 h. Following streptavidin-mediated pulldown, we could retrieve most biotinylated proteins (**Figure 3.1C**).

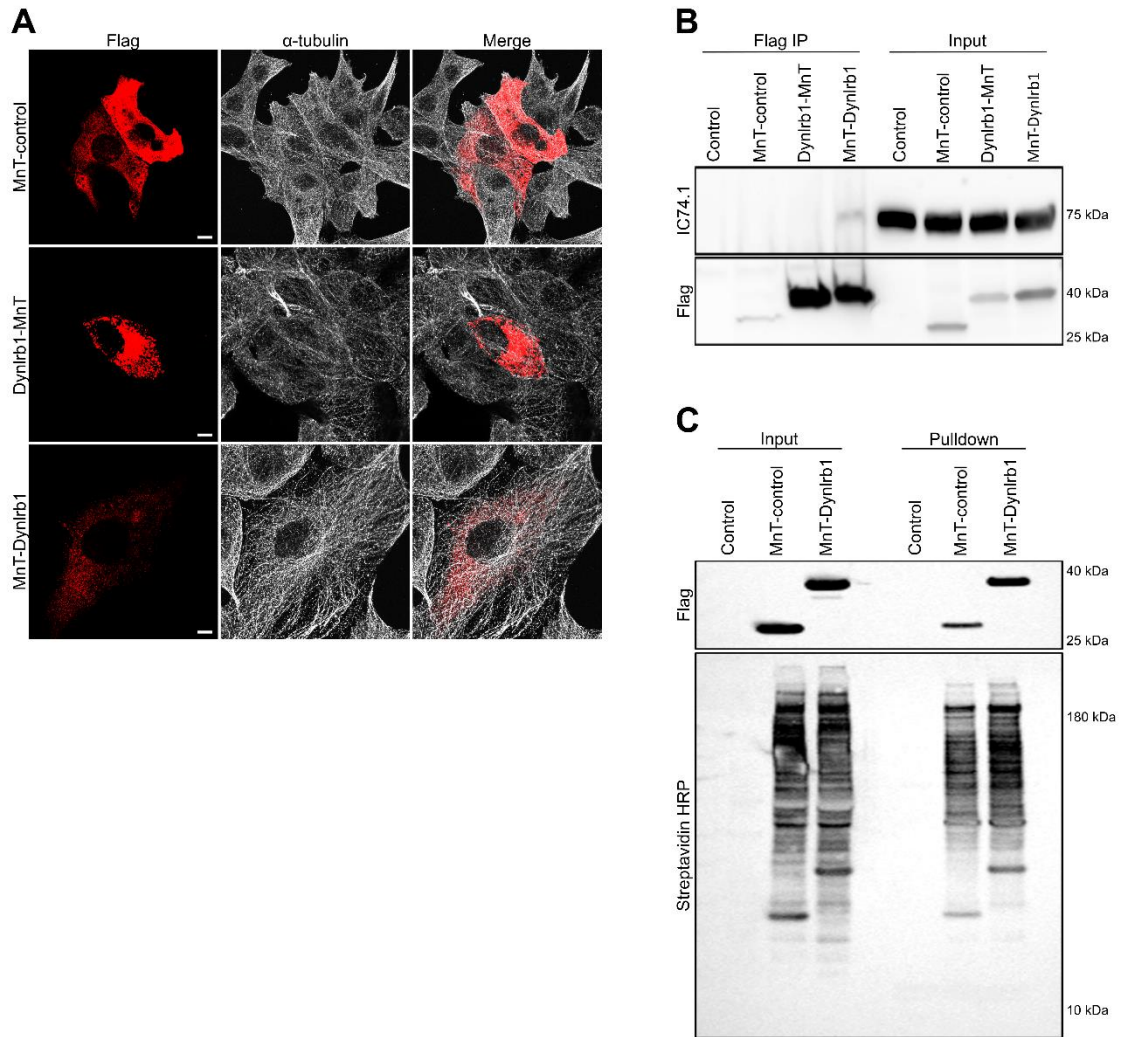


Figure 3.1. Optimization of miniTurbo fusion constructs in 3T3 cells. A) Representative images of 3T3 cells transfected with unconjugated miniTurbo (MnT-control) or miniTurbo fused to the C- (Dynlr1b1-MnT) or N-terminus (MnT-Dynlr1b1) domain of Dynlr1b1. The distribution of the flag-tagged proteins in the cytoplasm of transfected cells was revealed by flag staining (in red). Cells were labeled via anti-tubulin staining (in gray). Dynlr1b1-MnT protein clearly showed aggregation and toxicity. Scale bars 10 μ m, 5 μ m and 5 μ m respectively. B) Immunoprecipitation of flag-tagged proteins from 3T3 cells transfected with MnT-control, Dynlr1b1-MnT or MnT-Dynlr1b1. Dynein intermediate chain (IC74.1) was used to reveal incorporation in the dynein complex via western blot analysis. Non-transfected cells were used as a negative control. Only the N-terminal fusion protein (MnT-Dynlr1b1) was able to pulldown dynein intermediate chain. C) Western blot analysis of the streptavidin pulldown of biotinylated proteins in 3T3 cells transfected with MnT-control or MnT-Dynlr1b1. The expression is revealed using anti-flag antibody, while the extent of biotinylation is detected using streptavidin HRP.

We then transferred the MnT-control and the MnT-Dynlrb1 sequences to adeno-associated virus (AAV) vector backbone (**Figure 3.2A**) to transduce cultured dorsal root ganglia (DRG) neurons. Western blot analysis confirmed efficient expression of the flag-tagged proteins 6 days after infection (**Figure 3.2B**). The activity of the enzyme in transduced cultures was confirmed by revealing the extent of biotinylation via western blot analysis with streptavidin HRP (**Figure 3.2B**). We further validated the constructs' expression and ability to biotinylate proteins via immunofluorescence staining of transduced sensory neurons (**Figure 3.2C**).

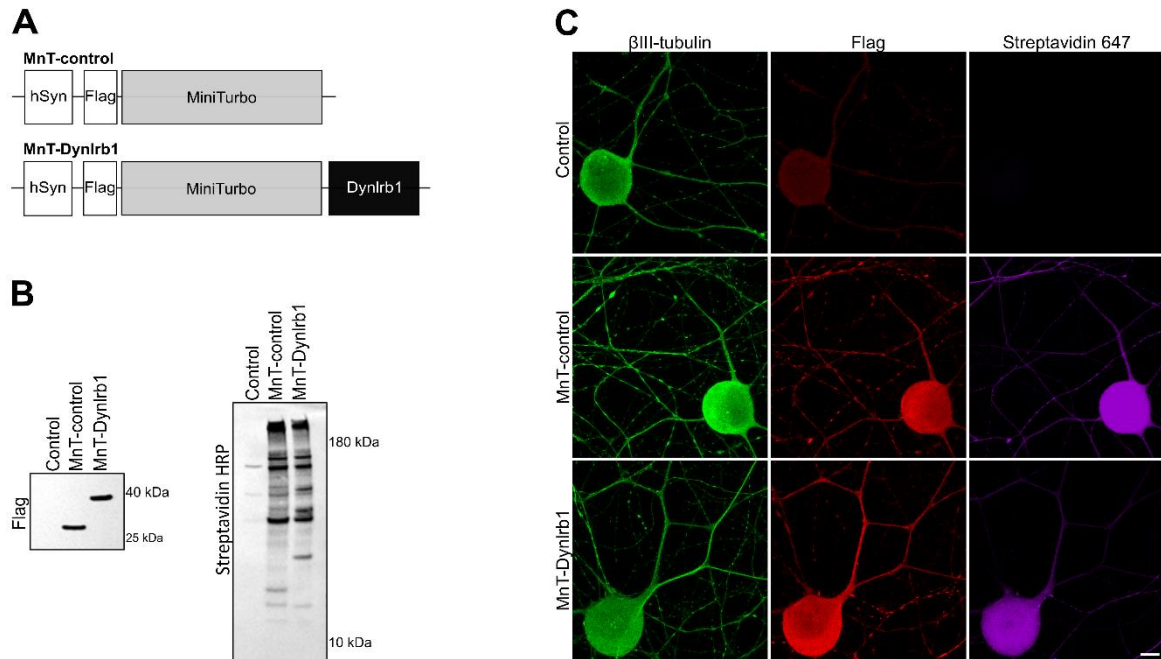


Figure 3.2. Optimization of proximity labeling in cultured DRG neurons. A) Schematic representation of the miniTurbo constructs used to infect DRG neurons. B) Western blot analysis of the expression and biotinylation pattern of MnT-control and MnT-Dynlrb1 detected using anti-flag and streptavidin HRP respectively. A non-transduced sample is included as a negative control. C) DRG neurons were transduced with MnT-control or MnT-Dynlrb1 and subjected to biotinylation. Non-transduced cells were also added as a control. Neurons are labeled with βIII-tubulin (green). The expression is revealed using an anti-flag antibody (red), while the extent of biotinylation is detected using streptavidin Alexa 647 (magenta). Scale bar 10 μm.

Furthermore, we took advantage of *in situ* proximity ligation assay (PLA), a technique that allows direct visualization of protein-protein close association (40 nm range, [126]) with high specificity and sensitivity [127], to validate the interaction between MnT-Dynlrb1 and the dynein complex in neuronal cultures. Indeed, robust association between MnT-Dynlrb1 and dynein heavy chain (Dync1h1) was detected in both neuronal cell bodies and axons (**Figure 3.3**). Thus, we confirmed MnT-Dynlrb1 incorporation in the dynein complex in DRG neurons.

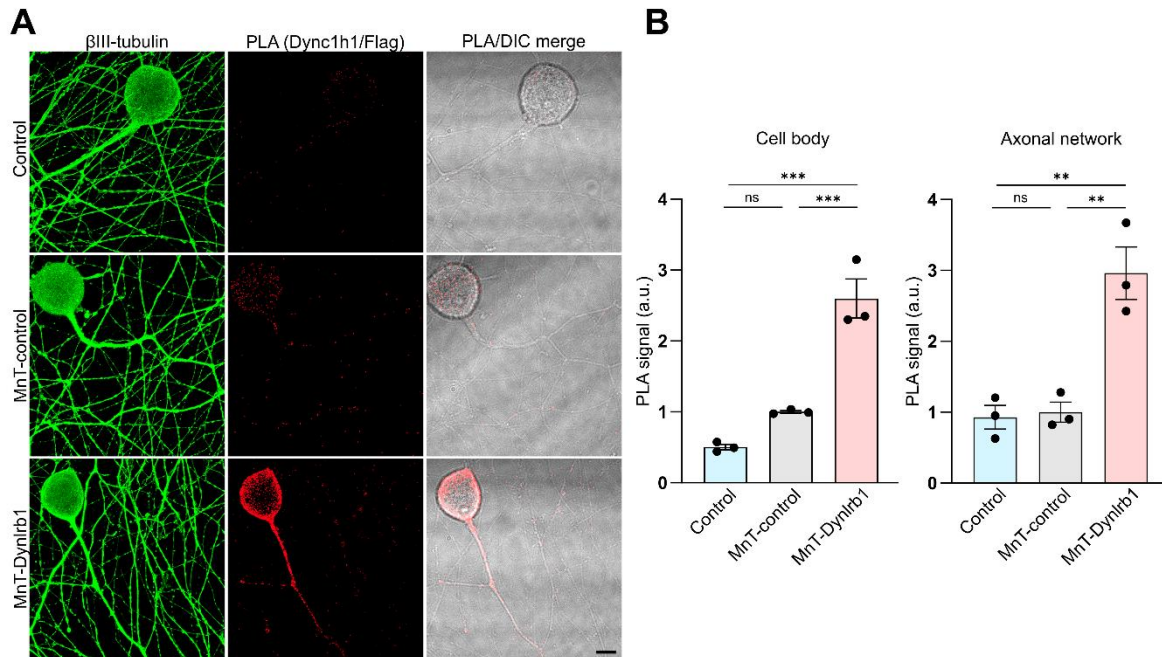


Figure 3.3. Validation of recombinant Dynlrb1 association with the dynein complex in sensory neurons. A) PLA analysis between dynein heavy chain (Dync1h1) and flag-tagged proteins (MnT-Dynlrb1 and MnT-control). Non-transduced cells were included as a control. Neurons are labeled with β III-tubulin (green). The PLA signal is in red. Scale bar 10 μ m. B) Quantification of the PLA experiment in A. PLA signal in the cell bodies and axons was quantified separately. Mean \pm SEM, ** $p < 0.01$, *** $p < 0.001$, ns, not significant, $n = 3$, one-way ANOVA followed by Tukey's HSD post hoc correction for multiple comparisons.

3.2. Identifying Dynlrb1 interactors in DRG neurons via mass spectrometry

To identify Dynlrb1 interactors, cultured DRG neurons transduced with either MnT-control or MnT-Dynlrb1 constructs were treated with 200 μ M biotin for 2 h to initiate labeling. Biotinylated proteins were captured by streptavidin magnetic beads, eluted, and subjected to liquid chromatography-tandem mass spectrometry (LC-MS/MS). Subsequent MaxQuant analysis identified 90 Dynlrb1 interactors significantly enriched over MnT-control ($FC \geq 2$; $p \leq 0.05$), including subunits of the dynein and dynactin complex (**Figure 3.4A & Table 1**). Bioinformatic analysis using the [g:Profile](#) server [128], highlighted an enrichment of proteins involved in protein transport as expected (**Figure 3.4B**), confirming the successful pulldown of Dynlrb1-related dynein complexes. mRNA translation and RNA binding were also represented in the proteomics hits (**Figure 3.4B**).

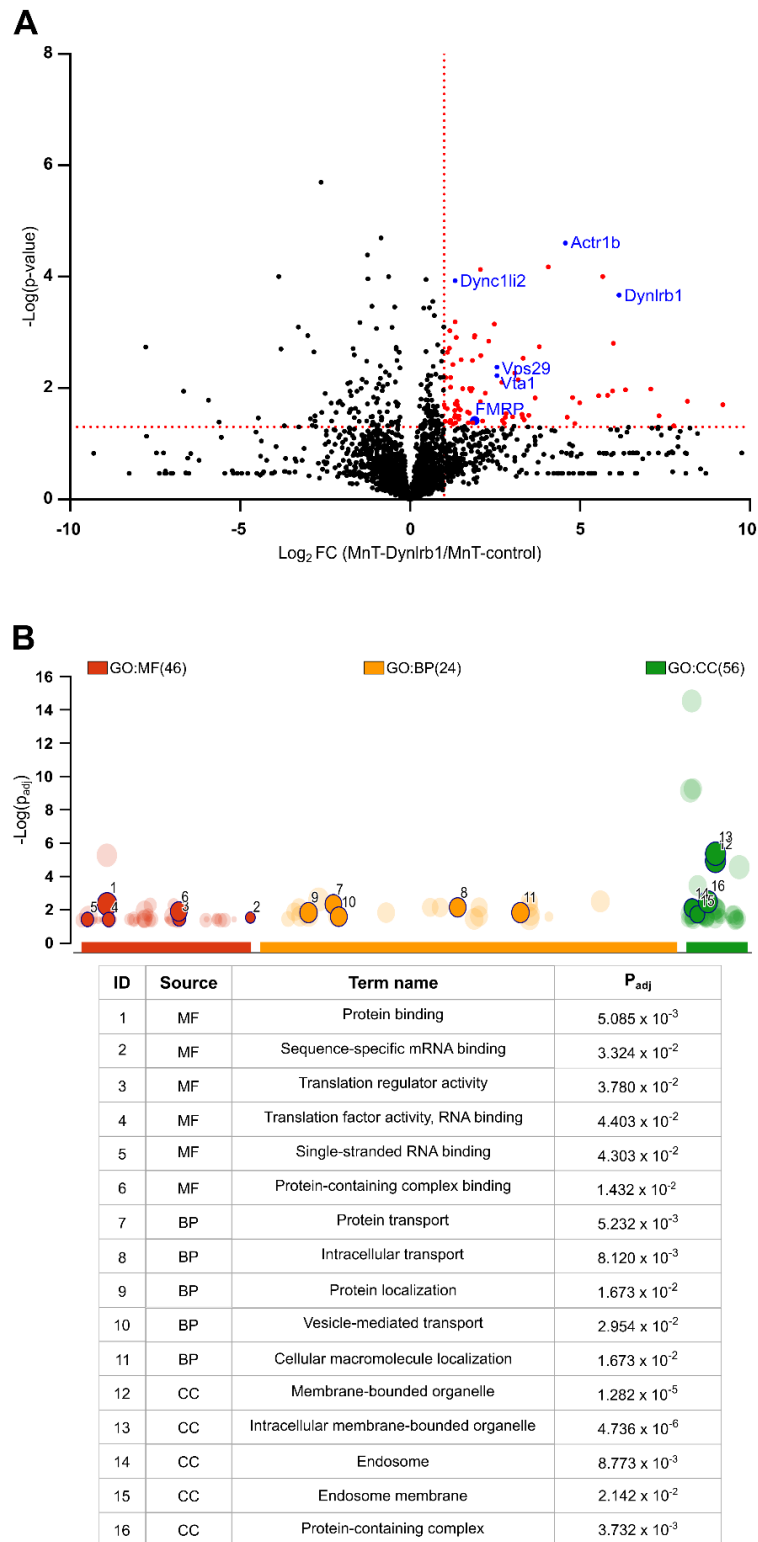


Figure 3.4. Mass spectrometry (MS) analysis of Dynlr1b1 interactors. A) Volcano plot of the MS analysis of DRG neurons transduced with MnT-control or MnT-Dynlr1b1 AAV constructs. Red and blue circles represent putative interactors. Vertical and horizontal dashed red lines mark two-fold change ($\log_2(2)=1$) compared to MnT-control and p-value of 0.05 ($-\log_{10}(0.05)=1.3$) respectively. B) Manhattan plot of the candidate hits from the MS analysis. Functional enrichment analysis was performed using the g:Profile server. GO categories associated with the MS hits are plotted vs the $-\log_{10}$ of the adjusted p-values (P_{adj}). Circles represent functional terms that are grouped, and color coded by data source (GO: gene ontology; MF: molecular function, BP: biological process, CC: cellular component). A few chosen categories are highlighted in the plot and table below the chart.

We selected three candidates for validation based on their role in intracellular trafficking and neuronal homeostasis: the vacuolar protein sorting associated protein 29 (Vps29), the vacuolar protein sorting-associated protein VTA1 homolog (Vta1), and FMRP. We used PLA to visualize the association between Dynlrb1 and the selected candidates as well as the subcellular localization of said interaction. Due to the lack of reliable antibodies against Dynlrb1, the PLA analysis was performed between the endogenous candidates and the flag-tagged MnT-control or MnT-Dynlrb1 proteins. Semi-endogenous PLA signal was previously shown to represent a valid protein interaction [129]. Reassuringly, all the candidate hits showed interaction with Dynlrb1 when compared to the miniTurbo control (**Figure 3.5., Figure 3.6.**). While Vps29-Dynlrb1 interaction was mainly axonal (**Figure 3.5A&B**), Vta1 and FMRP showed significant association with Dynlrb1 across both the somatic and axonal compartments (**Figure 3.5C&D, Figure 3.6.**). Because of the relevance of FMRP to neuronal pathology and the relative lack of data regarding its interaction with the dynein complex, we selected this candidate for further investigations.

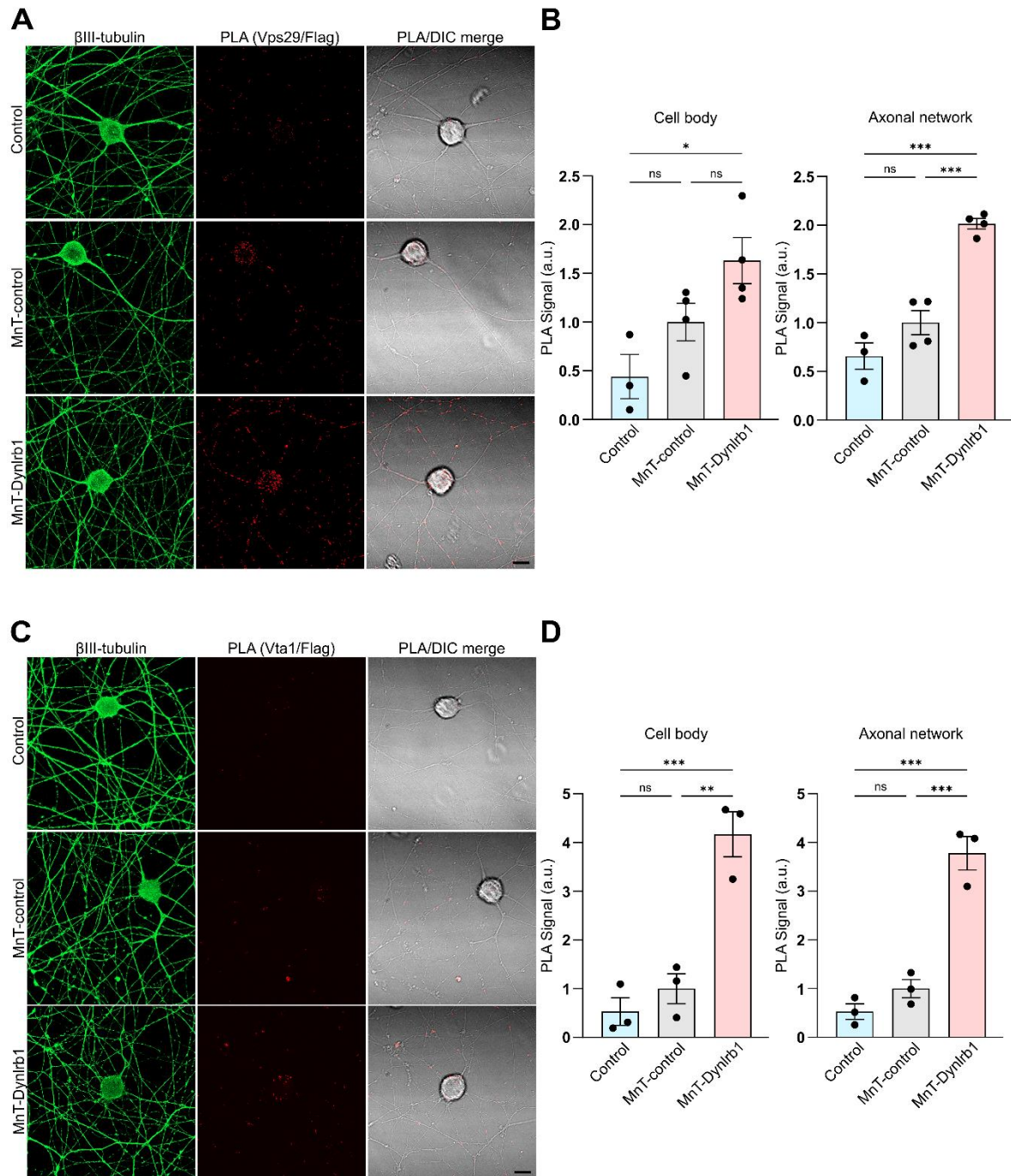


Figure 3.5. Validation of Dynlrb1-Vps29 and Vta1 interaction in DRG neurons. A) Representative images of PLA between Vps29 and flag-tagged proteins in neurons transduced with miniTurbo or MnT-Dynlrb1 AAVs. Non-transduced cells were included as a control. Neurons are labeled with β III-tubulin (green). The PLA signal is in red. Scale bar 10 μ m. B) Quantification of the PLA experiment in A. PLA signal in the cell bodies and axons was quantified separately. Mean \pm SEM, * $p < 0.05$, *** $p < 0.001$, ns not significant, $n \geq 3$, one-way ANOVA followed by Tukey's HSD post hoc correction for multiple comparisons. C) Representative images of PLA between Vta1 and flag-tagged proteins in neurons transduced with MnT-control or MnT-Dynlrb1. Non-transduced cells were included as a control. Neurons are labeled with β III-tubulin (green). The PLA signal is in red. Scale bar 10 μ m. D) Quantification of the PLA experiment in C. PLA signal in the cell bodies and axons was quantified separately. Mean \pm SEM, ** $p < 0.01$, *** $p < 0.001$, ns not significant, $n = 3$, one-way ANOVA followed by Tukey's HSD post hoc correction for multiple comparisons.

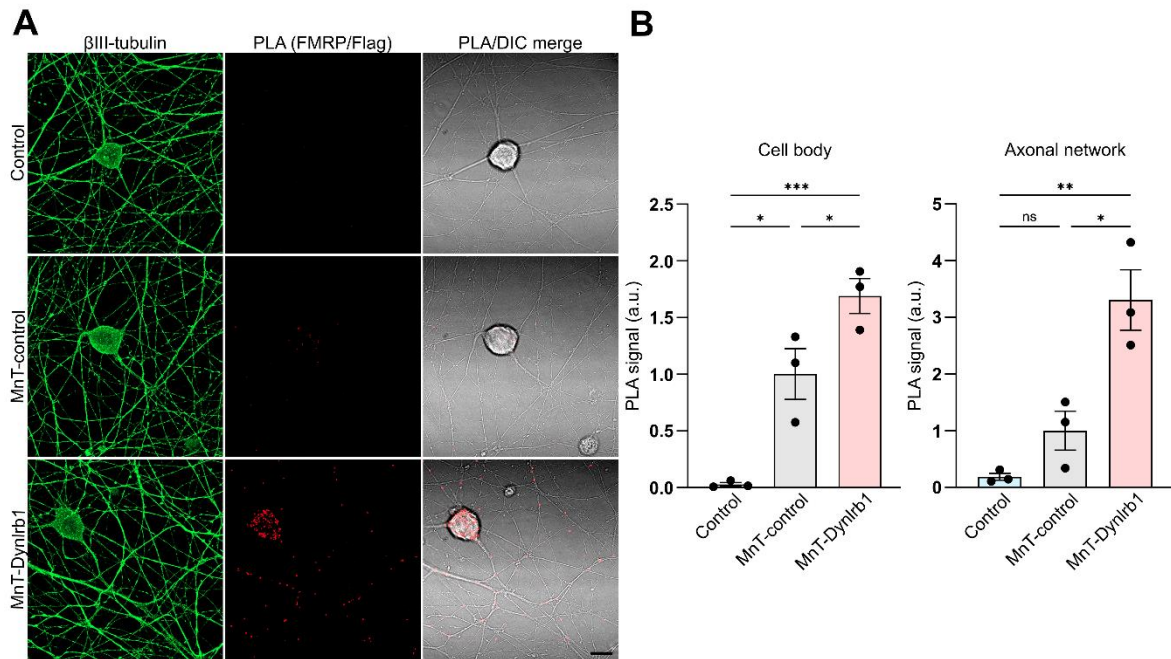


Figure 3.6. Validation of Dynlrb1-FMRP association in DRG neurons. A) Representative images of PLA between FMRP and flag-tagged proteins in DRG neurons transduced with MnT-control or MnT-Dynlrb1. Non-transduced cells were also added as a control. Neurons are labeled with β III-tubulin (green). The PLA signal is in red. Scale bar 10 μ m. B) Quantification of the PLA experiment in A. PLA signal in the cell bodies and axons was quantified separately. Mean \pm SEM, * $p < 0.05$, ** $p < 0.01$, *** $p < 0.001$, ns not significant, $n=3$, one-way ANOVA followed by Tukey's HSD post hoc correction for multiple comparisons.

3.3. FMRP associates with dynein and endolysosomes in wild type sensory axons

Interestingly, FMRP has been reported to interact with BicD, a dynein activating adaptor, driving its molecular transport into *Drosophila*'s neurons [27]. In addition, recent work demonstrated that RBPs complexed within RNA granules can gain indirect access to long-range transport by associating with already-motile Lamp1-positive endolysosomes, a process known as hitchhiking [62, 69]. Our previous data indicates that Dynlrb1 is crucial for lysosomal transport in DRG neurons [43], thus we decided to characterize FMRP's association with dynein and its axonal trafficking in relation to lysosomes in sensory axons. To obtain enough axonal lysate for a Co-IP assay, we isolated axoplasm from mouse sciatic nerve and immunoprecipitated FMRP. Indeed, we could recover dynein intermediate chain (IC74.1) in the FMRP pulldown (**Figure 3.7.**), confirming the association of FMRP with the dynein complex in axonal cytoplasm and suggesting the possibility of dynein-based axonal transport of FMRP.

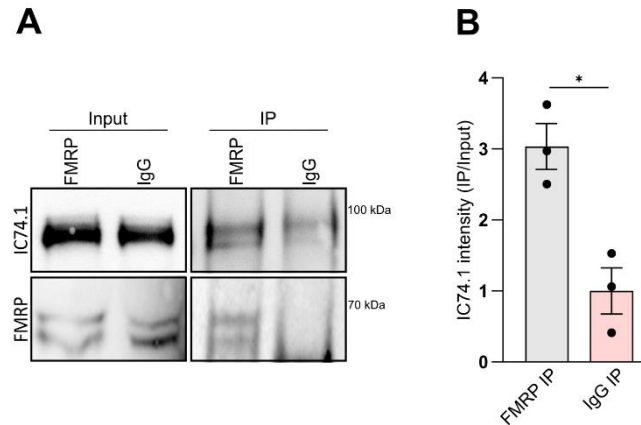


Figure 3.7. FMRP co-precipitates with the dynein complex in sensory axons. A) Western blot analysis of FMRP immunoprecipitation from axoplasm extracted from mouse sciatic nerve. Co-IP of dynein intermediate chain is revealed by immunostaining with IC74.1 antibody. B) Quantification of the pull-down in A. Mean \pm SEM, * $p < 0.05$, $n = 3$, unpaired t-test.

We then expressed EGFP-FMRP in cultured DRG neurons and performed time-lapse imaging together with lysotracker DND-99, a dye that allows for live labeling of lysosomes. Time-lapse imaging revealed that 56% and 63% of FMRP and endolysosomes respectively exhibited a processive directional movement in wild type neurons (**Figure 3.8A&B**), in agreement with previous observations [43], [88]. Interestingly, while most antero- and retrograde motile EGFP-FMRP granules trafficked with lysosomes, not all lysosomes co-trafficked with FMRP granules (**Figure 3.8A**). EGFP-FMRP positive carriers exhibited preferential retrograde trafficking in sensory axons (**Figure 3.8A&B**). Frequency distribution of EGFP-FMRP speed showed a characteristic peak in each direction (**Figure 3.8C-F**) with the anterograde peak closely aligning with that of lysotracker positive organelles (**Figure 3.8C&D**), whereas the retrograde peak revealed a selective association with a subpopulation of endolysosomes (**Figure 3.8E&F**). The observed retrograde bias in motility could support a model in which EGFP-FMRP is coupled with a subpopulation of lysotracker positive organelles for degradation in the soma. While local axonal degradation has been reported, the majority of enzymatically active degradative lysosomes reside in the soma [15], [21]. Retrograde shuttling, as opposed to the bidirectional transport described for EGFP-FMRP in dendrites of other neuronal types, could be more prominent in DRG, whose network is exclusively axonal. Indeed, unlike dendrites, axons are characterized by a uniform plus-ended microtubule polarity and dynein is a retrograde motor in this context [130]–[132].

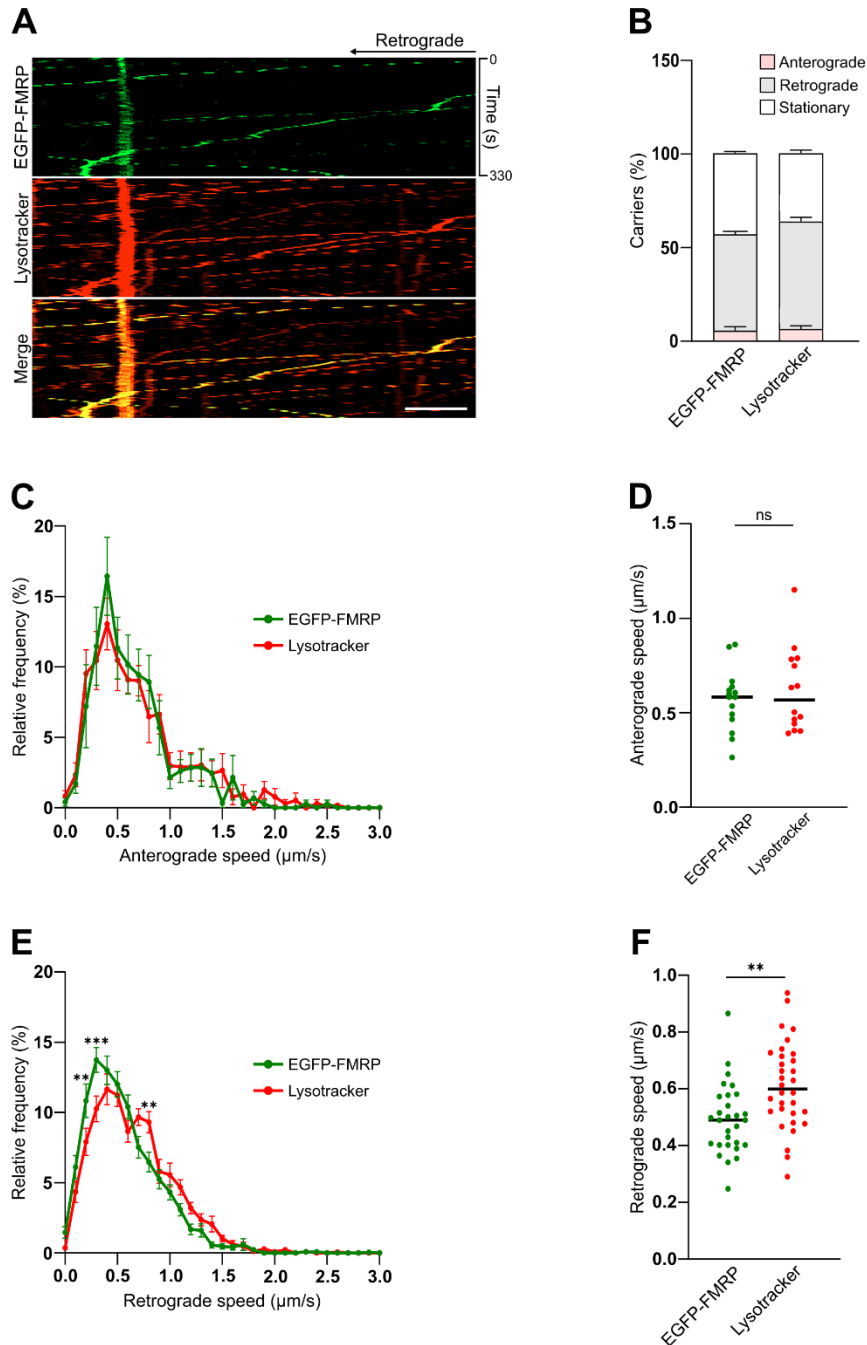


Figure 3.8. Analysis of FMRP trafficking in wild type sensory neurons. A) Representative kymograph of DRG neurons transfected with EGFP-FMRP construct (in green). Lysotracker was added to track lysosomal transport (in red). The merge between the two channels is in yellow. Scale bar 5 μm . B) Percentage of anterograde and retrograde versus stationary carriers in the experiment described in A. C) Anterograde speed distributions from the experiment described in A. Mean \pm SEM, $n > 14$ movies per group over three independent biological repeats, two-way ANOVA, followed by Sidak's multiple comparisons test. D) Medians of the instantaneous anterograde speeds of moving carriers in the experiment described in A. Mean \pm SEM, ns not significant, $n > 14$ movies per group over three independent biological repeats, unpaired t-test. E) Retrograde speed distributions from the experiment described in A. Mean \pm SEM, ** $p < 0.01$, *** $p < 0.001$, $n > 28$ movies per group over three independent biological repeats. Two-way ANOVA, followed by Sidak's multiple comparisons test. F) Medians of the instantaneous retrograde speeds of moving lysotracker and FMRP carriers in the experiment described in A. Mean \pm SEM, ** $p < 0.01$, $n > 28$ movies per group over three independent biological repeats, unpaired t-test.

Recently, Lippincott-Schwartz and Ward groups identified annexin A11 (Anxa11), a vesicular trafficking protein linked to ALS [29], [133], as the tethering adaptor for G3bp1 granules association with motile Lamp1-positive vesicles [29]. Interestingly, Anxa11 was one of the hits identified in our proteomics screen (**Table 1.**). Thus, we examined the impact of Anxa11 silencing, using an siRNA pool, on the association of endogenous FMRP to Lamp1 positive organelles using PLA. The efficiency of the knockdown was confirmed by western blot analysis (**Figure 3.9.**). Remarkably, PLA analysis revealed reduced FMRP association with Lamp1 organelles upon Anxa11 depletion across the somatic and axonal compartments (**Figure 3.10.**) suggesting that Anxa11 could mediate the docking of at least a pool of FMRP granules onto Lamp1-positive vesicles for long-range transport.

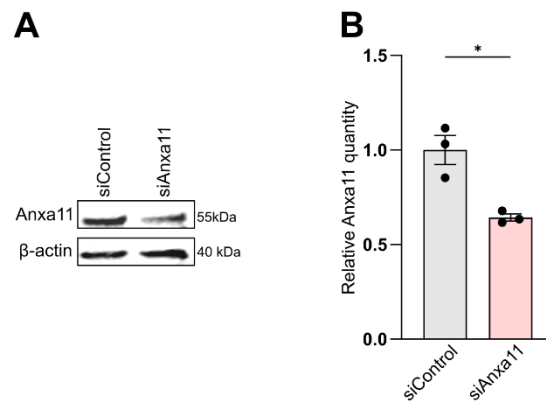


Figure 3.9. Efficiency of Anxa11 depletion in sensory neurons. A) Western blot analysis of Anxa11 protein levels in DRG neurons transfected with siControl or siAnxa11. B) Quantification of the experiment described in A. Mean ± SEM, n=3, * p<0.05, unpaired t-test.

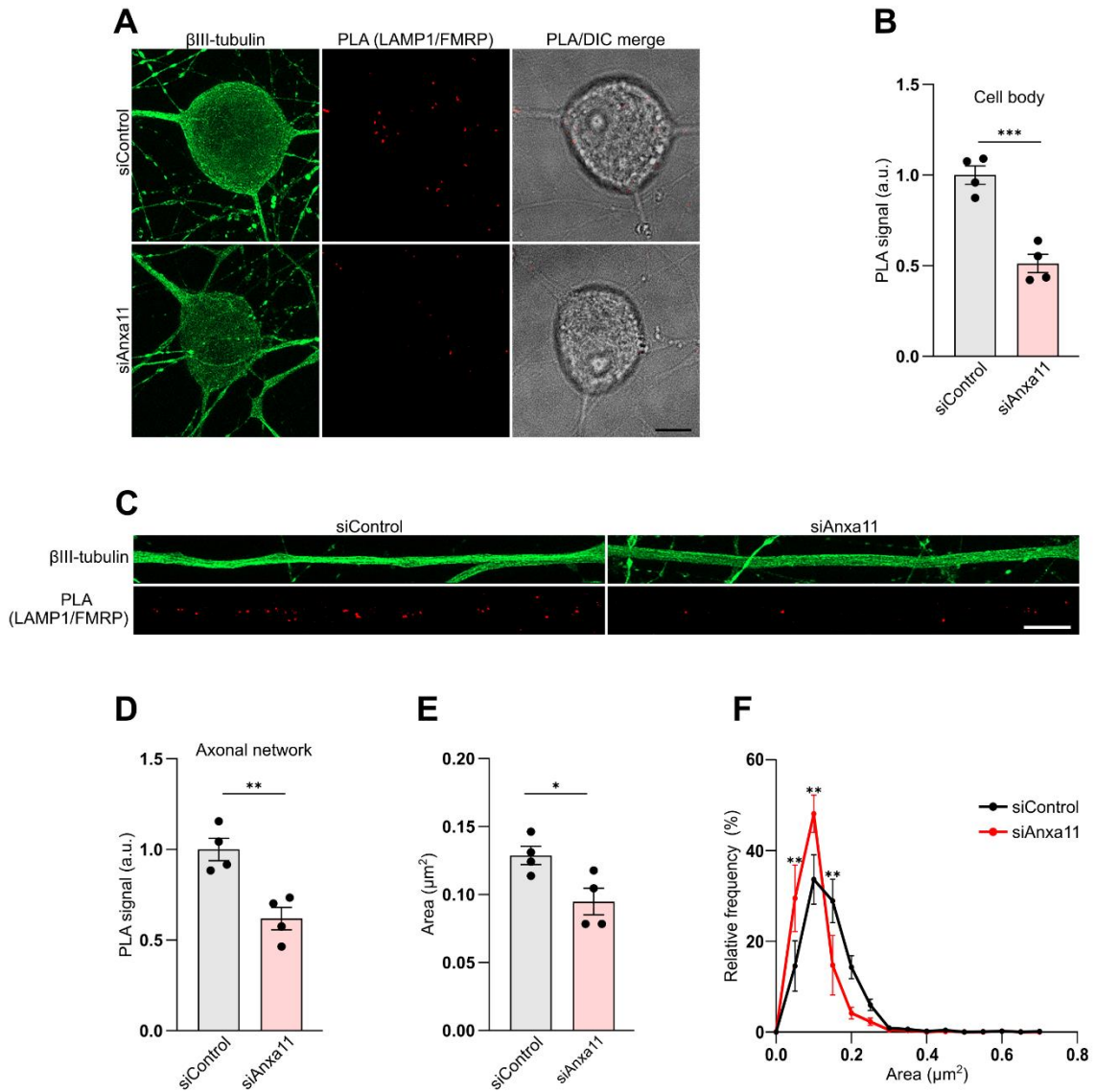


Figure 3.10. Depletion of Anxa11 reduces FMRP association with Lamp1 vesicles. A) Representative images of PLA between FMRP and Lamp1 in the somatic compartment of siControl and siAnxa11 DRG neurons. Neurons are labeled with β III-tubulin (green). PLA signal is in red. Scale bar 10 μm . B) Quantification of the PLA spots in A. Mean \pm SEM, *** $p < 0.001$, $n = 4$, unpaired t-test. C) Representative images of axonal Lamp1/FMRP PLA in siControl and siAnxa11 neurons labeled with β III-tubulin (green). PLA signal is in red. Scale bar 10 μm . D) Quantification of the PLA spots in C. Mean \pm SEM, ** $p < 0.01$, $n = 4$, unpaired t-test. E) Median of the PLA area described in A&C. Mean \pm SEM, * $p < 0.05$, $n = 4$, unpaired t-test. F) Relative frequency distribution of the PLA area for the experiment in A&C. ** $p < 0.01$, $n = 4$, two-way ANOVA followed by Sidak's multiple comparisons test.

3.4. FMRP axonal trafficking depends on Dynlrb1 levels

To test the role of Dynlrb1 in FMRP trafficking, we designed a small hairpin RNA (shRNA) against the coding sequence of Dynlrb1. Quantitative RT-PCR from cultured DRG neurons transduced with shDynlrb1 AAV showed 60% reduction in Dynlrb1 mRNA levels compared to a non-targeting shControl (Figure 3.11A). Given the critical role of Dynlrb1 in sensory neuron survival, we monitored our cultures for signs of toxicity. Six days after transduction with shDynlrb1, only minimal toxicity (8.5% reduction in the number of viable cells) was observed (Figure 3.11B&C).

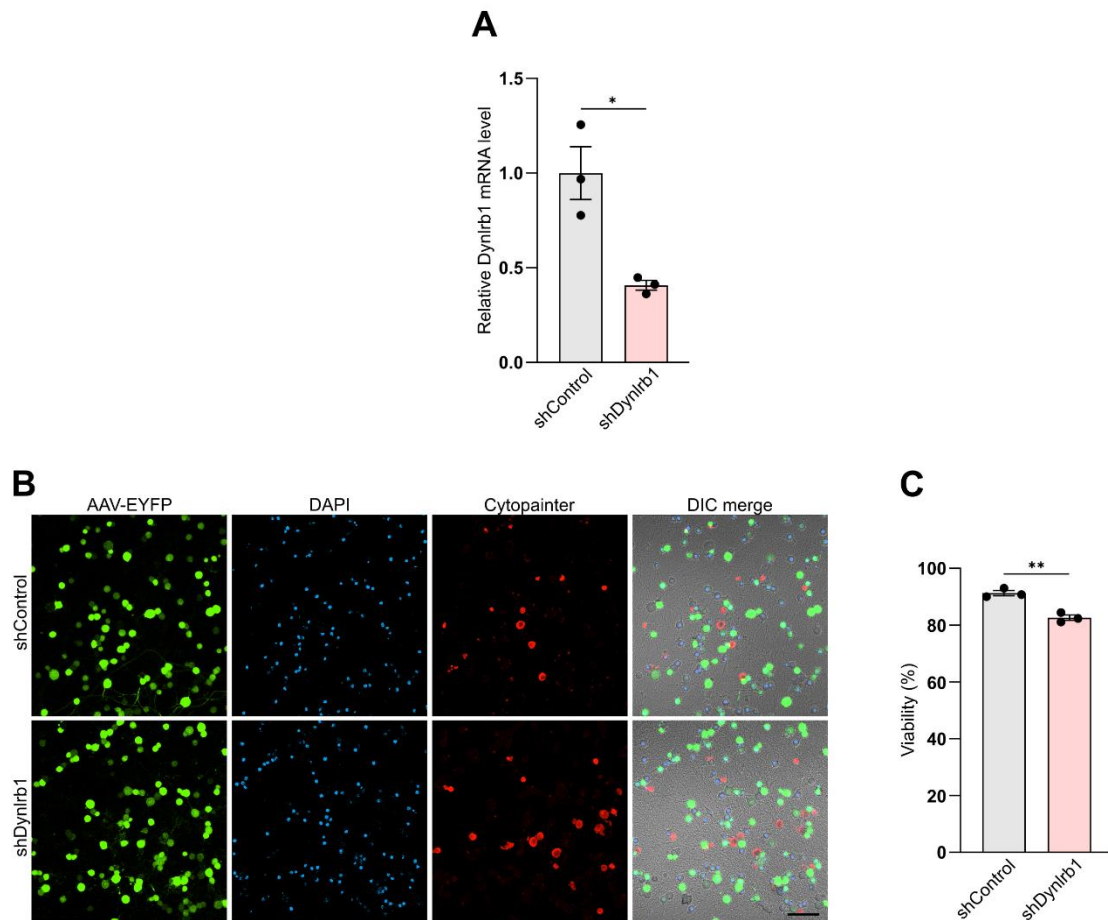


Figure 3.11. shRNA-mediated depletion of Dynlrb1 in DRG neurons. A) Quantitative RT-PCR analysis on RNA extracted from DRG neurons 8 days post-transduction with shControl or shDynlrb1. Mean \pm SEM, * $p < 0.05$, $n = 3$, unpaired t-test. B) Representative images of DRG neurons transduced with shControl or shDynlrb1 for 6 days and stained with cytopainter dye for 45 mins. Cells with compromised plasma membranes show high cytopainter fluorescence intensity (in red). Transduced neurons are labeled by EYFP expressed by the viral constructs (in green). Nuclei are visualized by DAPI (in blue). Scale bar 100 μm . C) Quantification of the experiment described in B. Mean \pm SEM, ** $p < 0.01$, $n = 3$, unpaired t-test.

We then proceeded to test whether shRNA-mediated knockdown of Dynlrb1 affects FMRP pairing with the dynein complex. PLA analysis revealed that the interaction of FMRP with dynein heavy chain (Dync1h1) (**Figure 3.12.**) is greatly reduced upon Dynlrb1 depletion suggesting that FMRP active transport could be dependent on Dynlrb1.

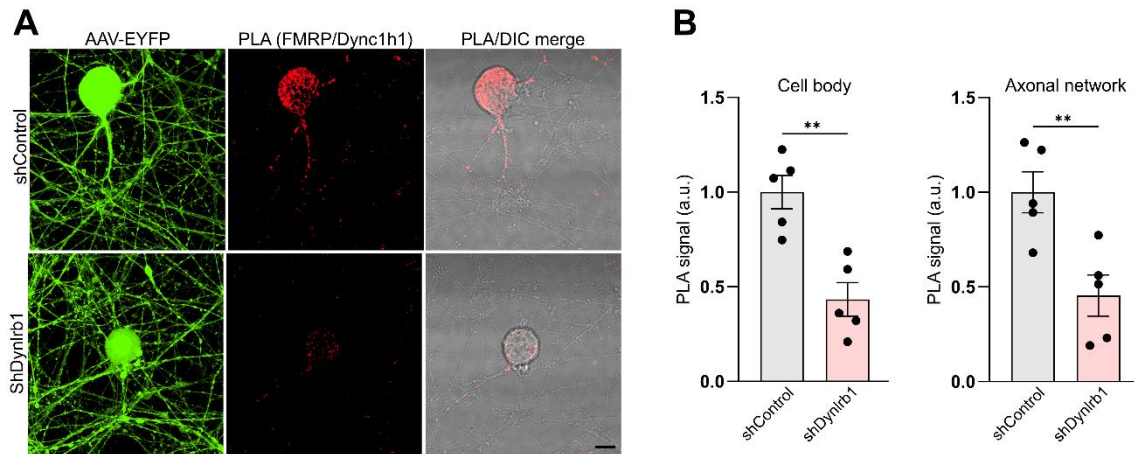


Figure 3.12. Dynlrb1 silencing impacts FMRP association with the dynein complex. A) Representative images of PLA between FMRP and dynein heavy chain (Dync1h1) in DRG neurons transduced with shControl or shDynlrb1 constructs. Transduced neurons are labeled by EYFP expressed by the viral constructs. The PLA signal is in red. Scale bar 10 μ m. B) Quantification of the PLA experiment in A. PLA signal in the cell bodies and axons was quantified separately. Mean \pm SEM, ** $p < 0.01$, $n = 5$, unpaired t-test.

Accordingly, we decided to test whether Dynlrb1 depletion would stall FMRP trafficking, inducing its axonal accumulation. Since our viral shRNA constructs express EYFP, we used an siRNA pool to test whether Dynlrb1 is required for EGFP-FMRP axonal motility. Dynlrb1 knockdown efficiency was confirmed by quantitative RT-PCR (**Figure 3.13.**).

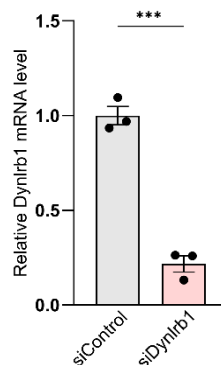


Figure 3.13. siRNA-mediated depletion of Dynlrb1 in DRG neurons. Quantitative RT-PCR analysis on RNA extracted from DRG neurons 3 days post-transfection with siControl or siDynlrb1. Mean \pm SEM, *** $p < 0.001$, $n = 3$, unpaired t-test.

As expected, depletion of Dynlrb1 via siRNA significantly increased the stationary pool of lysosomes at the expense of the mobile pool as previously described [43] (**Figure 3.14A&B**). Comparably, Dynlrb1 depletion impaired FMRP retrograde transport by increasing the number of stationary particles (**Figure 3.14A&B**) and further reduced the speed of both lysotracker- (**Figure 3.14C&D**) and FMRP-positive residual retrogradely moving carriers (**Figure 3.14E&F**). Interestingly, EGFP-FMRP stationary particles colocalized with stationary lysosomes (**Figure 3.14A**), thus confirming that the long-range transport of lysosomes and FMRP is closely linked and suggesting association between the two.

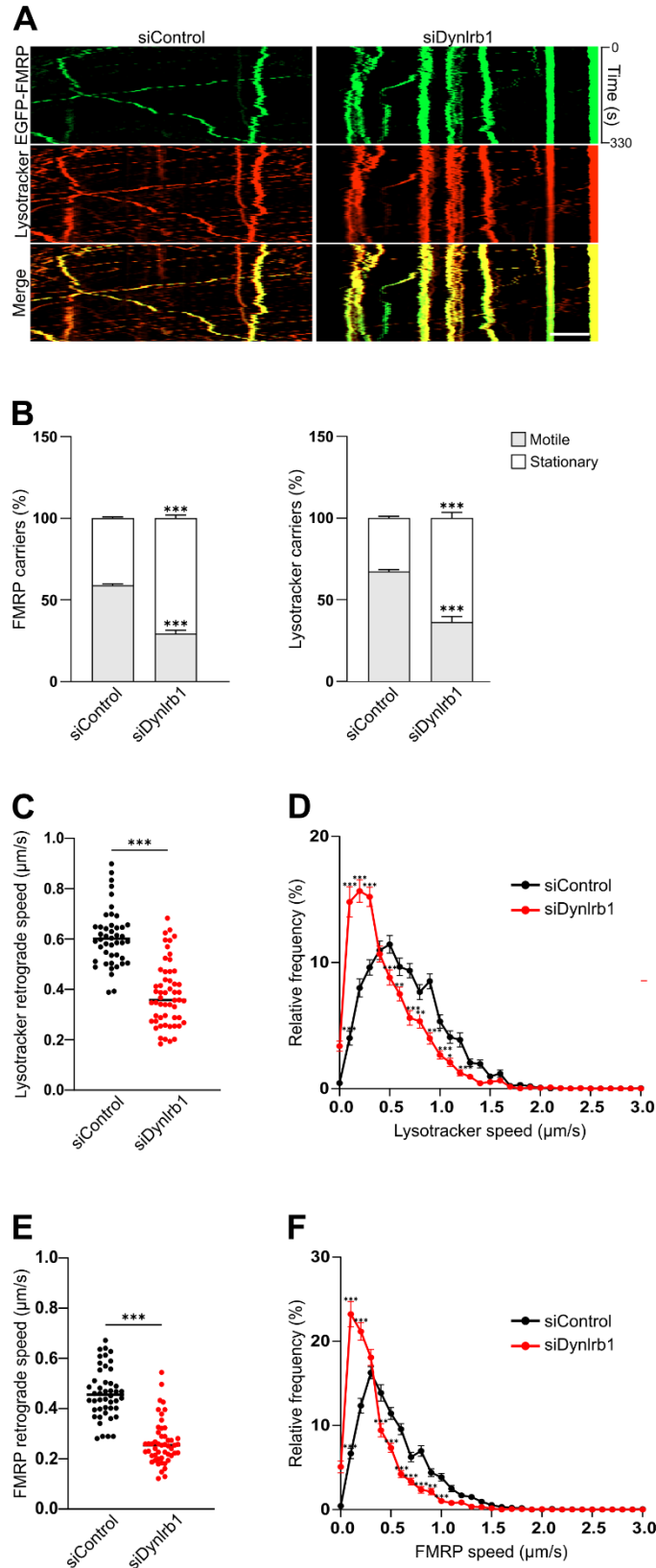


Figure 3.14. Dynlrb1 depletion negatively impacts FMRP trafficking. A) Representative kymographs of siControl and siDynlrb1 DRG neurons transfected with EGFP-FMRP construct (in green). Lysotracker was used to track lysosomal transport (in red). The merge between the two channels is in yellow. Scale bar 5 μm . B) Percentage of moving versus stationary carriers in the experiment described in A for both FMRP and lysotracker positive axonal carriers. Mean \pm SEM, *** $p < 0.001$, $n=3$, two-way ANOVA, followed by Sidak's multiple comparisons test.

Figure 3.14. (continued) C) Medians of the instantaneous retrograde speeds of lysotracker-positive moving carriers in siControl and siDynlrb1 DRG neurons transfected with EGFP-FMRP from the experiment described in A. Mean \pm SEM, *** $p < 0.001$, $n > 46$ movies per group over three independent biological repeats, unpaired t-test. D) Retrograde speed distributions of lysotracker-positive moving carriers from the experiment described in A. Mean \pm SEM, * $p < 0.05$, ** $p < 0.01$, *** $p < 0.001$, $n > 46$ movies per group over three independent biological repeats, two-way ANOVA followed by Sidak's multiple comparisons test. E) Medians of the instantaneous retrograde speeds of FMRP-positive moving carriers in the experiment described in A. Mean \pm SEM, *** $p < 0.001$, $n > 46$ movies per group over three independent biological repeats, unpaired t-test. F) Retrograde speed distributions of FMRP-positive moving carriers from the experiment described in A. Mean \pm SEM, ** $p < 0.01$, *** $p < 0.001$, $n > 46$ movies per group over three independent biological repeats, two-way ANOVA followed by Sidak's multiple comparisons test.

In line with impaired FMRP trafficking, we observed a significant increase in the number of endogenous FMRP puncta in axons of shDylnrb1 transduced neurons (**Figure 3.15A&Bi**). Dylnrb1 knockdown also perturbed FMRP axonal puncta size, inducing a statistically significant shift to larger puncta (**Figure 3.15Bii&Biii**).

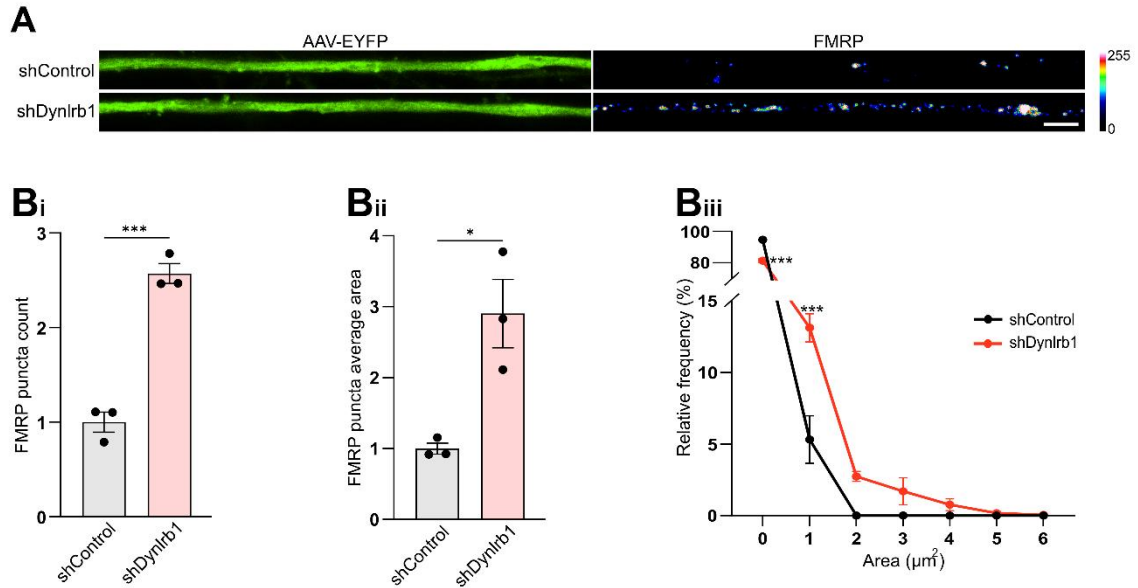


Figure 3.15. Dynlrb1 silencing induces intra-axonal accumulations of FMRP. A) Representative images of shControl or shDylnrb1 axons. FMRP axonal accumulation is revealed by staining with an anti-FMRP antibody (rainbow palette to highlight difference in intensity). Scale bar 5 µm. B) Quantification of the number (Bi), area (Bii) and relative frequency (Biii) of FMRP-positive puncta in the experiment described in A. Mean ± SEM, * p<0.05, *** p<0.001, n=3, unpaired t-test.

Super-resolution imaging of the enlarged FMRP puncta revealed them to be clusters of individual FMRP granules (**Figure 3.16A-D**). Further analysis confirmed a statistically significant increase in the number of puncta and a shift to a larger size (0.25 µm² - 0.75 µm²) (**Figure 3.16E**) in Dylnrb1 knockdown neurons. The abnormally enlarged axonal pool of FMRP in Dylnrb1 depleted neurons could result from an impairment in trafficking and/or degradation.

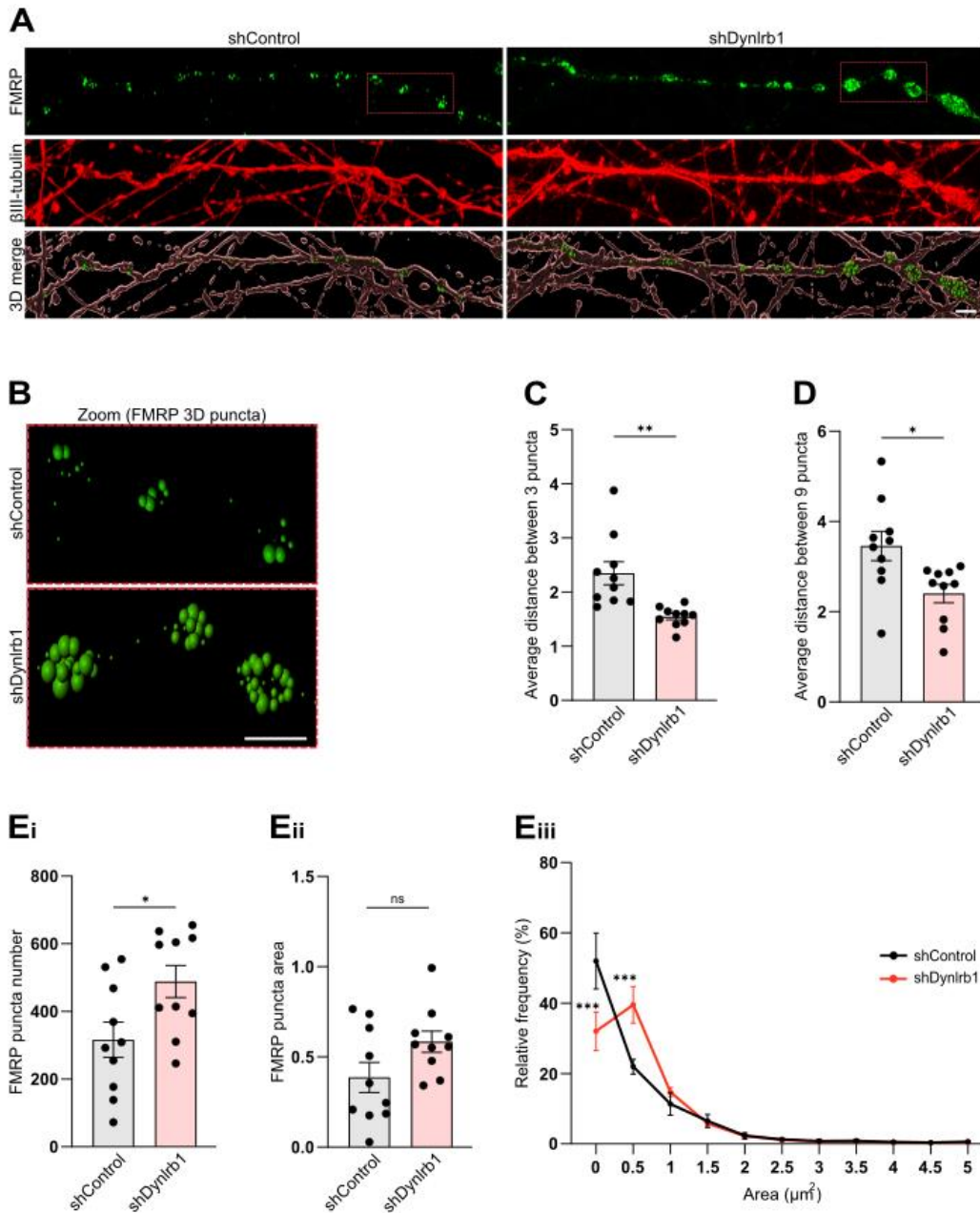


Figure 3.16. Super-resolution imaging of intra-axonal FMRP granules. A) Airyscan images of FMRP (in green) and β III-tubulin (in red), and the 3D merge of FMRP 3D spot detection and surface rendering in DRG neurons transduced with shControl or shDylnrb1. Scalebar 3 μm . B) FMRP puncta detection from the zoom in area shown in panel A (red box). Scalebar 3 μm . C&D) Quantification of axonal FMRP clustering with the average distance between 3 spots and 9 spots respectively. E) Quantification of FMRP puncta number (Ei), area (Eii), and relative frequency (Eiii). * $p < 0.05$, *** $p < 0.001$, ns not significant, unpaired t-test, $n = 10$ images per group.

To investigate whether the axonal transport deficit found in Dynlrb1 depleted neurons is specific to lysosomes and FMRP granules, we monitored mitochondrial dynamics. Mitochondria are shuttled bidirectionally by molecular motors, and alterations of their axonal transport have been linked to neurodegenerative diseases [4]. DRG neurons transfected with siControl or siDynlrb1 were incubated with mitotracker deep red to visualize active mitochondria. Time-lapse imaging revealed a reduction in the motile pool of mitochondria from 32 to 23% upon Dynlrb1 depletion (**Figure 3.17A&B**) with slower movements occurring more frequently despite not impacting the overall median speed (**Figure 3.17C-F**). Interestingly, mutant FMRP was previously reported to negatively impact mitochondrial transport in *Drosophila* axonal network without disrupting their speed of transport [134]. Previous work from our group has also reported that Dynlrb1 genetic depletion negatively affects the percentage of retrogradely motile signaling endosomes, but not their speed [43]. Remarkably, while our data highlights how Dynlrb1 silencing affects a broad range of cargos, lysosomes are affected to a much greater extent (**Figure 3.14**).

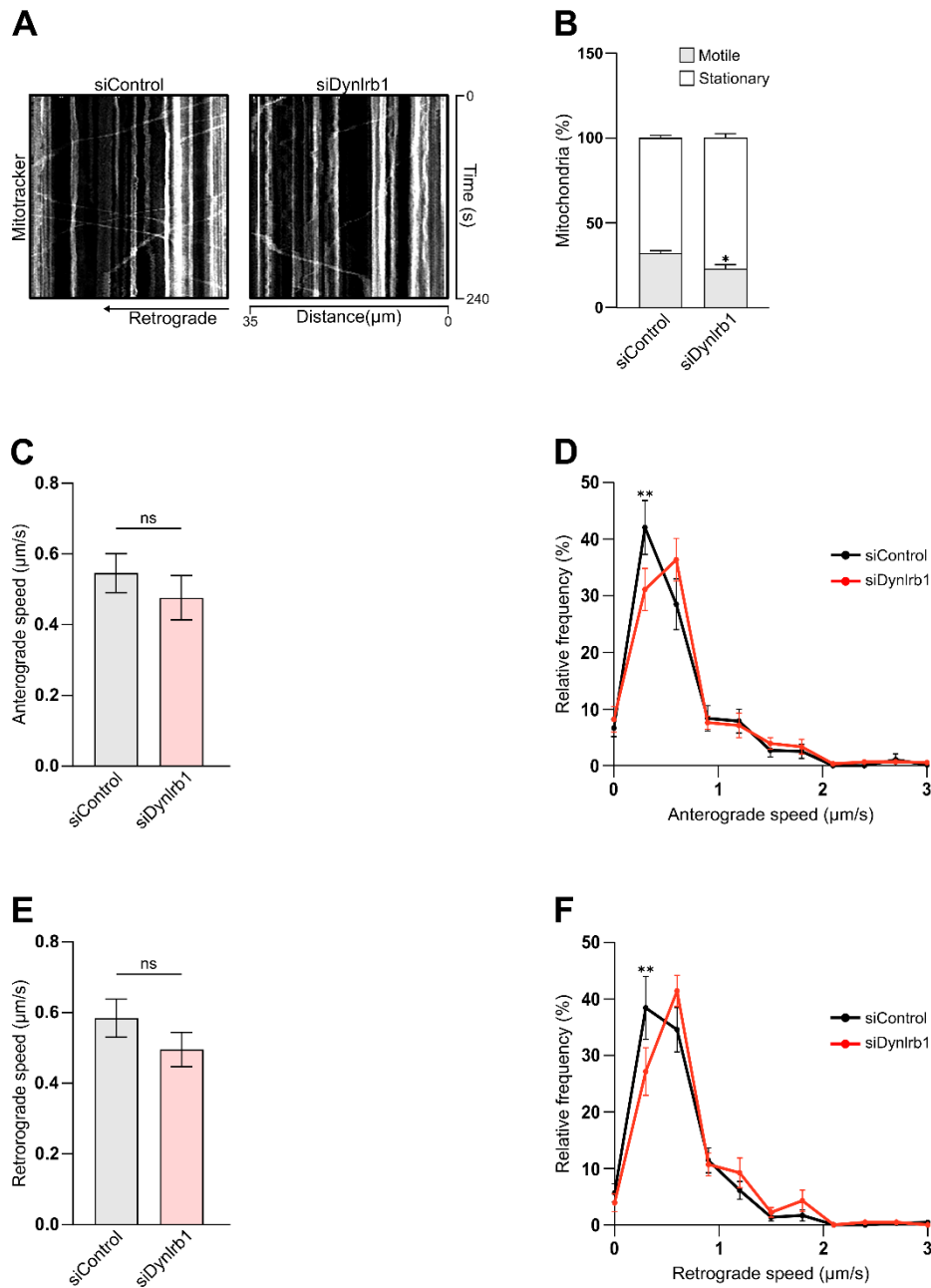


Figure 3.17. Dynlrb1 silencing negatively impacts mitochondrial trafficking. A) Representative kymographs of siControl and siDynlrb1 DRG neurons labeled with mitotracker (grayscale). B) Percentage of moving versus stationary carriers in the experiment described in A. Mean \pm SEM, * $p < 0.05$, $n = 3$, two-way ANOVA, followed by Sidak's multiple comparisons test. C) Medians of the anterograde speeds of mitotracker-positive moving carriers in siControl and siDynlrb1 DRG neurons from the experiment described in A. Mean \pm SEM, ns not significant, $n > 19$ movies per group over three independent biological repeats, unpaired t-test. D) Anterograde speed distributions of mitotracker moving carriers from the experiment described in A. Mean \pm SEM, ** $p < 0.01$, $n > 19$ movies per group over three independent biological repeats, two-way ANOVA followed by Sidak's multiple comparisons test. E) Medians of the retrograde speeds of mitotracker-positive moving carriers in siControl and siDynlrb1 DRG neurons from the experiment described in A. Mean \pm SEM, ns not significant, $n = 19$ movies per group over three independent biological repeats, unpaired t-test. F) Retrograde speed distributions of mitotracker moving carriers from the experiment described in A. Mean \pm SEM, ** $p < 0.01$, $n = 19$ movies per group over three independent biological repeats, two-way ANOVA followed by Sidak's multiple comparisons test.

3.5. Dynlrb1 regulates FMRP protein levels and function

As previously discussed, interaction between BicD and FMRP has been documented in *Drosophila* and absence of BicD has been reported to cause a significant reduction of FMRP protein levels in *Drosophila*'s larval brain [27]. However, mutations of the dynein motor, which might potentially alter FMRP trafficking, didn't affect its protein levels in *Drosophila* [27], [135], suggesting that the non-catalytic subunits of the dynein machinery might play a direct role in regulating FMRP protein levels. Thus, we tested whether Dynlrb1 knockdown affects FMRP protein levels in DRG neurons. Indeed, Dynlrb1 genetic depletion increased the overall FMRP protein levels (**Figure 3.18.**) and further promoted the formation of FMRP granules in DRG neuron soma (**Figure 3.18A**). Since LLPS is facilitated by the local concentration of RBPs [136], the observed increase in FMRP levels could have promoted or enhanced its condensation into granules upon Dynlrb1 silencing.

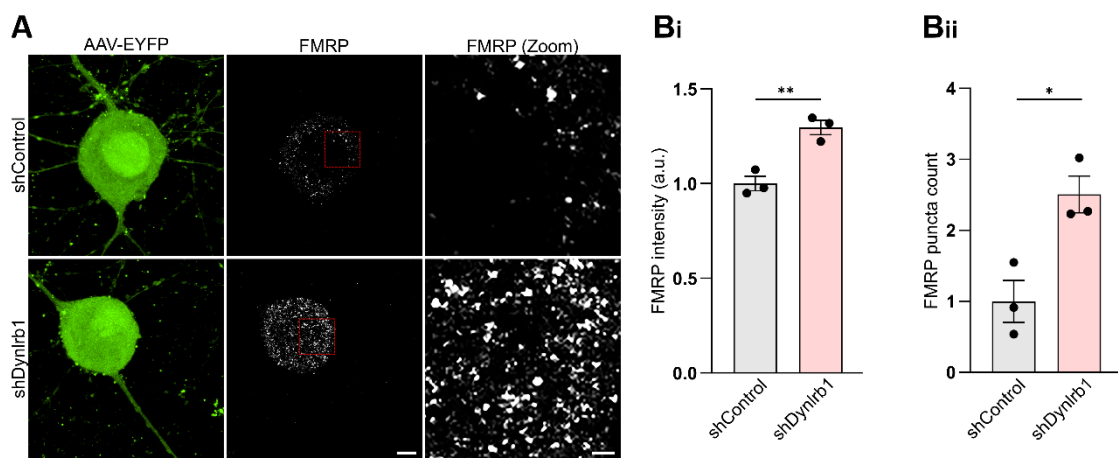


Figure 3.18. Genetic depletion of Dynlrb1 promotes FMRP granule formation. A) Representative images of cell bodies of DRG neurons transduced with shControl or shDynlrb1. Transduced neurons are labeled by EYFP expressed by the viral constructs (in green). FMRP granules are visualized by staining with an anti-FMRP antibody (grayscale). Scale bars 5 μ m and 1 μ m respectively. B) Quantification of FMRP intensity (Bi) and the number of FMRP-positive granules (Bii) in the experiment described in A. Mean \pm SEM, * $p < 0.05$, ** $p < 0.01$, $n = 3$, unpaired t-test.

FMRP has been reported to promote the formation of stress granules [136] and aberrant stress granules formation has been linked to neurodegeneration [137]. Thus, we examined whether the observed increase in FMRP levels could trigger the assembly and/or accumulation of stress granules in DRG neurons depleted of Dynlrb1. Stress granules were visualized by immunofluorescence staining of G3bp1, one of the most abundant RBPs that is crucial for stress granule formation [63]. Indeed, Dynlrb1 knockdown induced a significant increase in G3bp1 level (**Figure 3.19A&B**). Moreover, quantification of G3bp1 intra-axonal signal revealed a significant increase in the number of G3bp1 granules without significantly impacting their size (**Figure 3.19C**).

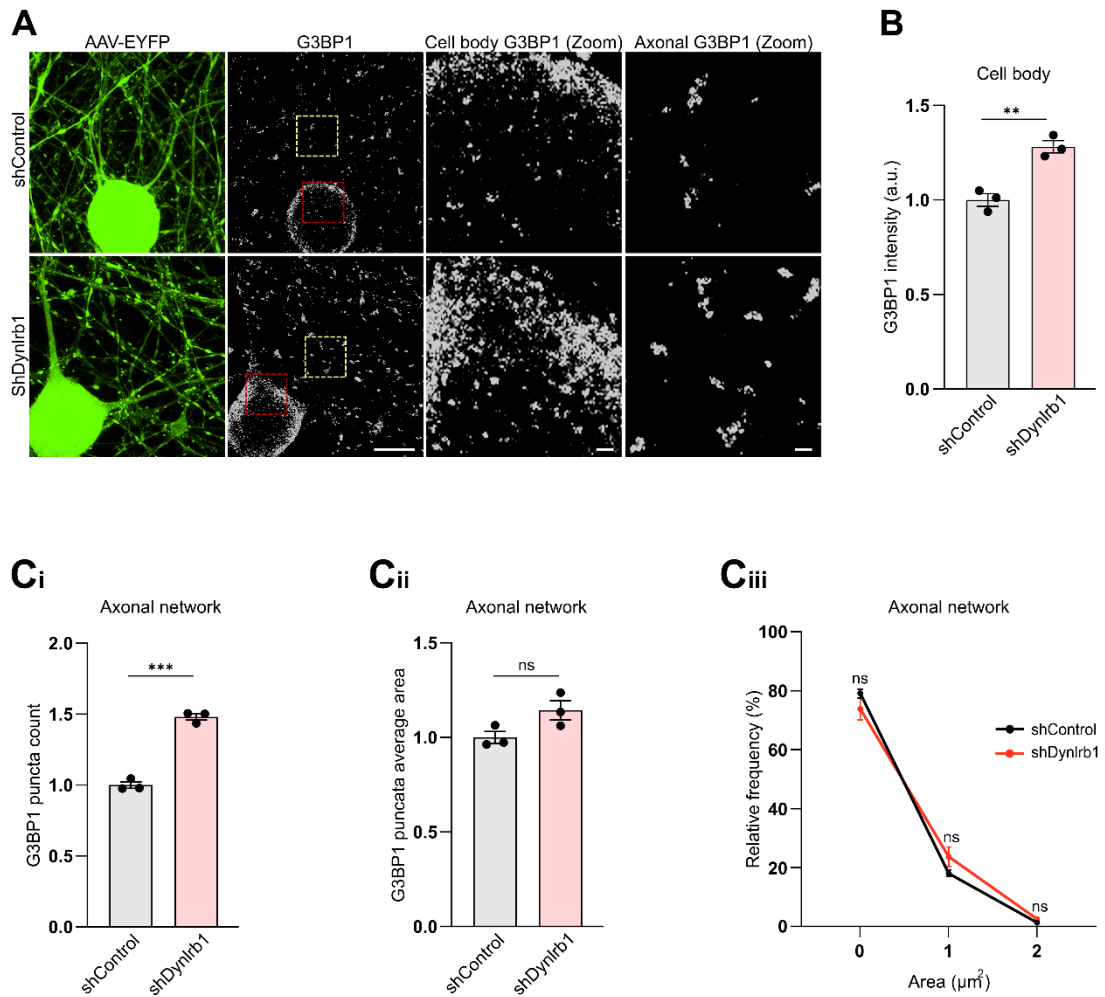


Figure 3.19. Dynlrb1 silencing induces stress granule formation. A) Representative images of shControl or shDynlrb1 DRG neurons. Stress granules are visualized with anti-G3bp1 antibody (grayscale). Transduced neurons are labeled by EYFP (in green). Scale bars 10 μm , 1 μm and 1 μm respectively. B) Quantification of somatic G3bp1 intensity. Mean \pm SEM, ** $p < 0.01$, $n = 3$, unpaired t-test. C) Quantification of the number (Ci), area (Cii) and relative frequency (Ciii) of axonal G3bp1 puncta. Mean \pm SEM, *** $p < 0.001$, ns not significant, $n = 3$, unpaired t-test.

We then tested whether the loss of Dynlrb1 impairs FMRP degradation by western blot analysis. Neuronal cultures transduced with shDynlrb1 or shControl were incubated for 6 h with the proteasome inhibitor (MG132) or a cocktail of lysosomal inhibitors (leupeptin, pepstatin A and E-64d) before protein extraction. Interestingly, both proteasomal and lysosomal inhibition led to a 2- to 2.5-fold increase in the levels of FMRP in shControl neurons (**Figure 3.20.**). In contrast, MG132 failed to elicit any significant increase of FMRP levels in shDynlrb1 neurons, whereas lysosomal inhibitors induced a minimal but non-significant increase in FMRP protein levels (**Figure 3.20.**). These data suggest that both the proteasomal and lysosomal pathways work hand in hand in adult sensory neurons to tightly control FMRP levels and that FMRP degradation capacity is saturated in DRG neurons depleted of Dynlrb1.

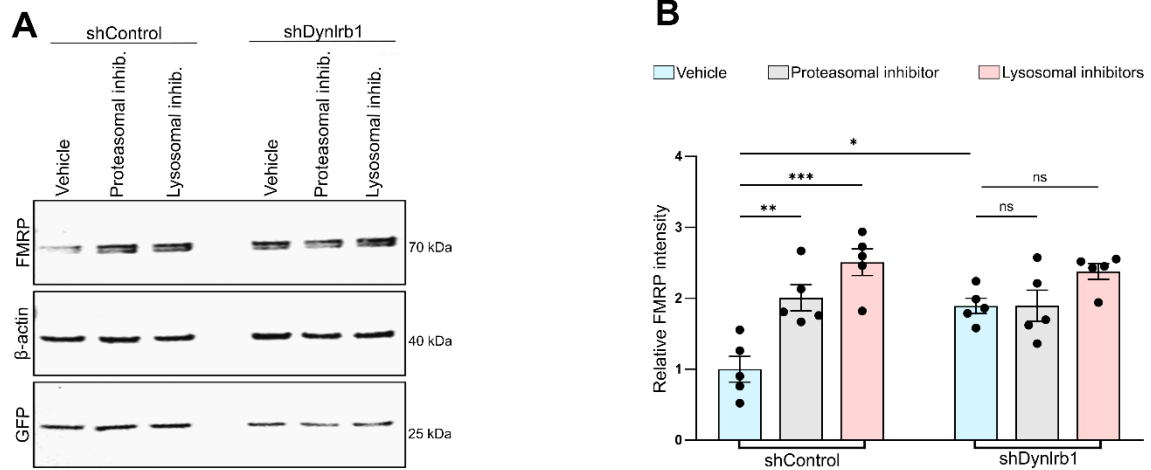


Figure 3.20. Genetic depletion of Dynlrb1 impairs FMRP degradation. A) Western blot analysis of FMRP protein levels in shControl or shDynlrb1 DRG neurons after incubation with proteasomal inhibitor (MG132), lysosomal inhibitors (leupeptin, pepstatin A and E-64d) or vehicles for 6 h. β -actin immunostaining was used to normalize FMRP levels. Viral transduction efficiency was visualized by an anti-GFP antibody. B) Quantification of the experiment described in A. Mean \pm SEM, $n=5$, * $p < 0.05$, ** $p < 0.01$, *** $p < 0.001$, ns not significant, one-way ANOVA followed by Tukey's HSD post hoc correction for multiple comparisons.

We next investigated whether the impaired FMRP degradation and the consequent dysregulation of its granule formation could affect the translation of its mRNA targets. We first assessed the localization of the microtubule-associated protein 1b (Map1b) mRNA, a well-known target of FMRP [138], with FMRP granules using RNA *in situ* hybridization (ISH) combined with immunofluorescence staining. Map1b mRNA exhibited a punctated staining pattern that colocalized with FMRP granules (**Figure 3.21A**). Interestingly, Map1b mRNA sequestration in FMRP granules was increased after Dynlrb1 depletion compared to shControl neurons (**Figure 3.21A&B**). The specificity of the Map1b signal was confirmed by the absence of the ISH signal upon hybridization of a negative control probe (**Figure 3.21C**).

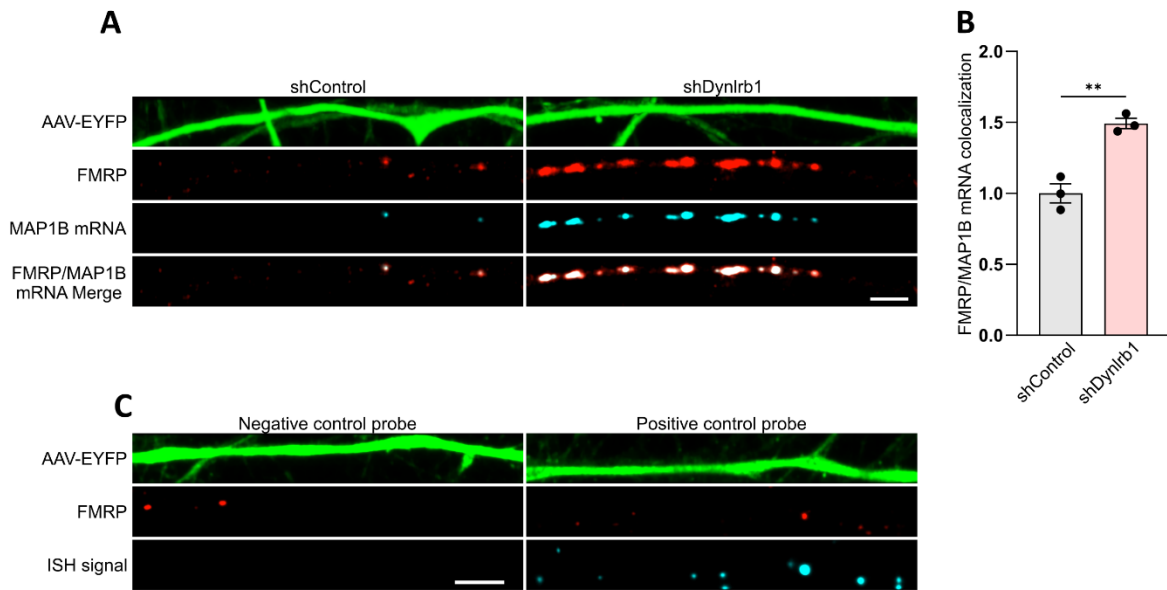


Figure 3.21. FMRP accumulations in Dynlrb1 depleted neurons sequester Map1b mRNA. A) Representative images of integrated in situ hybridization (ISH) for Map1b mRNA and FMRP immunostaining in DRG neurons transduced with shControl or shDynlrb1. Transduced neurons are labelled by EYFP expressed by the viral constructs (in green). ISH signal is in Turquoise. Scale bar 5 μ m. B) Quantification of the axonal colocalization between FMRP and Map1b mRNA in the experiment described in A. Mean \pm SEM, n=3, ** p<0.01, unpaired t-test. RNAscope controls for Map1b mRNA detection in DRG neurons A) Representative images of in situ hybridization signal obtained with negative and positive RNAscope control probes (in Turquoise). Neurons are labelled with EYFP expressed by the viral constructs (in green). FMRP immunostaining signal is in red. Scale bar 5 μ m.

Subsequently, we examined the effect of Dynlrb1 depletion on Map1b translation. Direct visualization of newly synthesized Map1b by combining puromycin labeling and PLA revealed a significant reduction in Map1b translation in Dynlrb1 knockdown neurons (**Figure 3.22A, C&D**). The specificity of the PLA signal was determined by pre-treatment with 40 μ M anisomycin, a protein synthesis inhibitor, as a negative control (**Figure 3.22B, C&D**). Collectively, these results are in accordance with previous literature correlating FMRP condensation with translation inhibition [65], [139], and could, at least in part, explain the impaired axonal outgrowth described in Dynlrb1 heterozygous mouse model [43].

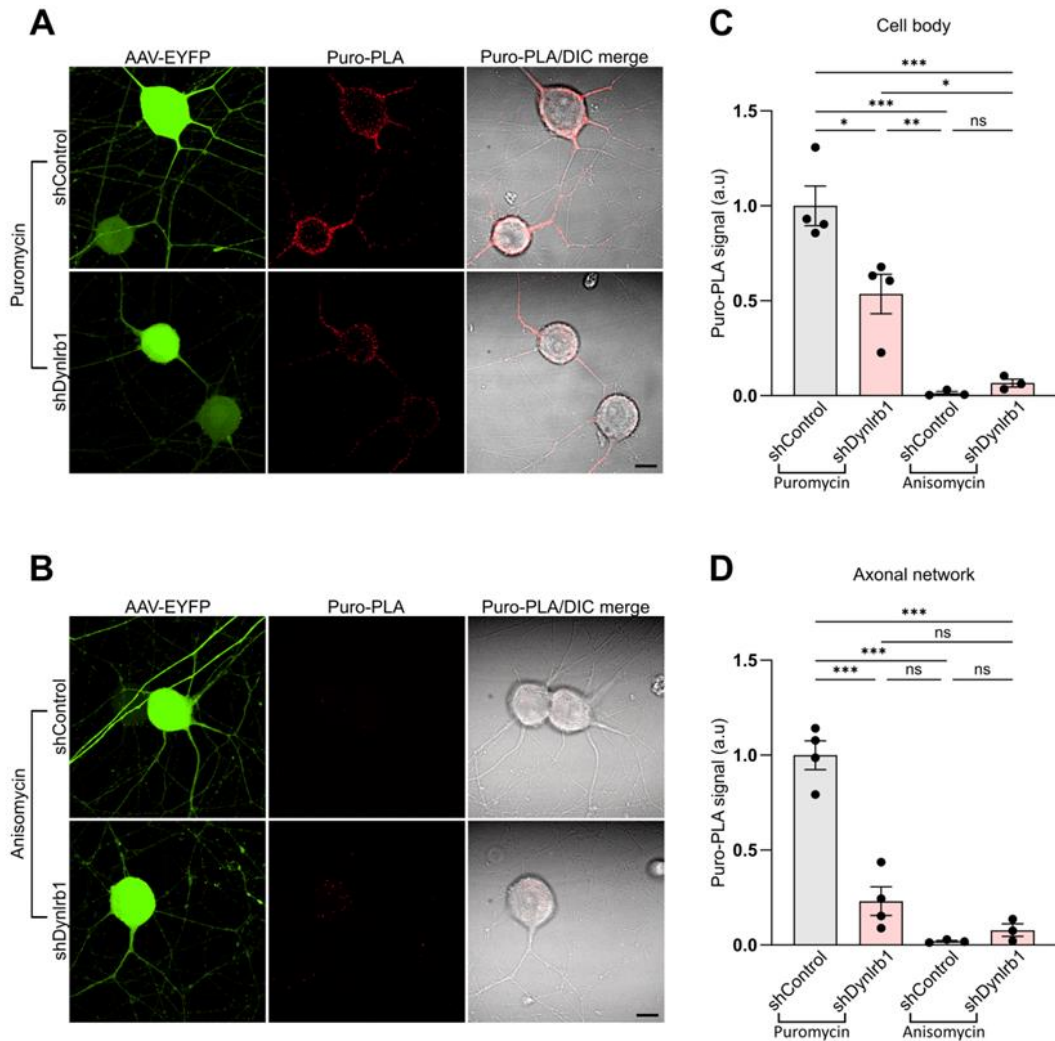


Figure 3.22. Dynlrb1 silencing impairs Map1b translation. A) Representative images of newly synthesized Map1b in puromycin treated shControl or shDynlrb1 DRG neurons detected by PLA between anti-puromycin and anti-Map1b antibodies. Neurons were incubated with puromycin for 10 min to label newly translated proteins. Transduced neurons are labeled by EYFP expressed by the viral constructs (in green). PLA signal is in red. Scale bar 10 μ m. B) Representative images of newly synthesized Map1b in anisomycin treated shControl or shDynlrb1 DRG neurons. Neurons were incubated with 40 μ M anisomycin for 30 min prior to incubation with puromycin for 10 min as a negative control for the PLA reaction in A. Transduced neurons are labeled by EYFP expressed by the viral constructs (in green). PLA signal is in red and detected by PLA between anti-puromycin and anti-Map1b antibodies. Scale bar 10 μ m. C&D) Quantification of the puro-PLA signal for the experiment described in A&B in the somatic and axonal compartments respectively. Mean \pm SEM, $n \geq 3$, * $p < 0.05$, ** $p < 0.01$, *** $p < 0.001$, ns not significant, one-way ANOVA followed by Tukey's HSD post hoc correction for multiple comparisons.

Chapter 4.

Discussion

Cytoplasmic dynein is the main retrograde molecular motor thus it plays a crucial role in all eukaryotic cells, particularly in highly polarized cells such as neurons. Indeed, disruption of the function of dynein, or its co-factor dynactin, has been implicated in motor neuron degeneration, including ALS [3], [5], [50]. More than 30 missense heterozygous mutations within the dynein heavy chain were linked to neurological disorders in humans. The link between *Dync1h1* mutations and disease was further reinforced by the motor and sensory deficits observed in the heterozygous *Dync1h1* mutant mouse models [3]. Comparably, conditional *Dynlrb1* depletion was shown to negatively impact proprioceptive neuronal survival, suggesting its involvement in dynein-dependent transport and signaling [43]. Two roadblock isoforms are expressed in mammalian cells, *Dynlrb1* and *Dynlrb2*. Similar to other subunits, isoform diversity could define distinct dynein populations with unique functions [9], [140]. Previous interactome studies for *Dynlrb1* yielded only a few hits [44]–[47]. Nonetheless, the observed neuronal loss upon *Dynlrb1* depletion cannot be fully explained by these interactions. Thus, we used a proximity labeling approach coupled with mass spectrometry to identify *Dynlrb1* interactome in sensory neurons.

To select candidates for further validation and characterization, the putative interactors list was refined through a literature review to highlight candidates involved in neuronal homeostasis (disruption of their interaction with *Dynlrb1* could contribute to the neuronal loss observed upon its depletion). While the list includes candidates with high enrichment values and statistical significance, we opted to prioritize the potential physiological significance of the interaction over its frequency. The three candidates chosen for validation are involved in intracellular trafficking and translational regulation and thus are also representative of the enriched GO categories in the functional enrichment analysis (**Figure 3.4B**). Given FMRP's implication in neurological disorders, its involvement in the proper functioning of the spinal sensory system as evident by the sensory deficits reported in patients afflicted with FXS and FXTAS [141], and the relative lack of data regarding its interaction with the dynein complex in mammalian systems, it was selected for further investigations.

Increasing evidence shows how mRNA, miRNA, and RNA granules hitchhike onto membranous organelles for long-range transport [30], and that late endosomes can act as a platform for mRNA translation [28]. Utilizing live imaging and PLA analysis, I show how the long-range transport of endolysosomes and FMRP granules is closely linked (**Figure 3.8.**) and dependent on *Dynlrb1* (**Figure 3.14.**). Speed distribution showed that FMRP anterograde peak aligns with that of the lysotracker-positive organelles while the retrograde peak displays a selective association with a pool of lysotracker-positive vesicles. Lysotracker can incorporate into mildly acidic organelles ($\text{pH} \leq 6$) thus labeling several organelles including lysosomes, late endosomes, and multivesicular bodies. It is possible that retrogradely trafficked FMRP only associates with one of these compartments. Whether FMRP pairing to endolysosomes is dependent on the degree of acidification requires further investigation.

Recently, Lippincott-Schwartz and Ward groups identified Anxa11 as an adaptor that tethers G3bp1 granules to Lamp1-positive organelles for long-range trafficking [29]. Anxa11 mutations impacting its propensity to phase separate and its association with lysosomal vesicles have been implicated in familial ALS pathogenesis [133]. Interestingly, Anxa11 was one of the candidates identified in our proteomics screen (**Table 1**). And subsequent PLA analysis suggests that at least a population of FMRP granules utilize the same molecular adaptor to dock on Lamp1-positive organelles in sensory neurons (**Figure 3.10**). Endolysosomes represent an ideal platform for the tethering of FMRP granules given the speed and extent of their transport. Moreover, the pairing of FMRP granules to lysosomes could provide an opportunity for internalization and degradation by microautophagy [29], [142]. Indeed, overexpressed FMRP was found inside lysosomal compartments via electron microscopy [143], and our data suggests a block of FMRP lysosomal degradation upon Dynlrb1 depletion (**Figure 3.20**). Furthermore, since FMRP-mediated translation is dependent on synaptic activity, retrograde transport of a pool of RNA granules could support a model in which mRNAs patrol different synaptic sites until being recruited by an active site rather than being permanently anchored at a specific synapse [65], [144]. Indeed, FMRP is a key regulator of the translation of critical proteins for synaptic signaling [59], [70]. Retrograde trafficking has been previously described for G3bp1 and La granules [25], [29]. And was also proposed to support the recycling of mRNAs back to the soma to regulate the copy number of specific axonal mRNAs [145].

The data presented in this thesis together with earlier work from our group [43] suggests the involvement of Dynlrb1 in the retrograde trafficking of a broad range of organelles in sensory neurons. The extent to which these cargos are impacted is variable, with the mitochondria (**Figure 3.17**) and the signaling endosomes [43] seemingly less affected than lysotracker-positive organelles, where both the speed profile and the frequency of mobile carriers are reduced to a greater extent (**Figure 3.14**). Thus, Dynlrb1 depletion could be impacting a specific pool of dynein recruited mostly to endolysosomes. Dynlrb1 could be involved in directly linking cargos and/or adaptor proteins to dynein. Alternatively, it could play a role in regulating dynein localization and/or processive motility. Dynlrb dimer binding to dynein intermediate chain provides one of three tail contact sites between dync1h1 dimer in phi (ϕ) conformation [11], [146]. While the ϕ conformation lacks processive motility, and structure-based mutation of the motor dimerization contact sites drives dynein into a more open conformation with higher affinity to both dynactin and MT, this conformation seems to play a significant regulatory role on account of the multiple mutations within the ϕ interface linked to SMA-LED and MCD [11]. Site-directed mutagenesis of the ϕ interface was shown to increase centrosomal dynein localization in mitotic cells [11]. Whether Dynlrb1, but not Dynlrb2, is required to stabilize the phi particle and thus regulate the axonal localization of at least a subpopulation of dynein remains to be assessed.

The two main degradative pathways in eukaryotic cells are the UPS and the autophagy-lysosomal system with the former mediating the degradation of the individual proteins marked with ubiquitin tags including damaged and misfolded proteins and the latter mostly removing aggregated proteins as well as damaged organelles [14]. Perturbation of either proteolytic pathways have been linked to neurodegenerative disorders [147], [148]. Herein, I show that Dynlrb1 silencing impairs both the lysosomal and proteasomal degradation of FMRP (**Figure 3.20**). The impaired lysosomal degradation could be, at least in part, explained by the impaired retrograde trafficking of acidic organelles. While some degradation can occur locally through degradative lysosomes being continuously delivered

to axonal tips [21], [149], the majority of enzymatically active degradative lysosomes reside in the soma which necessitate efficient dynein-dependent shuttling of mildly acidic organelles. Moreover, the proteomics data identified both Vps29 and Vta1 (**Figure 3.5., Table 1.**), two proteins involved in endosomal and multivesicular body sorting and lysosomal acidification [150]–[152]. It would be of interest to assess whether these associations pose any functional significance. In the context of proteasomal block, the N-terminal domain of FMRP is prone to intrinsically fold into β -rich structures, promoting the formation of fibrillar aggregates [153], [154]. Pioneering work from Ron Kopito's lab has shown that protein aggregation inhibits the UPS [155], with similar findings also reported from other groups [156], [157]. Upon the accumulation of aggregation-prone proteins beyond the capacity of the UPS, a state of proteostasis could be attained through dynein-mediated transport and formation of aggresomes. FMRP granules, induced by controlled overexpression of FMRP in motor neurons, were reported to sequester HDAC6, a protein that facilitates aggresome-mediated clearance of misfolded proteins and is involved in promoting autophagosomes-lysosomes fusion events [39] [158]. Furthermore, an *in silico* model proposed that NAGK activates dynein processive motility, via association with Dynlrb1, and accordingly reduces mutant huntingtin (mHtt Q74) and α -synuclein (α -syn A53T) aggregation in mouse brain cells [159]. Our proteomics screen did not identify NAGK as a Dynlrb1 interactor in DRG neurons. This can be explained by the difference in neuronal subtypes, the developmental/maturation stage (embryonic cortical neurons vs adult sensory neurons), or the experimental conditions. Nevertheless, follow-up work would be necessary to confirm the proposed model.

Alteration of RNA processing as a result of accumulation of RNP aggregates has been identified as a unifying mechanism underlying the pathogenesis of several neurodegenerative diseases, regardless of the underlying cause [160]. The data presented here shows that Dynlrb1 silencing in sensory neurons promotes aberrant FMRP accumulations (**Figure 3.15., Figure 3.18.**) that further trigger the formation of stress granule inclusions (**Figure 3.19.**). The extent of G3bp1 accumulation is lower compared to the one observed with FMRP, suggesting a secondary effect to FMRP accumulation. And that FMRP and G3bp1 granule populations might not completely overlap in sensory neurons. Nonetheless, Intra-axonal G3bp1 granule accumulation, reminiscent of the one observed in this work, was shown to negatively impact mRNA translation and axonal regeneration in sensory neurons [161]. A controlled FMRP overexpression paradigm in motor neurons was also shown to drive TDP43 accumulations [162].

FMRP's most studied functional role is translational regulation, where it interacts and represses the translation of hundreds of mRNAs [70]. One of its primary targets, distributed across neuronal sub-compartments, is Map1b [70]. Elevated Map1b levels were reported in FXS models as a consequence of the hypoassembly of FMRP granules [138], [163], [164]. The data presented here shows that FMRP accumulation and the enhanced granule formation upon Dynlrb1 depletion sequestered Map1b (**Figure 3.21**) and reduced its availability for translation (**Figure 3.22**). These findings are in line with the literature correlating FMRP condensation with translation inhibition [65], [139]. Map1b is involved in MT stabilization and axonal guidance [165]. Thus its impaired translation could, at least in part, explain the impaired axonal outgrowth described in Dynlrb1 heterozygous mouse [43].

Chapter 5.

Conclusion and Outlook

In this study, I utilized a proximity-based proteomics approach to screen for Dynlrb1 interactors in sensory neurons and identified FMRP as a Dynlrb1 interacting partner. Further analyses showed that FMRP undergoes axonal transport with endolysosomal organelles, likely utilizing Anxa11 as a hitchhiking adaptor. The data presented here supports a pathogenesis model whereby Dynlrb1 silencing stalls FMRP granule trafficking, a process intended to support FMRP clearance and potentially steer spatiotemporal mRNA translation. Moreover, Dynlrb1 depletion promotes FMRP granule formation, hence sequestering FMRP target mRNAs and reducing their availability for translation. Taken together, Dynlrb1 depletion can alter the finely tuned translation dynamics in sensory neurons, ultimately impacting their survival. This work identifies a role for Dynlrb1 in regulating mRNA translation in sensory neurons and correlates axonal transport as another factor in defining the correct phase separation equilibrium thus having a significant impact on neuronal homeostasis and disease pathogenesis. Our findings also pave the road for future work that aims to further investigate Dynlrb1 involvement in dynein trafficking and survival signaling.

5.1. Further investigation of the role of Dynlrb1 in dynein-mediated trafficking

Dynlrb1 depletion was shown to impact a broad range of cargos to different extents, which raises the possibility of involvement of Dynlrb1 in promoting the localization or the motility of the dynein motor. Dynein localization to axonal tips upon Dynlrb1 depletion could be assessed through immunofluorescence staining for Dync1h1. Active dynein localization by kinesin to axonal tips could also be assessed as described before [166]. An inducible cargo trafficking assay in cells depleted of Dynlrb1 could offer some insight into dynein processive motility in the presence or absence of Dynlrb1. Additionally, a cryo-electron microscopy study of the dynein forms (Phi vs open dynein) as well as its association with dynactin in the absence of Dynlrb1 would shed additional light on the mechanisms involved.

5.2. Investigation of the role of Dynlrb1 in regulating FMRP's post-translational modifications

The data presented in **Figure 3.18.** shows that Dynlrb1 depletion results in a significant increase in the number of FMRP granules. which could be, at least in part, attributed to the impairment of FMRP degradation. FMRP's phase separation and degradation are finely tuned with post-translational modifications. Activity-dependent PP2A dephosphorylation promotes FMRP granule disassembly, release of mRNAs for translation, and further triggers FMRP ubiquitination and degradation [65]. An alternative analysis of our proteomics data identifies several subunits of the PP2A enzyme. Thus, it would be interesting to investigate whether Dynlrb1 could regulate FMRP post-translational modifications. To assess this aspect, the level of phosphorylated FMRP would be detected via western blotting and/or immunofluorescence staining upon Dynlrb1 depletion. Additionally, the association

between PP2A and FMRP could be assessed using a proximity ligation assay in the presence and absence of Dynlrb1. This would be also coupled with an assessment of PP2A activity using a PP2A immunoprecipitation phosphatase assay kit.

5.3. Validation of Anxa11 recruitment as a hitchhiking adaptor for FMRP granules

While our data linking FMRP granules and endolysosomal compartments (**Figure 3.8.**, **Figure 3.10.**) is very intriguing, a few more aspects should be addressed in future work. For instance, an electron microscopy study would be essential to ensure that the bulk of FMRP granules is tethered to the endolysosomal membranes rather than being engulfed inside these organelles. In addition, time-lapse imaging of EGFP-FMRP and lysotracker-positive organelles co-trafficking upon Anxa11 depletion should be performed. A better, yet more technically challenging, alternative would be to monitor the co-trafficking of EGFP-FMRP granules and Anxa11 fused to a fluorescent reporter.

5.4. The involvement of Dynlrb1 in neuronal homeostasis

While the work presented in this thesis focuses on characterizing the functional significance of Dynlrb1-FMRP interaction, the proteomics data represents an array of interacting candidates for Dynlrb1 that will be useful for further investigations of Dynlrb1 involvement in neuronal homeostasis. One interesting interactor is Vps29, which associates with Dynlrb1 within the axonal compartment (**Figure 3.5.**). Vps29 is one of three subunits of the retromer cargo recognition complex involved in the proper functioning of the autophagy-lysosomal pathway. The complex was shown to promote the autophagic-mediated clearance of tau [167]. A role in regulating lysosomal acidification, through regulating v-ATPase levels, was also recently proposed in a Vps29 mutant *Drosophila* model [152]. Moreover, the retromer is involved in sorting a variety of cargos including cation-independent mannose 6-phosphate receptors and metabotropic glutamate receptors [168]–[170]. Perturbations of the level or the function of the complex have been linked to neurodegenerative diseases and dynein dysfunction was shown to mimic the features of retromer loss [171]. It will be of interest to explore the involvement of Dynlrb1 with the retromer complex to sustain endocytic sorting and clearance pathways.

5.5. Characterization of FMRP targets in sensory neurons

An additional intriguing aspect would be the impact of FMRP granule accumulation on axonal RNA localization in sensory neurons. FMRP research over the last few decades focused almost solely on the neurodevelopmental defects associated with FMRP depletion within CNS neurons. Identification of FMRP target mRNA for translational repression and localization in sensory neurons could deepen our understanding of nociceptive control and plasticity and could potentially open new therapeutic avenues for the treatment of pain disorders in FXS, FXTAS as well as neuropathic pain.

5.6. Further insights into the link between FMRP granules and neurodegenerative pathologies

Finally, this work raises interesting insights beyond the scope of dynein trafficking and signaling. Whereas hyperassembly of RNP granules and defects of RNA processing were described for a variety of RBPs and further linked to neurodegenerative disease pathogenesis, FMRP's hyperassembly received little attention. FMRP does not function in isolation, it was shown to assemble with TDP43, a prominent RBP involved in ALS pathogenesis, into the same RNPs and cooperatively regulate the translation of specific mRNAs, *Map1b* for instance [172]. FMRP overexpression was also shown to drive the formation of TDP43 inclusions in motor neurons [162]. Moreover, FMRP interacts with FUS (fused in sarcoma), another RBP implicated in ALS. FUS-ALS mutant was shown to sequester FMRP and reduce the translation of its target mRNAs [139]. These observations raise the possibility of the potential involvement of FMRP in ALS pathology. For instance, while FUS aggregation impairs FMRP function, could FMRP accumulations drive FUS aggregation as previously proposed for TDP43. Could FMRP hyperassembly and/or loss of function contribute to ALS pathogenesis. Fragile X proteins are involved in the processing of a subset of miRNAs that were downregulated in the serum of presymptomatic ALS patients [173] and were shown to aggregate in lumbar spinal cord samples from familial and sporadic ALS patients [174].

References

- [1] S. Maday, A. E. Twelvetrees, A. J. Moughamian, and E. L. F. Holzbaur, “Axonal Transport: Cargo-Specific Mechanisms of Motility and Regulation,” *Neuron*, vol. 84, no. 2. Cell Press, pp. 292–309, Oct. 22, 2014. doi: 10.1016/j.neuron.2014.10.019.
- [2] L. Guillaud, S. E. El-Agamy, M. Otsuki, and M. Terenzio, “Anterograde Axonal Transport in Neuronal Homeostasis and Disease,” *Front. Mol. Neurosci.*, vol. 13, p. 556175, 2020, doi: 10.3389/fnmol.2020.556175.
- [3] G. Schiavo, L. Greensmith, M. Hafezparast, and E. M. C. Fisher, “Cytoplasmic dynein heavy chain: The servant of many masters,” *Trends in Neurosciences*, vol. 36, no. 11. Elsevier Current Trends, pp. 641–651, Nov. 01, 2013. doi: 10.1016/j.tins.2013.08.001.
- [4] J. N. Sleight, A. M. Rossor, A. D. Fellows, A. P. Tosolini, and G. Schiavo, “Axonal transport and neurological disease,” *Nature Reviews Neurology*, vol. 15, no. 12. Nature Research, pp. 691–703, Dec. 01, 2019. doi: 10.1038/s41582-019-0257-2.
- [5] L. G. Bilslund, E. Sahai, G. Kelly, M. Golding, L. Greensmith, and G. Schiavo, “Deficits in axonal transport precede ALS symptoms in vivo,” *Proc. Natl. Acad. Sci. U. S. A.*, vol. 107, no. 47, pp. 20523–20528, Nov. 2010, doi: 10.1073/PNAS.1006869107/-DCSUPPLEMENTAL.
- [6] J. N. Sleight *et al.*, “Boosting peripheral BDNF rescues impaired in vivo axonal transport in CMT2D mice” *JCI Insight*, vol. 8, no. 9, May 2023, doi: 10.1172/JCI.INSIGHT.157191.
- [7] S. L. Reck-Peterson, W. B. Redwine, R. D. Vale, and A. P. Carter, “The cytoplasmic dynein transport machinery and its many cargoes,” *Nature Reviews Molecular Cell Biology*, vol. 19, no. 6. Nature Publishing Group, pp. 382–398, Jun. 01, 2018. doi: 10.1038/s41580-018-0004-3.
- [8] A. P. Carter, “Crystal clear insights into how the dynein motor moves,” *Journal of Cell Science*, vol. 126, no. 3. pp. 705–713, Feb. 01, 2013. doi: 10.1242/jcs.120725.
- [9] K. K. Pfister, “Distinct functional roles of cytoplasmic dynein defined by the intermediate chain isoforms,” *Experimental Cell Research*, vol. 334, no. 1. Academic Press Inc., pp. 54–60, May 15, 2015. doi: 10.1016/j.yexcr.2014.12.013.
- [10] K. K. Pfister *et al.*, “Genetic analysis of the cytoplasmic dynein subunit families,” *PLoS Genetics*, vol. 2, no. 1. Public Library of Science, pp. 11–26, Jan. 2006. doi: 10.1371/journal.pgen.0020001.
- [11] K. Zhang *et al.*, “Cryo-EM Reveals How Human Cytoplasmic Dynein Is Auto-inhibited and Activated,” *Cell*, vol. 169, no. 7, pp. 1303-1314.e18, Jun. 2017, doi: 10.1016/j.cell.2017.05.025.
- [12] M. A. Olenick and E. L. F. Holzbaur, “dynein activators and adaptors at a glance,” *J. Cell Sci.*, vol. 132, no. 6, Mar. 2019, doi: 10.1242/JCS.227132/57494.
- [13] C. G. Chung, H. Lee, and S. B. Lee, “Mechanisms of protein toxicity in neurodegenerative diseases,” *Cellular and Molecular Life Sciences*, vol. 75, no. 17. Birkhauser Verlag AG, pp. 3159–3180, Sep. 01, 2018. doi: 10.1007/s00018-018-2854-4.
- [14] V. Kumar, N. Sami, T. Kashav, A. Islam, F. Ahmad, and M. I. Hassan, “Protein aggregation and neurodegenerative diseases: From theory to therapy,” *Eur. J. Med. Chem.*, vol. 124, pp. 1105–1120, Nov. 2016, doi: 10.1016/j.ejmech.2016.07.054.
- [15] J. C. Roney, X. T. Cheng, and Z. H. Sheng, “Neuronal endolysosomal transport and lysosomal functionality in maintaining axonostasis,” *J. Cell Biol.*, vol. 221, no. 3, Mar. 2022, doi: 10.1083/JCB.202111077/213000.
- [16] B. Ravikumar *et al.*, “Dynein mutations impair autophagic clearance of aggregate-prone proteins,” *Nat. Genet.*, vol. 37, no. 7, Art. no. 7, Jul. 2005, doi: 10.1038/ng1591.
- [17] E. Christoforidou, F. A. Simoes, D. Gordon, K. Talbot, and M. Hafezparast, “Aberrant dynein function promotes TDP-43 aggregation and upregulation of p62 in male mice harboring transgenic human TDP-43,” *Amyotroph. Lateral Scler. Front. Degener.*, vol. 24, no. 7–8, pp. 746–755, Oct. 2023, doi: 10.1080/21678421.2023.2239276.
- [18] J. Pu, C. M. Guardia, T. Keren-Kaplan, and J. S. Bonifacino, “Mechanisms and functions of lysosome positioning,” *Journal of Cell Science*, vol. 129, no. 23. Company of Biologists Ltd, pp. 4329–4339, 2016. doi: 10.1242/jcs.196287.
- [19] S. Gowrishankar, Y. Wu, and S. M. Ferguson, “Impaired JIP3-dependent axonal lysosome transport promotes amyloid plaque pathology,” *J. Cell Biol.*, vol. 216, no. 10, pp. 3291–3305, Oct. 2017, doi: 10.1083/jcb.201612148.
- [20] S. E. Cason, S. S. Mogre, E. L. F. Holzbaur, and E. F. Koslover, “Spatiotemporal analysis of axonal autophagosome–lysosome dynamics reveals limited fusion events and slow maturation,” *Mol. Biol. Cell*, vol. 33, no. 13, Nov. 2022, doi: 10.1091/MBC.E22-03-0111/ASSET/IMAGES/LARGE/MBC-33-AR123-G008.JPEG.

- [21] T. Farfel-Becker, J. C. Roney, X.-T. Cheng, S. Li, S. R. Cuddy, and Z.-H. Sheng, “Neuronal Soma-Derived Degradative Lysosomes Are Continuously Delivered to Distal Axons to Maintain Local Degradation Capacity,” *Cell Rep.*, vol. 28, no. 1, pp. 51-64.e4, Jul. 2019, doi: 10.1016/j.celrep.2019.06.013.
- [22] S. E. Cason, P. J. Carman, C. Van Duyne, J. Goldsmith, R. Dominguez, and E. L. F. Holzbaur, “Sequential dynein effectors regulate axonal autophagosome motility in a maturation-dependent pathway,” *J. Cell Biol.*, vol. 220, no. 7, p. e202010179, May 2021, doi: 10.1083/jcb.202010179.
- [23] H. J. Wiedner and J. Giudice, “It’s not just a phase: function and characteristics of RNA-binding proteins in phase separation,” *Nat. Struct. Mol. Biol.*, vol. 28, no. 6, Art. no. 6, Jun. 2021, doi: 10.1038/s41594-021-00601-w.
- [24] N. Gershoni-Emek *et al.*, “Proteomic Analysis of Dynein-Interacting Proteins in Amyotrophic Lateral Sclerosis Synaptosomes Reveals Alterations in the RNA-Binding Protein Staufen1,” *Mol. Cell. Proteomics MCP*, vol. 15, no. 2, pp. 506–522, Feb. 2016, doi: 10.1074/mcp.M115.049965.
- [25] E. A. Van Niekerk, D. E. Willis, J. H. Chang, K. Reumann, T. Heise, and J. L. Twiss, “Sumoylation in axons triggers retrograde transport of the RNA-binding protein La,” *Proc. Natl. Acad. Sci. U. S. A.*, vol. 104, no. 31, pp. 12913–12918, Jul. 2007, doi: 10.1073/PNAS.0611562104/SUPPL_FILE/11562MOVIE2.MOV.
- [26] G. S. Wilkie and I. Davis, “Drosophila wingless and pair-rule transcripts localize apically by dynein-mediated transport of RNA particles,” *Cell*, vol. 105, no. 2, pp. 209–219, Apr. 2001, doi: 10.1016/S0092-8674(01)00312-9.
- [27] A. Bianco, M. Dienstbier, H. K. Salter, G. Gatto, and S. L. Bullock, “Bicaudal-D regulates fragile X mental retardation protein levels, motility, and function during neuronal morphogenesis,” *Curr. Biol.*, vol. 20, no. 16, pp. 1487–1492, Aug. 2010, doi: 10.1016/j.cub.2010.07.016.
- [28] J.-M. Cioni *et al.*, “Late Endosomes Act as mRNA Translation Platforms and Sustain Mitochondria in Axons,” *Cell*, vol. 176, no. 1–2, pp. 56–72.e15, Jan. 2019, doi: 10.1016/j.cell.2018.11.030.
- [29] Y. C. Liao *et al.*, “RNA Granules Hitchhike on Lysosomes for Long-Distance Transport, Using Annexin A11 as a Molecular Tether,” *Cell*, vol. 179, no. 1, p. 147, Sep. 2019, doi: 10.1016/J.CELL.2019.08.050.
- [30] J. R. Christensen and S. L. Reck-Peterson, “Hitchhiking Across Kingdoms: Cotransport of Cargos in Fungal, Animal, and Plant Cells,” *Httpsdoiorg101146annurev-Cellbio-120420-104341*, vol. 38, pp. 155–178, Oct. 2022, doi: 10.1146/ANNUREV-CELLBIO-120420-104341.
- [31] L. De Conti, M. Baralle, and E. Buratti, “Neurodegeneration and RNA-binding proteins,” *Wiley Interdiscip. Rev. RNA*, vol. 8, no. 2, p. e1394, Mar. 2017, doi: 10.1002/WRNA.1394.
- [32] A. Jishi, X. Qi, and H. C. Miranda, “Implications of mRNA translation dysregulation for neurological disorders,” *Semin. Cell Dev. Biol.*, vol. 114, p. 11, Jun. 2021, doi: 10.1016/J.SEMCDB.2020.09.005.
- [33] S. B. Yu and G. Pekkurnaz, “Mechanisms Orchestrating Mitochondrial Dynamics for Energy Homeostasis,” *Journal of Molecular Biology*, vol. 430, no. 21. Academic Press, pp. 3922–3941, Oct. 19, 2018. doi: 10.1016/j.jmb.2018.07.027.
- [34] X. T. Cheng, N. Huang, and Z. H. Sheng, “Programming axonal mitochondrial maintenance and bioenergetics in neurodegeneration and regeneration,” *Neuron*, vol. 110, no. 12, pp. 1899–1923, Jun. 2022, doi: 10.1016/J.NEURON.2022.03.015.
- [35] J. T. Canty, A. Hensley, M. Aslan, A. Jack, and A. Yildiz, “TRAK adaptors regulate the recruitment and activation of dynein and kinesin in mitochondrial transport,” *Nat. Commun.*, vol. 14, no. 1, Art. no. 1, Mar. 2023, doi: 10.1038/s41467-023-36945-8.
- [36] D. Villarroya-Campos, G. Schiavo, and O. M. Lazo, “The many disguises of the signalling endosome,” *Febs Lett.*, vol. 592, no. 21, pp. 3615–3632, Nov. 2018, doi: 10.1002/1873-3468.13235.
- [37] K. Deinhardt *et al.*, “Rab5 and Rab7 Control Endocytic Sorting along the Axonal Retrograde Transport Pathway,” *Neuron*, vol. 52, no. 2, pp. 293–305, Oct. 2006, doi: 10.1016/j.neuron.2006.08.018.
- [38] R. Garcia-Mata, Y.-S. Gao, and E. Sztul, “Hassles with Taking Out the Garbage: Aggravating Aggresomes,” *Traffic*, vol. 3, no. 6, pp. 388–396, 2002, doi: 10.1034/j.1600-0854.2002.30602.x.
- [39] Y. Kawaguchi, J. J. Kovacs, A. McLaurin, J. M. Vance, A. Ito, and T.-P. Yao, “The Deacetylase HDAC6 Regulates Aggresome Formation and Cell Viability in Response to Misfolded Protein Stress,” *Cell*, vol. 115, no. 6, pp. 727–738, Dec. 2003, doi: 10.1016/S0092-8674(03)00939-5.
- [40] M. Gamerdinger, A. M. Kaya, U. Wolfrum, A. M. Clement, and C. Behl, “BAG3 mediates chaperone-based aggresome-targeting and selective autophagy of misfolded proteins,” *EMBO Rep.*, vol. 12, no. 2, pp. 149–156, Feb. 2011, doi: 10.1038/embor.2010.203.
- [41] L. Calderilla-Barbosa *et al.*, “Interaction of SQSTM1 with the motor protein dynein – SQSTM1 is required for normal dynein function and trafficking,” *J. Cell Sci.*, vol. 127, no. 18, pp. 4052–4063, Sep. 2014, doi: 10.1242/jcs.152363.
- [42] A. B. Bowman, R. S. Patel-King, S. E. Benashski, J. M. McCaffery, L. S. B. Goldstein, and S. M. King, “Drosophila roadblock and chlamydomonas LC7: A conserved family of dynein-associated proteins

- involved in axonal transport, flagellar motility, and mitosis,” *J. Cell Biol.*, vol. 146, no. 1, pp. 165–179, Jul. 1999, doi: 10.1083/jcb.146.1.165.
- [43] M. Terenzio *et al.*, “DYNLRB1 is essential for dynein mediated transport and neuronal survival,” *Neurobiol. Dis.*, p. 104816, Feb. 2020, doi: 10.1016/j.nbd.2020.104816.
- [44] M. A. Islam, S. R. Sharif, H. Lee, and I. S. Moon, “N-acetyl-D-glucosamine kinase promotes the axonal growth of developing neurons,” *Mol. Cells*, vol. 38, no. 10, pp. 876–885, Oct. 2015, doi: 10.14348/molcells.2015.0120.
- [45] M. A. Islam, S. R. Sharif, H. S. Lee, D. H. Seog, and I. S. Moon, “N-acetyl-D-glucosamine kinase interacts with dynein light-chain roadblock type 1 at Golgi outposts in neuronal dendritic branch points,” *Exp. Mol. Med.*, vol. 47, no. 8, p. e177, Aug. 2015, doi: 10.1038/emm.2015.48.
- [46] B. Wanschers, R. Van De Vorstenbosch, M. Wijers, B. Wieringa, S. M. King, and J. Fransen, “Rab6 family proteins interact with the dynein light chain protein DYNLRB1,” *Cell Motil. Cytoskeleton*, vol. 65, no. 3, pp. 183–196, Mar. 2008, doi: 10.1002/cm.20254.
- [47] Q. Tang *et al.*, “A novel transforming growth factor-beta receptor-interacting protein that is also a light chain of the motor protein dynein,” *Mol. Biol. Cell*, vol. 13, no. 12, pp. 4484–96, Dec. 2002, doi: 10.1091/mbc.e02-05-0245.
- [48] J. Gepner *et al.*, “Cytoplasmic dynein function is essential in *Drosophila melanogaster*,” *Genetics*, vol. 142, no. 3, pp. 865–78, Mar. 1996.
- [49] A. Harada, Y. Takei, Y. Kanai, Y. Tanaka, S. Nonaka, and N. Hirokawa, “Golgi vesiculation and lysosome dispersion in cells lacking cytoplasmic dynein,” *J. Cell Biol.*, vol. 141, no. 1, pp. 51–59, Apr. 1998, doi: 10.1083/jcb.141.1.51.
- [50] M. Hafezparast *et al.*, “Mutations in dynein link motor neuron degeneration to defects in retrograde transport,” *Science*, vol. 300, no. 5620, pp. 808–812, May 2003, doi: 10.1126/science.1083129.
- [51] H. S. Ilieva *et al.*, “Mutant dynein (Loa) triggers proprioceptive axon loss that extends survival only in the SOD1 ALS model with highest motor neuron death,” *Proc. Natl. Acad. Sci. U. S. A.*, vol. 105, no. 34, pp. 12599–12604, Aug. 2008, doi: 10.1073/pnas.0805422105.
- [52] K. M. Ori-McKenney, J. Xu, S. P. Gross, and R. B. Vallee, “A cytoplasmic dynein tail mutation impairs motor processivity,” *Nat. Cell Biol.*, vol. 12, no. 12, pp. 1228–1234, Dec. 2010, doi: 10.1038/ncb2127.
- [53] H. T. Hoang, M. A. Schlager, A. P. Carter, and S. L. Bullock, “DYNC1H1 mutations associated with neurological diseases compromise processivity of dynein-dynactin-cargo adaptor complexes,” *Proc. Natl. Acad. Sci. U. S. A.*, vol. 114, no. 9, pp. E1597–E1606, Feb. 2017, doi: 10.1073/pnas.1620141114.
- [54] M. G. Marzo, J. M. Griswold, K. M. Ruff, R. E. Buchmeier, C. P. Fees, and S. M. Markus, “Molecular basis for dyneinopathies reveals insight into dynein regulation and dysfunction,” *eLife*, vol. 8, p. e47246, Jul. 2019, doi: 10.7554/eLife.47246.
- [55] M. N. Weedon *et al.*, “Exome Sequencing Identifies a DYNC1H1 Mutation in a Large Pedigree with Dominant Axonal Charcot-Marie-Tooth Disease,” *Am. J. Hum. Genet.*, vol. 89, no. 2, pp. 308–312, Aug. 2011, doi: 10.1016/j.ajhg.2011.07.002.
- [56] M. J. Farrer *et al.*, “DCTN1 mutations in Perry syndrome,” *Nat. Genet.*, vol. 41, no. 2, pp. 163–165, Feb. 2009, doi: 10.1038/ng.293.
- [57] T. Konno, O. A. Ross, H. A. G. Teive, J. Sławek, D. W. Dickson, and Z. K. Wszolek, “DCTN1-related neurodegeneration: Perry syndrome and beyond,” *Parkinsonism and Related Disorders*, vol. 41, Elsevier Ltd, pp. 14–24, Aug. 01, 2017, doi: 10.1016/j.parkreldis.2017.06.004.
- [58] F. M. Laird *et al.*, “Motor neuron disease occurring in a mutant dynactin mouse model is characterized by defects in vesicular trafficking,” *J. Neurosci.*, vol. 28, no. 9, pp. 1997–2005, Feb. 2008, doi: 10.1523/JNEUROSCI.4231-07.2008.
- [59] J. D. Richter and X. Zhao, “The Molecular Biology of FMRP: New Insights into Fragile X Syndrome,” *Nat. Rev. Neurosci.*, vol. 22, no. 4, p. 209, Apr. 2021, doi: 10.1038/S41583-021-00432-0.
- [60] R. Hagerman and P. Hagerman, “Fragile X-associated tremor/ataxia syndrome: pathophysiology and management,” *Curr. Opin. Neurol.*, vol. 34, no. 4, pp. 541–546, Aug. 2021, doi: 10.1097/WCO.0000000000000954.
- [61] G. Hoem *et al.*, “The FMRpolyGlycine Protein Mediates Aggregate Formation and Toxicity Independent of the CGG mRNA Hairpin in a Cellular Model for FXTAS,” *Front. Genet.*, vol. 10, 2019, Accessed: Aug. 21, 2023. [Online]. Available: <https://www.frontiersin.org/articles/10.3389/fgene.2019.00249>
- [62] A. Lai, A. N. Valdez-Sinon, and G. J. Bassell, “Regulation of RNA granules by FMRP and implications for neurological diseases,” *Traffic Cph. Den.*, vol. 21, no. 7, pp. 454–462, Jul. 2020, doi: 10.1111/tra.12733.
- [63] S. Hofmann, N. Kedersha, P. Anderson, and P. Ivanov, “Molecular mechanisms of stress granule assembly and disassembly,” *Biochim. Biophys. Acta BBA - Mol. Cell Res.*, vol. 1868, no. 1, p. 118876, Jan. 2021, doi: 10.1016/j.bbamcr.2020.118876.

- [64] J. C. Darnell *et al.*, “Kissing complex RNAs mediate interaction between the Fragile-X mental retardation protein KH2 domain and brain polyribosomes,” *Genes Dev.*, vol. 19, no. 8, pp. 903–918, Apr. 2005, doi: 10.1101/gad.1276805.
- [65] B. Tsang *et al.*, “Phosphoregulated FMRP phase separation models activity-dependent translation through bidirectional control of mRNA granule formation,” *Proc. Natl. Acad. Sci. U. S. A.*, vol. 116, no. 10, pp. 4218–4227, 2019, doi: 10.1073/PNAS.1814385116/-DCSUPPLEMENTAL.
- [66] S. Ceman, W. T. O’Donnell, M. Reed, S. Patton, J. Pohl, and S. T. Warren, “Phosphorylation influences the translation state of FMRP-associated polyribosomes,” *Hum. Mol. Genet.*, vol. 12, no. 24, pp. 3295–3305, Dec. 2003, doi: 10.1093/hmg/ddg350.
- [67] V. C. Nalavadi, R. S. Muddashetty, C. Gross, and G. J. Bassell, “Dephosphorylation-Induced Ubiquitination and Degradation of FMRP in Dendrites: A Role in Immediate Early mGluR-Stimulated Translation,” *J. Neurosci.*, vol. 32, no. 8, pp. 2582–2587, Feb. 2012, doi: 10.1523/JNEUROSCI.5057-11.2012.
- [68] H. Siomi, M. C. Siomi, R. L. Nussbaum, and G. Dreyfuss, “The protein product of the fragile X gene, FMR1, has characteristics of an RNA-binding protein,” *Cell*, vol. 74, no. 2, pp. 291–298, Jul. 1993, doi: 10.1016/0092-8674(93)90420-U.
- [69] G. Dölen *et al.*, “Correction of fragile X syndrome in mice,” *Neuron*, vol. 56, no. 6, pp. 955–962, Dec. 2007, doi: 10.1016/j.neuron.2007.12.001.
- [70] J. C. Darnell *et al.*, “FMRP stalls ribosomal translocation on mRNAs linked to synaptic function and autism,” *Cell*, vol. 146, no. 2, p. 247, Jul. 2011, doi: 10.1016/J.CELL.2011.06.013.
- [71] S. R. Thomson *et al.*, “Cell-Type-Specific Translation Profiling Reveals a Novel Strategy for Treating Fragile X Syndrome,” *Neuron*, vol. 95, no. 3, pp. 550-563.e5, Aug. 2017, doi: 10.1016/j.neuron.2017.07.013.
- [72] S. Das Sharma *et al.*, “Widespread Alterations in Translation Elongation in the Brain of Juvenile Fmr1 Knockout Mice,” *Cell Rep.*, vol. 26, no. 12, pp. 3313-3322.e5, Mar. 2019, doi: 10.1016/j.celrep.2019.02.086.
- [73] A. Hien, G. Molinaro, B. Liu, K. M. Huber, and J. D. Richter, “Ribosome profiling in mouse hippocampus: plasticity-induced regulation and bidirectional control by TSC2 and FMRP,” *Mol. Autism*, vol. 11, no. 1, p. 78, Oct. 2020, doi: 10.1186/s13229-020-00384-9.
- [74] B. Liu *et al.*, “Regulatory discrimination of mRNAs by FMRP controls mouse adult neural stem cell differentiation,” *Proc. Natl. Acad. Sci. U. S. A.*, vol. 115, no. 48, pp. E11397–E11405, Nov. 2018, doi: 10.1073/pnas.1809588115.
- [75] Y. Feng, D. Absher, D. E. Eberhart, V. Brown, H. E. Malter, and S. T. Warren, “FMRP associates with polyribosomes as an mRNP, and the I304N mutation of severe fragile X syndrome abolishes this association,” *Mol. Cell*, vol. 1, no. 1, pp. 109–118, Dec. 1997, doi: 10.1016/s1097-2765(00)80012-x.
- [76] E. Chen, M. R. Sharma, X. Shi, R. K. Agrawal, and S. Joseph, “Fragile X mental retardation protein regulates translation by binding directly to the ribosome,” *Mol. Cell*, vol. 54, no. 3, pp. 407–417, May 2014, doi: 10.1016/j.molcel.2014.03.023.
- [77] H. Shu, E. Donnard, B. Liu, S. Jung, R. Wang, and J. D. Richter, “FMRP links optimal codons to mRNA stability in neurons,” *Proc. Natl. Acad. Sci.*, vol. 117, no. 48, pp. 30400–30411, Dec. 2020, doi: 10.1073/pnas.2009161117.
- [78] G. Hanson and J. Collier, “Codon optimality, bias and usage in translation and mRNA decay,” *Nat. Rev. Mol. Cell Biol.*, vol. 19, no. 1, pp. 20–30, Jan. 2018, doi: 10.1038/nrm.2017.91.
- [79] F. Zhang *et al.*, “Fragile X mental retardation protein modulates the stability of its m6A-marked messenger RNA targets,” *Hum. Mol. Genet.*, vol. 27, no. 22, p. 3936, Nov. 2018, doi: 10.1093/hmg/ddy292.
- [80] E. Santini *et al.*, “Reducing eIF4E-eIF4G interactions restores the balance between protein synthesis and actin dynamics in fragile X syndrome model mice,” *Sci. Signal.*, vol. 10, no. 504, p. eaan0665, Nov. 2017, doi: 10.1126/scisignal.aan0665.
- [81] P. Jin *et al.*, “Biochemical and genetic interaction between the fragile X mental retardation protein and the microRNA pathway,” *Nat. Neurosci.*, vol. 7, no. 2, Art. no. 2, Feb. 2004, doi: 10.1038/nn1174.
- [82] R. S. Muddashetty *et al.*, “Reversible inhibition of PSD-95 mRNA translation by miR-125a, FMRP phosphorylation, and mGluR signaling,” *Mol. Cell*, vol. 42, no. 5, pp. 673–688, Jun. 2011, doi: 10.1016/j.molcel.2011.05.006.
- [83] J. N. S. Vargas, J. N. Sleigh, and G. Schiavo, “Coupling axonal mRNA transport and local translation to organelle maintenance and function,” *Curr. Opin. Cell Biol.*, vol. 74, pp. 97–103, Feb. 2022, doi: 10.1016/J.CEB.2022.01.008.
- [84] I. Dalla Costa *et al.*, “The functional organization of axonal mRNA transport and translation,” *Nat. Rev. Neurosci.* 2020 222, vol. 22, no. 2, pp. 77–91, Dec. 2020, doi: 10.1038/s41583-020-00407-7.

- [85] R. Goering *et al.*, “FMRP promotes RNA localization to neuronal projections through interactions between its RGG domain and G-quadruplex RNA sequences,” *eLife*, vol. 9, p. e52621, doi: 10.7554/eLife.52621.
- [86] M. A. McClintock *et al.*, “RNA-directed activation of cytoplasmic dynein-1 in reconstituted transport RNPs,” *eLife*, vol. 7, Jun. 2018, doi: 10.7554/ELIFE.36312.
- [87] S. Baumann, A. Komissarov, M. Gili, V. Ruprecht, S. Wieser, and S. P. Maurer, “A reconstituted mammalian APC-kinesin complex selectively transports defined packages of axonal mRNAs,” *Sci. Adv.*, vol. 6, no. 11, 2020, doi: 10.1126/SCIADV.AAZ1588/SUPPL_FILE/AAZ1588_SM.PDF.
- [88] R. El Fatimy *et al.*, “Tracking the Fragile X Mental Retardation Protein in a Highly Ordered Neuronal RiboNucleoParticles Population: A Link between Stalled Polyribosomes and RNA Granules,” *PLoS Genet.*, vol. 12, no. 7, p. e1006192, Jul. 2016, doi: 10.1371/JOURNAL.PGEN.1006192.
- [89] L. N. Antar, R. Afroz, J. B. Dichtenberg, R. C. Carroll, and G. J. Bassell, “Metabotropic glutamate receptor activation regulates fragile x mental retardation protein and FMR1 mRNA localization differentially in dendrites and at synapses,” *J. Neurosci. Off. J. Soc. Neurosci.*, vol. 24, no. 11, pp. 2648–2655, Mar. 2004, doi: 10.1523/JNEUROSCI.0099-04.2004.
- [90] L. N. Antar, C. Li, H. Zhang, R. C. Carroll, and G. J. Bassell, “Local functions for FMRP in axon growth cone motility and activity-dependent regulation of filopodia and spine synapses,” *Mol. Cell. Neurosci.*, vol. 32, no. 1–2, pp. 37–48, 2006, doi: 10.1016/j.mcn.2006.02.001.
- [91] C. Li, G. J. Bassell, and Y. Sasaki, “Fragile X Mental Retardation Protein is Involved in Protein Synthesis-Dependent Collapse of Growth Cones Induced by Semaphorin-3A,” *Front. Neural Circuits*, vol. 3, p. 11, 2009, doi: 10.3389/neuro.04.011.2009.
- [92] R. Fan and K.-O. Lai, “Understanding how kinesin motor proteins regulate postsynaptic function in neuron,” *FEBS J.*, vol. 289, no. 8, pp. 2128–2144, 2022, doi: 10.1111/febs.16285.
- [93] J. B. Dichtenberg, S. A. Swanger, L. N. Antar, R. H. Singer, and G. J. Bassell, “A Direct Role for FMRP in Activity-Dependent Dendritic mRNA Transport Links Filopodial-Spine Morphogenesis to Fragile X Syndrome,” *Dev. Cell*, vol. 14, no. 6, pp. 926–939, Jun. 2008, doi: 10.1016/j.devcel.2008.04.003.
- [94] D.-I. Kao, G. M. Aldridge, I. J. Weiler, and W. T. Greenough, “Altered mRNA transport, docking, and protein translation in neurons lacking fragile X mental retardation protein,” *Proc. Natl. Acad. Sci. U. S. A.*, vol. 107, no. 35, pp. 15601–15606, Aug. 2010, doi: 10.1073/pnas.1010564107.
- [95] P. S. Estes, M. O’Shea, S. Clasen, and D. C. Zarnescu, “Fragile X protein controls the efficacy of mRNA transport in *Drosophila* neurons,” *Mol. Cell. Neurosci.*, vol. 39, no. 2, pp. 170–179, Oct. 2008, doi: 10.1016/j.mcn.2008.06.012.
- [96] M. R. Akins, H. F. LeBlanc, E. E. Stackpole, E. Chyung, and J. R. Fallon, “Systematic mapping of Fragile X granules in the mouse brain reveals a potential role for presynaptic FMRP in sensorimotor functions,” *J. Comp. Neurol.*, vol. 520, no. 16, pp. 3687–3706, 2012, doi: 10.1002/cne.23123.
- [97] M. R. Akins *et al.*, “Axonal ribosomes and mRNAs associate with fragile X granules in adult rodent and human brains,” *Hum. Mol. Genet.*, vol. 26, no. 1, pp. 192–209, Jan. 2017, doi: 10.1093/hmg/ddw381.
- [98] S. Markmiller *et al.*, “Context-Dependent and Disease-Specific Diversity in Protein Interactions within Stress Granules,” *Cell*, vol. 172, no. 3, pp. 590–604.e13, Jan. 2018, doi: 10.1016/j.cell.2017.12.032.
- [99] B. Di Marco *et al.*, “Fragile X mental retardation protein (FMRP) and metabotropic glutamate receptor subtype 5 (mGlu5) control stress granule formation in astrocytes,” *Neurobiol. Dis.*, vol. 154, p. 105338, Jul. 2021, doi: 10.1016/j.nbd.2021.105338.
- [100] T. H. Kim, B. Tsang, R. M. Vernon, N. Sonenberg, L. E. Kay, and J. D. Forman-Kay, “Phospho-dependent phase separation of FMRP and CAPRIN1 recapitulates regulation of translation and deadenylation,” *Science*, vol. 365, no. 6455, pp. 825–829, Aug. 2019, doi: 10.1126/science.aax4240.
- [101] Y. Luo, Z. Na, and S. A. Slavoff, “P-Bodies: Composition, Properties, and Functions,” *Biochemistry*, vol. 57, no. 17, pp. 2424–2431, May 2018, doi: 10.1021/acs.biochem.7b01162.
- [102] E. K. Lee *et al.*, “hnRNP C promotes APP translation by competing with FMRP for APP mRNA recruitment to P bodies,” *Nat. Struct. Mol. Biol.*, vol. 17, no. 6, Art. no. 6, Jun. 2010, doi: 10.1038/nsmb.1815.
- [103] J. C. Darnell, K. B. Jensen, P. Jin, V. Brown, S. T. Warren, and R. B. Darnell, “Fragile X mental retardation protein targets G quartet mRNAs important for neuronal function,” *Cell*, vol. 107, no. 4, pp. 489–499, Nov. 2001, doi: 10.1016/s0092-8674(01)00566-9.
- [104] S. Stefanovic, G. J. Bassell, and M. R. Mihailescu, “G quadruplex RNA structures in PSD-95 mRNA: potential regulators of miR-125a seed binding site accessibility,” *RNA*, vol. 21, no. 1, pp. 48–60, Jan. 2015, doi: 10.1261/rna.046722.114.
- [105] S. Stefanovic, B. A. DeMarco, A. Underwood, K. R. Williams, G. J. Bassell, and M. Rita Mihailescu, “Fragile X mental retardation protein interactions with a G quadruplex structure in the 3'-untranslated

- region of NR2B mRNA,” *Mol. Biosyst.*, vol. 11, no. 12, pp. 3222–3230, 2015, doi: 10.1039/C5MB00423C.
- [106] L. Menon, S. A. Mader, and M.-R. Mihailescu, “Fragile X mental retardation protein interactions with the microtubule associated protein 1B RNA,” *RNA*, vol. 14, no. 8, pp. 1644–1655, Aug. 2008, doi: 10.1261/rna.1100708.
- [107] M. Ascano *et al.*, “FMRP targets distinct mRNA sequence elements to regulate protein expression,” *Nature*, vol. 492, no. 7429, pp. 382–386, Dec. 2012, doi: 10.1038/nature11737.
- [108] M. Li *et al.*, “Identification of FMR1-regulated molecular networks in human neurodevelopment,” *Genome Res.*, vol. 30, no. 3, pp. 361–374, Mar. 2020, doi: 10.1101/gr.251405.119.
- [109] K. Sawicka *et al.*, “FMRP has a cell-type-specific role in CA1 pyramidal neurons to regulate autism-related transcripts and circadian memory,” *eLife*, vol. 8, p. e46919, Dec. 2019, doi: 10.7554/eLife.46919.
- [110] “FMRP binding to a ranked subset of long genes is revealed by coupled CLIP and TRAP in specific neuronal cell types | bioRxiv.” Accessed: Sep. 11, 2023. [Online]. Available: <https://www.biorxiv.org/content/10.1101/762500v1.full>
- [111] S. S. Tran *et al.*, “Widespread RNA editing dysregulation in brains from autistic individuals,” *Nat. Neurosci.*, vol. 22, no. 1, Art. no. 1, Jan. 2019, doi: 10.1038/s41593-018-0287-x.
- [112] I. Napoli *et al.*, “The Fragile X Syndrome Protein Represses Activity-Dependent Translation through CYFIP1, a New 4E-BP,” *Cell*, vol. 134, no. 6, pp. 1042–1054, Sep. 2008, doi: 10.1016/j.cell.2008.07.031.
- [113] P. Samavarchi-Tehrani, R. Samson, and A.-C. Gingras, “Proximity dependent biotinylation: key enzymes and adaptation to proteomics approaches,” *Mol. Cell. Proteomics*, p. mcp.R120.001941, Mar. 2020, doi: 10.1074/mcp.r120.001941.
- [114] A. C. Gingras, K. T. Abe, and B. Raught, “Getting to know the neighborhood: using proximity-dependent biotinylation to characterize protein complexes and map organelles,” *Current Opinion in Chemical Biology*, vol. 48. Elsevier Ltd, pp. 44–54, Feb. 01, 2019. doi: 10.1016/j.cbpa.2018.10.017.
- [115] S. E. El-Agamy, L. Guillaud, K. Kono, Y. Wu, and M. Terenzio, “FMRP long-range transport and degradation are mediated by Dynlrb1 in sensory neurons,” *Mol. Cell. Proteomics*, vol. 0, no. 0, Sep. 2023, doi: 10.1016/j.mcpro.2023.100653.
- [116] M. F. Emily, L. Agrawal, P. Barzaghi, M. Otsuki, and M. Terenzio, “Use of Microfluidics Chambers to Image Axonal transport in Adult Sensory Neurons,” *Methods Mol. Biol. Clifton NJ*, vol. 2431, pp. 271–288, 2022, doi: 10.1007/978-1-0716-1990-2_14.
- [117] K. Y. Chan *et al.*, “Engineered AAVs for efficient noninvasive gene delivery to the central and peripheral nervous systems,” *Nat. Neurosci.*, vol. 20, no. 8, pp. 1172–1179, Aug. 2017, doi: 10.1038/nn.4593.
- [118] K. Dorgans, D. Guo, K. Kurima, J. Wickens, and M. Y. Uusisaari, “Designing AAV Vectors for Monitoring the Subtle Calcium Fluctuations of Inferior Olive Network in vivo,” *Front. Cell. Neurosci.*, vol. 16, p. 172, Apr. 2022, doi: 10.3389/FNCEL.2022.825056/XML/NLM.
- [119] T. C. Branon *et al.*, “Efficient proximity labeling in living cells and organisms with TurboID,” *Nat. Biotechnol.*, vol. 36, no. 9, pp. 880–887, Oct. 2018, doi: 10.1038/nbt.4201.
- [120] H. Yu *et al.*, “Tet3 regulates synaptic transmission and homeostatic plasticity via DNA oxidation and repair,” *Nat. Neurosci.*, vol. 18, no. 6, pp. 836–843, Jun. 2015, doi: 10.1038/NN.4008.
- [121] A. Stetler *et al.*, “Identification and characterization of the methyl arginines in the fragile X mental retardation protein Fmrp,” *Hum. Mol. Genet.*, vol. 15, no. 1, pp. 87–96, Jan. 2006, doi: 10.1093/HMG/DDI429.
- [122] I. Rishal *et al.*, “Axoplasm isolation from peripheral nerve,” *Dev. Neurobiol.*, vol. 70, no. 2, pp. 126–133, 2010, doi: 10.1002/dneu.20755.
- [123] R. Fischer and B. M. Kessler, “Gel-aided sample preparation (GASP)—A simplified method for gel-assisted proteomic sample generation from protein extracts and intact cells,” *PROTEOMICS*, vol. 15, no. 7, pp. 1224–1229, Apr. 2015, doi: 10.1002/PMIC.201400436.
- [124] J. Rappsilber, M. Mann, and Y. Ishihama, “Protocol for micro-purification, enrichment, pre-fractionation and storage of peptides for proteomics using StageTips,” *Nat. Protoc.*, vol. 2, no. 8, pp. 1896–1906, Aug. 2007, doi: 10.1038/NPROT.2007.261.
- [125] P. Marfull-Oromí, K. Onishi, X. Han, J. R. Yates, and Y. Zou, “The Fragile X Messenger Ribonucleoprotein 1 Participates in Axon Guidance Mediated by the Wnt/Planar Cell Polarity Pathway,” *Neuroscience*, vol. 508, pp. 76–86, Jan. 2023, doi: 10.1016/j.neuroscience.2022.09.018.
- [126] R. Sable, N. Jambunathan, S. Singh, S. Pallerla, K. G. Kousoulas, and S. Jois, “Proximity ligation assay to study protein–protein interactions of proteins on two different cells,” *BioTechniques*, vol. 65, no. 3, pp. 149–157, Sep. 2018, doi: 10.2144/btn-2018-0049.

- [127] O. Söderberg *et al.*, “Direct observation of individual endogenous protein complexes in situ by proximity ligation,” *Nat. Methods* 2006 312, vol. 3, no. 12, pp. 995–1000, Oct. 2006, doi: 10.1038/nmeth947.
- [128] U. Raudvere *et al.*, “g:Profiler: a web server for functional enrichment analysis and conversions of gene lists (2019 update),” *Nucleic Acids Res.*, vol. 47, no. W1, pp. W191–W198, Jul. 2019, doi: 10.1093/nar/gkz369.
- [129] A. Gajadhar and A. Guha, “A proximity ligation assay using transiently transfected, epitope-tagged proteins: Application for in situ detection of dimerized receptor tyrosine kinases,” *BioTechniques*, vol. 48, no. 2, pp. 145–152, Feb. 2010, doi: 10.2144/000113354/ASSET/IMAGES/LARGE/FIGURE5.JPEG.
- [130] D. S. Smith and J. H. Skene, “A transcription-dependent switch controls competence of adult neurons for distinct modes of axon growth,” *J. Neurosci. Off. J. Soc. Neurosci.*, vol. 17, no. 2, pp. 646–658, Jan. 1997, doi: 10.1523/JNEUROSCI.17-02-00646.1997.
- [131] P. W. Baas, L. A. White, and S. R. Heidemann, “Microtubule polarity reversal accompanies regrowth of amputated neurites,” *Proc. Natl. Acad. Sci.*, vol. 84, no. 15, pp. 5272–5276, Aug. 1987, doi: 10.1073/pnas.84.15.5272.
- [132] J.-Q. Zheng *et al.*, “A Functional Role for Intra-Axonal Protein Synthesis during Axonal Regeneration from Adult Sensory Neurons,” *J. Neurosci.*, vol. 21, no. 23, pp. 9291–9303, Dec. 2001, doi: 10.1523/JNEUROSCI.21-23-09291.2001.
- [133] B. N. Smith *et al.*, “Mutations in the vesicular trafficking protein annexin A11 are associated with amyotrophic lateral sclerosis,” *Sci. Transl. Med.*, vol. 9, no. 388, p. eaad9157, May 2017, doi: 10.1126/scitranslmed.aad9157.
- [134] A. Yao *et al.*, “Drosophila FMRP regulates microtubule network formation and axonal transport of mitochondria,” *Hum. Mol. Genet.*, vol. 20, no. 1, pp. 51–63, Jan. 2011, doi: 10.1093/hmg/ddq431.
- [135] S. C. Ling, P. S. Fahrner, W. T. Greenough, and V. I. Gelfand, “Transport of Drosophila fragile X mental retardation protein-containing ribonucleoprotein granules by kinesin-1 and cytoplasmic dynein,” *Proc. Natl. Acad. Sci. U. S. A.*, vol. 101, no. 50, p. 17428, Dec. 2004, doi: 10.1073/PNAS.0408114101.
- [136] C. L. Riggs, N. Kedersha, P. Ivanov, and P. Anderson, “Mammalian stress granules and P bodies at a glance,” *J. Cell Sci.*, vol. 133, no. 16, Aug. 2020, doi: 10.1242/JCS.242487/225735.
- [137] B. Wolozin and P. Ivanov, “Stress granules and neurodegeneration,” *Nat. Rev. Neurosci.*, vol. 20, no. 11, pp. 649–666, Nov. 2019, doi: 10.1038/s41583-019-0222-5.
- [138] R. Lu *et al.*, “The fragile X protein controls microtubule-associated protein 1B translation and microtubule stability in brain neuron development,” *Proc. Natl. Acad. Sci. U. S. A.*, vol. 101, no. 42, pp. 15201–15206, Oct. 2004, doi: 10.1073/PNAS.0404995101.
- [139] N. Birsa *et al.*, “FUS-ALS mutants alter FMRP phase separation equilibrium and impair protein translation,” *Sci. Adv.*, vol. 7, no. 30, p. eabf8660, Jul. 2021, doi: 10.1126/sciadv.abf8660.
- [140] S. He *et al.*, “Distinct dynein complexes defined by DYNLRB1 and DYNLRB2 regulate mitotic and male meiotic spindle bipolarity,” *Nat. Commun.*, vol. 14, no. 1, Art. no. 1, Mar. 2023, doi: 10.1038/s41467-023-37370-7.
- [141] T. J. Price and O. K. Melemedjian, “Fragile X Mental Retardation Protein (FMRP) and the Spinal Sensory System,” *Results Probl. Cell Differ.*, vol. 54, pp. 41–59, 2012, doi: 10.1007/978-3-642-21649-7_4.
- [142] W. W. Y. Yim and N. Mizushima, “Lysosome biology in autophagy,” *Cell Discov.* 2020 61, vol. 6, no. 1, pp. 1–12, Feb. 2020, doi: 10.1038/s41421-020-0141-7.
- [143] E. W. Khandjian, “Biology of the fragile X mental retardation protein, an RNA-binding protein,” *Biochem. Cell Biol. Biochim. Biol. Cell.*, vol. 77, no. 4, pp. 331–342, 1999.
- [144] M. Doyle and M. A. Kiebler, “Focus Review Mechanisms of dendritic mRNA transport and its role in synaptic tagging,” *EMBO J.*, vol. 30, pp. 3540–3552, 2011, doi: 10.1038/emboj.2011.278.
- [145] E. Corradi *et al.*, “Axonal precursor miRNAs hitchhike on endosomes and locally regulate the development of neural circuits,” *EMBO J.*, vol. 39, no. 6, p. e102513, Mar. 2020, doi: 10.15252/EMBJ.2019102513.
- [146] M. Ansar *et al.*, “ARTICLE Bi-allelic Variants in DYNC112 Cause Syndromic Microcephaly with Intellectual Disability, Cerebral Malformations, and Dysmorphic Facial Features,” *Am. J. Hum. Genet.*, vol. 104, May 2019, doi: 10.1016/j.ajhg.2019.04.002.
- [147] S. Finkbeiner, “The Autophagy Lysosomal Pathway and Neurodegeneration,” *Cold Spring Harb. Perspect. Biol.*, vol. 12, no. 3, p. a033993, Mar. 2020, doi: 10.1101/cshperspect.a033993.
- [148] Q. Zheng *et al.*, “Dysregulation of Ubiquitin-Proteasome System in Neurodegenerative Diseases,” *Front. Aging Neurosci.*, vol. 8, 2016, Accessed: Aug. 21, 2023. [Online]. Available: <https://www.frontiersin.org/articles/10.3389/fnagi.2016.00303>

- [149] J. C. Roney *et al.*, “Lipid-mediated motor-adaptor sequestration impairs axonal lysosome delivery leading to autophagic stress and dystrophy in Niemann-Pick type C,” *Dev. Cell*, vol. 56, no. 10, p. 1452, May 2021, doi: 10.1016/J.DEVCEL.2021.03.032.
- [150] I. Azmi *et al.*, “Recycling of ESCRTs by the AAA-ATPase Vps4 is regulated by a conserved VSL region in Vta1,” *J. Cell Biol.*, vol. 172, no. 5, pp. 705–717, Feb. 2006, doi: 10.1083/jcb.200508166.
- [151] H. Ye *et al.*, “Retromer subunit, VPS29, regulates synaptic transmission and is required for endolysosomal function in the aging brain,” *eLife*, vol. 9, p. e51977, doi: 10.7554/eLife.51977.
- [152] H. Ye, P. Bagchi, T. Wu, E. B. Dammer, N. T. Seyfried, and J. M. Shulman, “Retromer subunit, VPS29, regulates vacuolar-type ATPase and lysosomal acidification in the aging brain,” *Alzheimers Dement.*, vol. 18, no. S4, p. e065045, 2022, doi: 10.1002/alz.065045.
- [153] D. Santorelli *et al.*, “Folding Mechanism and Aggregation Propensity of the KH0 Domain of FMRP and Its R138Q Pathological Variant,” *Int. J. Mol. Sci.*, vol. 23, no. 20, p. 12178, Oct. 2022, doi: 10.3390/ijms232012178.
- [154] L. Sjekloća, K. Pauwels, and A. Pastore, “On the aggregation properties of FMRP--a link with the FXTAS syndrome?,” *FEBS J.*, vol. 278, no. 11, pp. 1912–1921, Jun. 2011, doi: 10.1111/j.1742-4658.2011.08108.x.
- [155] N. F. Bence, R. M. Sampat, and R. R. Kopito, “Impairment of the Ubiquitin-Proteasome System by Protein Aggregation,” *Science*, vol. 292, no. 5521, pp. 1552–1555, May 2001, doi: 10.1126/science.292.5521.1552.
- [156] C. McKinnon *et al.*, “Early-onset impairment of the ubiquitin-proteasome system in dopaminergic neurons caused by α -synuclein,” *Acta Neuropathol. Commun.*, vol. 8, no. 1, p. 17, Feb. 2020, doi: 10.1186/s40478-020-0894-0.
- [157] L. G. G. C. Verhoef, K. Lindsten, M. G. Masucci, and N. P. Dantuma, “Aggregate formation inhibits proteasomal degradation of polyglutamine proteins,” *Hum. Mol. Genet.*, vol. 11, no. 22, pp. 2689–2700, Oct. 2002, doi: 10.1093/hmg/11.22.2689.
- [158] J.-Y. Lee *et al.*, “HDAC6 controls autophagosome maturation essential for ubiquitin-selective quality-control autophagy,” *EMBO J.*, vol. 29, no. 5, pp. 969–980, Mar. 2010, doi: 10.1038/emboj.2009.405.
- [159] M. K. H. Ripon *et al.*, “N-acetyl-D-glucosamine kinase binds dynein light chain roadblock 1 and promotes protein aggregate clearance,” *Cell Death Dis.*, vol. 11, no. 8, p. 619, Aug. 2020, doi: 10.1038/s41419-020-02862-7.
- [160] R. Abouward and G. Schiavo, “Walking the line: mechanisms underlying directional mRNA transport and localisation in neurons and beyond,” *Cell. Mol. Life Sci.*, vol. 78, no. 6, pp. 2665–2681, 2021, doi: 10.1007/s00018-020-03724-3.
- [161] P. K. Sahoo *et al.*, “Axonal G3BP1 stress granule protein limits axonal mRNA translation and nerve regeneration,” *Nat. Commun.*, vol. 9, no. 1, p. 3358, Aug. 2018, doi: 10.1038/s41467-018-05647-x.
- [162] “Aggregation of the nucleic acid-binding protein TDP-43 occurs via distinct routes that are coordinated with stress granule formation - Journal of Biological Chemistry.” Accessed: Sep. 14, 2023. [Online]. Available: [https://www.jbc.org/article/S0021-9258\(20\)38993-6/fulltext#seccesstitle70](https://www.jbc.org/article/S0021-9258(20)38993-6/fulltext#seccesstitle70)
- [163] F. Zalfa *et al.*, “The Fragile X Syndrome Protein FMRP Associates with BC1 RNA and Regulates the Translation of Specific mRNAs at Synapses,” *Cell*, vol. 112, no. 3, pp. 317–327, Feb. 2003, doi: 10.1016/S0092-8674(03)00079-5.
- [164] Y. Guo *et al.*, “Elevated levels of FMRP-target MAP1B impair human and mouse neuronal development and mouse social behaviors via autophagy pathway,” *Nat. Commun.*, vol. 14, no. 1, Art. no. 1, Jun. 2023, doi: 10.1038/s41467-023-39337-0.
- [165] J. A. D. Rio *et al.*, “MAP1B Is Required for Netrin 1 Signaling in Neuronal Migration and Axonal Guidance,” *Curr. Biol.*, vol. 14, no. 10, pp. 840–850, May 2004, doi: 10.1016/j.cub.2004.04.046.
- [166] A. E. Twelvetrees *et al.*, “The Dynamic Localization of Cytoplasmic Dynein in Neurons Is Driven by Kinesin-1,” *Neuron*, vol. 90, no. 5, pp. 1000–1015, Jun. 2016, doi: 10.1016/j.neuron.2016.04.046.
- [167] J. M. Carosi *et al.*, “Retromer regulates the lysosomal clearance of MAPT/tau,” *Autophagy*, vol. 17, no. 9, pp. 2217–2237, Sep. 2021, doi: 10.1080/15548627.2020.1821545.
- [168] J.-J. Liu, “Retromer-Mediated Protein Sorting and Vesicular Trafficking,” *J. Genet. Genomics*, vol. 43, no. 4, pp. 165–177, Apr. 2016, doi: 10.1016/j.jgg.2016.02.006.
- [169] T.-B. Lin *et al.*, “VPS26A-SNX27 Interaction-Dependent mGluR5 Recycling in Dorsal Horn Neurons Mediates Neuropathic Pain in Rats,” *J. Neurosci. Off. J. Soc. Neurosci.*, vol. 35, no. 44, pp. 14943–14955, Nov. 2015, doi: 10.1523/JNEUROSCI.2587-15.2015.
- [170] C. N. Arighi, L. M. Hartnell, R. C. Aguilar, C. R. Haft, and J. S. Bonifacino, “Role of the mammalian retromer in sorting of the cation-independent mannose 6-phosphate receptor,” *J. Cell Biol.*, vol. 165, no. 1, pp. 123–133, Apr. 2004, doi: 10.1083/jcb.200312055.
- [171] N. Kimura, E. Samura, K. Suzuki, S. Okabayashi, N. Shimozawa, and Y. Yasutomi, “Dynein Dysfunction Reproduces Age-Dependent Retromer Deficiency: Concomitant Disruption of Retrograde

- Trafficking Is Required for Alteration in β -Amyloid Precursor Protein Metabolism,” *Am. J. Pathol.*, vol. 186, no. 7, pp. 1952–1966, Jul. 2016, doi: 10.1016/j.ajpath.2016.03.006.
- [172] P. Majumder, J.-F. Chu, B. Chatterjee, K. B. S. Swamy, and C.-K. J. Shen, “Co-regulation of mRNA translation by TDP-43 and Fragile X Syndrome protein FMRP,” *Acta Neuropathol. (Berl.)*, vol. 132, no. 5, pp. 721–738, 2016, doi: 10.1007/s00401-016-1603-8.
- [173] S. Mueller, L. Decker, S. Menge, A. C. Ludolph, and A. Freischmidt, “The Fragile X Protein Family in Amyotrophic Lateral Sclerosis,” *Mol. Neurobiol.*, vol. 60, no. 7, p. 3898, 2023, doi: 10.1007/s12035-023-03330-x.
- [174] A. Freischmidt *et al.*, “A serum microRNA sequence reveals fragile X protein pathology in amyotrophic lateral sclerosis,” *Brain J. Neurol.*, vol. 144, no. 4, pp. 1214–1229, May 2021, doi: 10.1093/brain/awab018.

Appendix

Table 1. Dynlrb1 putative interactors in DRG neurons

Gene ID	Gene Name
U2surp	U2 snrnp-associated SURP domain containing
Eif2s3y	Eukaryotic translation initiation factor 2, subunit 3
Dnajc2	Dnaj heat shock protein family member C2
Mrpl21	Mitochondrial ribosomal protein L21
Tecr	Trans-2,3-enoyl-coa reductase
Acs15	Acyl-coa synthetase long-chain family member 5
Dynlrb1	Dynein light chain roadblock-type 1
Ssb	Small RNA binding exonuclease protection factor La
Mtfr11	Mitochondrial fission regulator 1-like
C3ar1	Complement component 3a receptor 1
Psmg1	Proteasome assembly chaperone 1
Cog2	Component of oligomeric golgi complex 2
Col3a1	Collagen, type III, alpha 1
Nup133	Nucleoporin 133
Dusp11	Dual specificity phosphatase 11
Vac14	Vac14 homolog
Actr1b	ARP1 actin-related protein 1B, centractin beta
Ppm1a	Protein phosphatase 1A, magnesium dependent, alpha isoform
Ppm1b	Protein phosphatase 1B, magnesium dependent, beta isoform
Acaa1a	Acetyl-Coenzyme A acyltransferase 1A
Acaa1b	Acetyl-Coenzyme A acyltransferase 1B
Pak1ip1	PAK1 interacting protein 1
Cenpv	Centromere protein V
Setd3	SET domain containing 3
Tmpo	Thymopoietin
Tmem65	Transmembrane protein 65
Srp14	Signal recognition particle 14
Pnpla6	Patatin-like phospholipase domain containing 6
Epm2aip1	EPM2A (laforin) interacting protein 1
Cops6	COP9 signalosome subunit 6
Sacs	Sacsin
Efr3a	EFR3 homolog A
Pxn	Paxillin
Dgkh	Diacylglycerol kinase, eta
Atxn2l	Ataxin 2-like
Cmas	Cytidine monophospho-N-acetylneuraminic acid synthetase
Fam91a1	Family with sequence similarity 91, member A1
Vta1	Vesicle (multivesicular body) trafficking 1
Vps29	VPS29 retromer complex component
Rab11fip5	RAB11 family interacting protein 5 (class I)
Ubp2	Ubiquitin-associated protein 2
Aldoc	Aldolase C, fructose-bisphosphate
Eif3k	Eukaryotic translation initiation factor 3, subunit K
Primpol	Primase and polymerase (DNA-directed)
Hip1r	Huntingtin interacting protein 1 related
Arhgef12	Rho guanine nucleotide exchange factor 12
Ret	Ret proto-oncogene

Fmr1	Fragile X messenger ribonucleoprotein 1
Hnrnp1l	Heterogeneous nuclear ribonucleoprotein L-like
Dnajb1	Dnaj heat shock protein family member B1
Sec24c	SEC24 homolog C, COPII coat complex component
Stx8	Syntaxin 8
Chordc1	Cysteine& histidine-rich domain containing zinc binding protein 1
Map1s	Microtubule-associated protein
Nisch	Nischarin
Kifc1	Kinesin family member C1
Kifc5b	Kinesin family member C5B
Gstm1	Glutathione S-transferase, mu 1
Get4	Golgi to ER traffic protein 4
Anxa11	Annexin A11
Cplx1	Complexin 1
Thop1	Thimet oligopeptidase 1
Ubr4	Ubiquitin protein ligase E3 component n-recognin 4
Ufm1	Ubiquitin-fold modifier 1
Ddx19a	DEAD box helicase 19a
Ddx19b	DEAD box helicase 19b
Usp7	Ubiquitin specific peptidase 7
Eef1a2	Eukaryotic translation elongation factor 1 alpha 2
Dusp3	Dual specificity phosphatase 3
Aacs	Acetoacetyl-coA synthetase
Myg1	Melanocyte proliferating gene 1
Ola1	Obg-like Atpase 1
Ckb	Creatine kinase, brain
Dync1li2	Dynein, cytoplasmic 1 light intermediate chain 2
Rpl18	Ribosomal protein L18
Glrx3	Glutaredoxin 3
Otub1	OTU domain, ubiquitin aldehyde binding 1
Aip	Aryl-hydrocarbon receptor-interacting protein
Rps19	Ribosomal protein S19
Best2	Bestrophin 2
G6pdx	Glucose-6-phosphate dehydrogenase X-linked
Faf1	Fas-associated factor 1
Nrd1	Nardilysin, N-arginine dibasic convertase, NRD convertase 1
Gdi1	Guanosine diphosphate dissociation inhibitor 1
Pabpc4	Poly(A) binding protein, cytoplasmic 4
Pitrm1	Pitriylsin metallepetidase 1
Ap3b2	Adaptor-related protein complex 3, beta 2 subunit
Gclm	Glutamate-cysteine ligase, modifier subunit
Adss	Adenylosuccinate synthetase, non-muscle
Nif3l1	Ngg1 interacting factor 3-like 1